Assessing the viability of implementing significantly oversized holes in high strength friction grip bolted connections

Towards the increased modularity of bridge decks and ease of their replacement

Master's Thesis

Eric Barelts

Faculty of Civil Engineering and Geosciences
Delft University of Technology
December 2022, Delft

TU Delft

Assessing the viability of implementing significantly oversized holes in high strength friction grip bolted connections

Towards the increased modularity of bridge decks and ease of their replacement

by

Eric Barelts

In partial fulfilment of the requirements for the degree of

Master of Science
in Civil Engineering

at the Faculty of Civil Engineering and Geosciences, Delft University of Technology,
to be defended publicly on Wednesday December 21, 2022 at 15:00.

Student number: 4282140

Thesis committee:

Dr. Ir	M. Pavlovic	TU Delft	Chair
Ir.	A. Christoforidou	TU Delft	Supervisor
Dr. Ir.	F. Kavoura	TU Delft	
Dr. Ir.	A. Cabboi	TU Delft	

An electronic version of this thesis is available at https://repository.tudelft.nl/

TU Delft

PREFACE

This master thesis is my final step in the completion of the Master Civil Engineering at Delft University of Technology. I started my journey at TU Delft with the intention of working on projects that would yield tangible results in the near future. This was the case with the subject of my Bachelor thesis and I intended to do the same with my Master's thesis.

The subject for this thesis was initially presented to me as a possibility to solve a problem as part of a product that could be implemented in the near future. This subject gradually shrunk in scope as I was far too ambitious at the start.

This thesis report is the end result, a first foray in experimental research on this subject meant to demonstrate the viability of this concept for future use. It is thus encouraged for more research to be conducted on this subject, which this thesis intends to facilitate by providing recommendations for future experiments and documentation of the lessons learned. I look forward to future research results and hopefully the eventual implementation of this proposed concept.

I would like to thank Marko Pavlovic, Florentia Kavoura and Alessandro Cabboi of my committee for providing feedback during our meetings. Special thanks go to my daily supervisor and committee member Angeliki Christoforidou for her help and patience during the writing of my thesis. I would also like to thank both Peter de Vries and Fred Schilperoort for thinking along and helping make the experiments possible. Finally I would like to thank both my father and my friends Derek and Jason for taking the time to read my thesis and provide feedback.

ABSTRACT

The development towards a circular economy has many hurdles to overcome. For the construction sector an important step in this process is the transition towards reusing structural elements. Prefabrication of elements is a significant step towards achieving this concept. However, a case where both prefabrication and reuse are limited is the replacement of bridge decks. Headed bolts are welded to the steel supporting elements and encased in grout to connect them to the concrete deck elements. This method prevents reuse of the deck elements and hinders reuse of the steel supporting elements.

Research and literature exists on a number of alternative shear connectors that increase the modularity of these elements. The best alternatives have a single limitation in common: the allowed deviation for the placement of the shear connectors and bolt holes is smaller than is feasibly possible. The variances of element placement during construction add up to make it incredibly hard for these low tolerance connections to be made. The bolt hole diameter can be increased to increase the deviation tolerances. The large nominal hole clearance this results in needs to be considered. This can be done by using either resin injected bolts or High Strength Friction Grip (HSFG) bolted connections. Using HSFG bolted connections is preferred due to the shorter time spent on site and minimal waste, but research on the subject is sparse.

A proposed HSFG bolted connection that implements significantly oversized holes, defined as bolt holes with a nominal hole clearance roughly equal to the bolt diameter, and cover plates was designed together with both a control and regular connection to compare its behaviour with. The control connection is identical to the proposed connection with the exception of its holes which are normal sized. The regular connection has normal holes and does not include cover plates. Finite Element Models (FEM) were made of these connections that were subjected to static loading in a Finite Element Analysis (FEA). Test specimens of these connections were made and subjected to fatigue loading.

The numerical results of the static FEA showed that the use of cover plates reduced the stiffness and slip load of the connection. The second observation was the small impact that the hole size had on the slip load when using cover plates. This small impact becomes negligible at design preload.

The experimental results showed that the impact of larger bolt holes increased the loss of preload by roughly 1% during both short term relaxation and fatigue loading. The effect of the bolt hole size on the slip after fatigue loading was also concluded to be negligible, but the effect of the cover plates was concluded to be detrimental.

It was overall concluded that the use of significantly oversized holes in HSFG bolted connections with cover plates is viable. The negative effects caused by the cover plates and required longer bolt make it preferrable for large disc springs to be used instead of thick cover plates. The proven viability of the concept allows for further research on the subject. Recommendations on specific tests and alternative and improved test setups have also been given.

Contents

LIST OF FIGURES

LIST OF TABLES

GLOSSARY

Term	Definition
Clamping length	The distance between the bolt head and nut.
Faying surface	A surface that is in contact with another surface to form a joint.
Friction resistance	Force resisting displacement through friction between two or more contacting surfaces.
Full head slip load	Applied load present in a friction connection where interfacing faying surfaces are slipping without the friction resistance increasing further.
LVDT (Linear Variable Differential Transformer)	Measurement tool that uses an electrical transformer to measure linear displacement.
Nominal hole clearance	The difference between the nominal hole diameter and the nominal bolt diameter.
Significantly oversized hole	A bolt hole with a nominal hole clearance roughly equal to the used bolt diameter
Slip load	The applied load present in a friction connection when the first slip starts.
Slip resistance	The applied load needed for slip to occur in a friction connection according to EN 1993-1-8.
Strain bolt	Bolt with internal strain gauge.
Strain gauge	Measurement device that uses electrical resistance to measure strain in an object.

LIST OF ABBREVIATIONS

Abbreviation	Full Meaning
FEA	Finite Element Analysis
FEM	Finite Element Model
FRP	Fibre Reinforced Polymer
HSFG	High Strength Friction Grip
SLS	Serviceability Limit State
ULS	Ultimate Limit State

1 INTRODUCTION

1.1 BACKGROUND

With the world moving towards a more circular economy, recycling is starting to lack as a solution with downgrading being common. Steel structural elements are at the forefront of this trend, since they have the benefit of a long service life, universal profile dimensions and ease of dismantling due to mechanical fasteners. Steel supporting structures can outlive other parts of a structure due to degradation or stricter design codes. Examples of this are floors in buildings and bridge decks. Prefabrication has simultaneously become the norm for faster construction and the search for more complete prefabricated elements is still ongoing.

Observing both trends together presents a challenge when combining these principles in certain cases. A specific case which demonstrates this problem is the replacement of bridge decks. Older bridges in the Netherlands are approaching the end of their service life due to deterioration of the bridge decks, increasingly higher traffic loads and stricter design codes. The steel superstructures of these bridges are in good condition and their service life can be extended with proper maintenance. The resulting solution is the replacement of the bridge decks with either prefabricated concrete deck elements or novel Fibre Reinforced Polymer (FRP) web-core panels. In cases where composite action is not present it could be induced with the new bridge decks to increase strength and stiffness. To ensure these replacement decks align with the principle of a circular economy, the shear connectors should be demountable. Current practice for steel-concrete composite decks is the use of headed studs welded to the steel girders. These connecters are connected to the deck by embedding them in grout. This method makes demounting the decks labour intensive and prevents the decks from being reused if possible. Newer demountable shear connectors have started to be tested in recent years, but face obstacles to be viable. Rather than welded studs, these consist of bolted connections that are attached to the steel girders and similar to the studs are embedded in grout to connect them to the deck elements. The novel FRP decks work similarly, the major difference being the use of resin to embed the shear connectors rather than grout. More recent research has focussed on the possibilities of incorporating the shear connectors during prefabrication or for the connectors to not be embedded in the deck elements. Both methods require unfeasible precision for the placement of the connector and the hole in the steel girder, which hampers their viability. The solution to this problem is found in the increase of the nominal hole clearance, which causes more problems. To solve this next problem, both resin injected bolts and High Strength Friction Grip (HSFG) bolted connections have been suggested. The behaviour of both when used in conjunction with significantly oversized holes, defined as bolt holes with a nominal hole clearance roughly equal to the bolt diameter, is currently insufficiently documented and design codes lack extensive guidelines for their use in such connections. Though resin injected bolts are more mature in this field, they have the downside of a higher time requirement on site during construction. HSFG connections lack significant research in this case, but could provide a preferable construction method if shown to be viable.

1.2 Problem Statement

Further development of demountable shear connectors in bridge decks is dependent on the possibility for these connectors to be placed during prefabrication or be fully independent of the deck elements. This promotes a higher degree of modularity and reuse in bridge construction and in extension in general floor construction where prefabricated floor elements are used. The deviation tolerance for bolt and hole placement needs to be increased to facilitate this. This can be achieved by increasing the nominal hole clearance, which needs to be compensated for. While both resin injected bolts and HSFG bolted connections are possible solutions, HSFG connections have the benefit of a lower time requirement on site and less waste. The use of HSFG bolted connections may be preferrable, but knowledge on the behaviour of HSFG connections with significantly oversized holes is scarce. Their use is thus hampered by this knowledge gap, which prevents further progress in prefabrication and reuse of both concrete and FRP deck elements.

1.3 Objective and Research Question

This thesis aims to document the influence that the hole size and nominal hole clearance have on the static and fatigue slip behaviour of HSFG bolted connections. More specifically, the impact that bolt holes with a nominal hole clearance roughly equal to the used bolt diameter, called significantly oversized holes, have on these behaviours. To quantify this influence, points of reference are needed. To this extent three connections are designed: a proposed connection with significantly oversized bolt holes and cover plates, a control connection identical to the proposed connection with normal bolt holes and cover plates and a regular connection with normal bolt holes and no cover plates. Based on the data collected from experiments conducted using these connections, the following questions will be answered:

To what extent is the static and fatigue slip behaviour of, and loss of bolt preload in a high strength friction grip bolted connection influenced by the bolt hole size and nominal hole clearance?

Sub questions:

- How large is the influence of the bolt hole size and nominal hole clearance on the slip load when comparing the HSFG proposed, control and regular connections?
- How large is the influence of the bolt hole size and nominal hole clearance on the total slip suffered during fatigue loading when comparing the HSFG proposed, control and regular connections?
- How large is the influence of the bolt hole size and nominal hole clearance on the short term relaxation when comparing the HSFG proposed and control connections?
- How large is the influence of the bolt hole size and the nominal hole clearance on the loss of preload suffered during fatigue loading when comparing the HSFG proposed, control and regular connections?

1.4 Outline, Research Approach and Methodology

This thesis is divided in six chapters:

Chapter 1 – Introduction:
The introduction gives a background and broad description of the subject. This includes the opportunity, problem, objective, approach and research question.

Chapter 2 – Literature review:
The literature review has three major goals: showing the need for the research subject, documenting the current knowledge base on the subject and finding related work that could be used to assist in the conduction of the research in this report.

Chapter 3 – Connection design:
This chapter aims to design the novel proposed HSFG bolted connection and derives from it both a control connection where the only difference is the bolt hole size and a regular connection with normal sized bolt holes and without cover plates. This is achieved by using the design codes EN 1993-1-8 and EN 1993-1-9, related literature and the Finite Element Analysis program Abaqus.

Chapter 4 – Finite Element Analysis:
A Finite Element Model is constructed with the goal of gaining further insight in the static slip behaviour of all three connections. This chapter provides the required information to replicate the models used and further analyses the slip, stiffness and slip load of each connection.

Chapter 5 – Experiments:
This chapter covers the fatigue tests conducted. It describes the testing setup and procedure and documents the resulting data on both the short term bolt relaxation and the slip and loss of preload due to fatigue loading. Any unwanted influences on the data are described and the results adjusted to minimize their impact. The data of the different tests specimens is compared and the differences are analysed.

Chapter 6 – Conclusions and Recommendations:
The gathered data and the analysis of this data found in chapters 4 and 5 is used to form conclusions on the slip behaviour and loss of preload as a consequence of static and fatigue loading. These conclusions are used to answer the sub questions and research question and provide recommendations for further research, such as improved testing setups and alternative parts to be used.

2 LITERATURE REVIEW

2.1 BRIDGE DECK CONNECTORS

Due to their lower weight and higher stiffness, steel-concrete composite beams started to be extensively used in the construction of bridges during the 1950s. Development of shear connectors led to the use of early versions of the modern headed stud connector in the 1970s. In depth research on this subject was conducted by Ollgaard et al. (1971) during this period. The composite action of these composite beams is ensured by shear studs welded to the steel girder which are embedded in the precast beam or deck using grout as seen in Figure 2.1a. The design rules of these structures are described in EN 1994-1-1. The use of welded shear connectors and cast-in-situ concrete generates significant waste during deconstruction, hinders reuse of the steel girders and prevents reuse of the deck elements. This is not in line with the emerging principle of a circular economy.

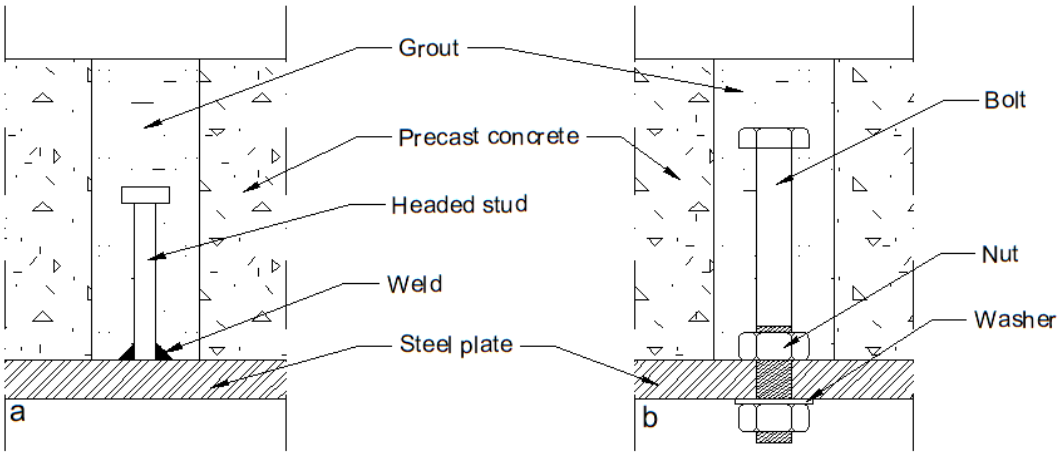

Figure 2.1 - a) Welded headed stud shear connector; b) Demountable bolted shear connector

Strides have been made in the use of demountable shear connectors, such as the one seen in Figure 2.1b, in response to this problem. A variety of options is shown in Figure 2.2. In these connections the bolts are connected to the top flange of the steel girder and then embedded in the concrete deck element, replacing welded studs. This allows for demounting of the concrete elements during deconstruction. Even though Eurocode 4 currently only supports tests for shear studs, a significant amount of research has been conducted on these demountable shear connectors. After comparative tests between a bolted shear connector and a headed stud were conducted by Pavlović et al. (2013, p. 148-149) a number of conclusions were made. The connection used consisted of M16 grade 8.8 bolts with a single embedded nut. The results showed that under static loading, the shear resistance was equal to 95% of that of a similar connection using welded headed studs. The downside was the significant reduction in stiffness, which was reduced by 50%. This reduction was contributed to slip in the hole and threads-to-hole penetration, among other causes.

Several bolt types have been tested over time to determine their viability as demountable shear connectors. Blind bolts were researched as possible demountable shear connectors by Wijesiri Pathirana et al. (2016, p. 193) for both composite beams and non-composite beams. It was concluded that the strength and stiffness behaviour of the blind bolts was comparable to that of the welded studs. In tests conducted by Hawkins (1987), the results of anchor bolts without an embedded nut showed a 20% reduction in shear resistance and 85% stiffness reduction when compared to welded studs. The use of HSFG bolted connections was the subject of research by Dallam (1968). This research showed that, with no slip at serviceability load, the ultimate shear resistance reached up to twice the value of welded headed studs with similar dimensions.

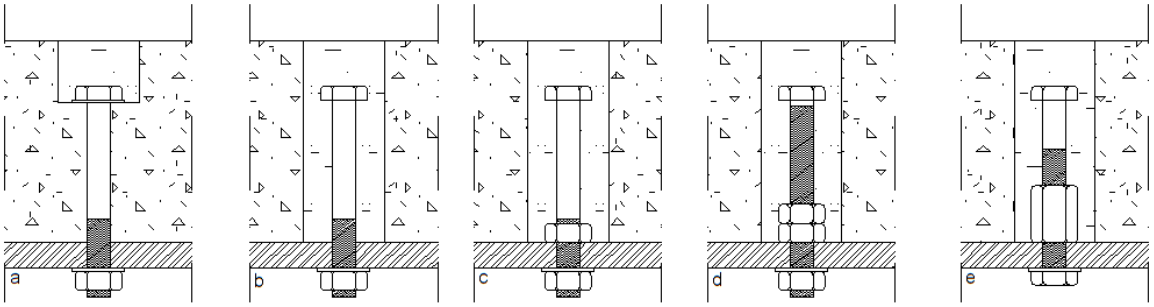

Figure 2.2 - Demountable shear connectors: a) Friction grip bolt; b) Embedded bolt; c) Embedded bolt, single nut; d) Embedded bolt, double nut; e) Embedded bolt with coupler

Kwon et al. (2010) noted that an additional benefit of the use of demountable shear connectors is the introduction of composite action in bridges that were designed without it using post-installed shear connectors. By doing this, the carrying capacity of these structures can be increased to meet the demands of higher loads and more recent design codes. In research by Dedic & Klaiber (1984) and more recently by Kwon et al. (2010) a number bolts in HSFG bolted connections were tested under fatigue loading to document their behaviour and shear resistance. Kwon et al. (2010, p. 539) concluded that the fatigue strength of the post-installed shear connectors was significantly higher than that of welded headed studs, which resulted in a reduction of the number of connectors required. The use of HSFG demountable shear connectors was further researched by Suwaed & Karavasilis (2020, p. 16) who concluded that this type of connector fulfils the SLS and ULS requirements when designed in accordance with EN 1994-1-1.

Similar to the demountable shear connectors in steel-concrete composite beams, research has been conducted on possible demountable shear connectors in FRP decks. Zhou & Keller (2005) explored the possibilities for adhesive bonding, mechanical joints and hybrid joints. Satasivam et al. (2017) focussed on blind bolts and proposed their use as shear connectors for FRP decks. Overall, the principles of demountable shear connectors are similar for both concrete and FRP decks when the interactions between the shear connectors and steel superstructure are the focus.

In most of the mentioned methods for demountable shear connectors, the connectors themselves are embedded in the deck elements during construction. The holes they are placed in are filled with either grout or polymers for concrete and FRP decks respectively. These connectors are practically permanently embedded, and the filling compound creates a permanent bond between the deck and steel girder. This solves the problem of deconstruction, but the time spent on site remains the same.

A number of solutions to include the connectors during prefabrication have been proposed over time. Through bolt shear connectors as seen in Figure 2.3c and d, which lack the requirement of a filling compound, have been tested by Chen et al. (2014) and Kozma et al. (2019) among others. Both identified the low tolerance for deviation of hole placement as the main disadvantage of this method. Another proposed solution by Yang et al. (2018) and Kozma et al. (2019) was the use of inserted bolts with a coupler to allow for the external bolt to be replaceable, these can be seen in Figure 2.3a and b. This solution had the same limitation of requiring precise hole placement due to the low deviations allowed. Kozma et al. (2019, p. 47) proposed the use of either HSFG bolted connections or epoxy resin injected bolts to allow for a larger nominal hole clearance and in turn a higher tolerance for deviation. Correia et al. (2017, p. 795) noted that resin injected bolts could be a cheaper alternative to fitted bolts when HSFG bolted connections are not possible.

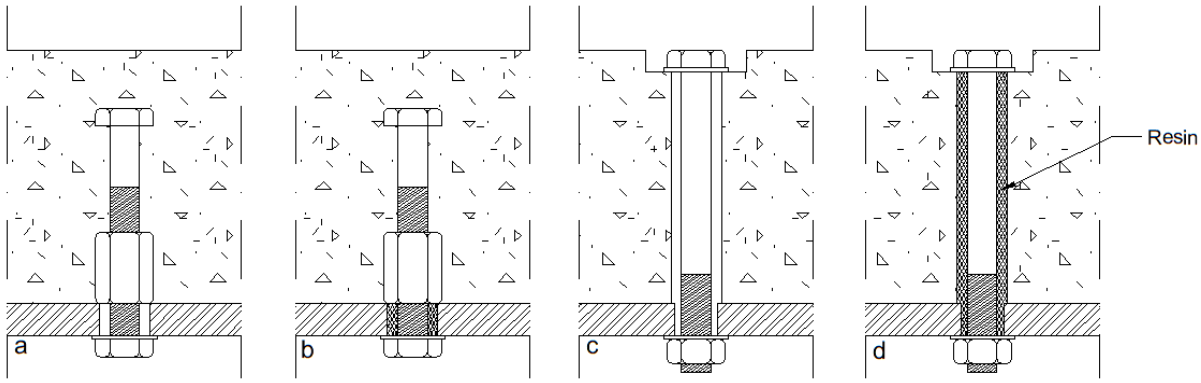

Figure 2.3 - Novel demountable shear connectors: a) Precast embedded coupler; b) Precast embedded coupler with resin; c) Through bolt; d) Through bolt with resin

Correia et al. (2017, p. 804) also concluded that resin injected bolts have a lower fatigue resistance than HSFG bolted connections. Solutions for this downside were researched by Nijgh (2017, p. 113-114), who focussed on further possibilities of resin and other injection materials, such as grout, resin and a proposed reinforced resin. This proposed reinforced resin consisted of steel shot enveloped by resin, which was injected afterwards. This produced a continuous matrix of resin that held the load bearing steel shot together. The results showed both a 86% increase in slip load and a reduction in creep when compared to regular resin. This proposed steel reinforced resin was further studied by Nijgh et al. (2018) with the goal of modelling it for further calculations. The subject was later picked up by Xin et al. (2019) who furthered the modelling knowledge of the material and joint.

2.2 High Strength Friction Grip Bolted Connections

Bolted connections loaded in shear can be broadly categorized in bearing connections and friction connections, sketches of which are shown in Figure 2.4. Traditional bolted connections transfer the load through the bolt shaft into the bearings of the connected plates. Friction connections transfer this load through the friction between the connected plates which is induced by the clamping force in the bolt. These High Strength Friction Grip connections normally consist of high strength bolts, such as grade 10.9, placed in a normal sized hole. Compared to bearing connections, significant tightening of the bolts is needed, and the faying surfaces need to have the required friction coefficient to transfer the forces properly. Proper faying surfaces are not always available such as during renovation of older structures. Some of the advantages of HSFG bolted connections are the higher fatigue resistance and stiffness. Cullimore (1982) demonstrated that the fatigue strength of HSFG bolted joints is higher than the fatigue strength of butt welds. It was also noted that slip would not occur and the bolt shaft would thus not interact with the side of the hole due to the high preload of the bolt. Another consequence of this high preload was the comparatively low variance of the force in the bolt which reduced fatigue damage. By combining these factors, it can be concluded that the longer fatigue life for both the bolt and hole in HSFG bolted connections proves useful for connections that are cyclically loaded such as those found in bridges. Design guidelines for these HSFG bolted connections are laid out in EN 1993-1-8 for static cases and in EN 1993-1-9 for fatigue cases. Further design standards on the preparation and execution of steel connections are found in EN 1090-2.

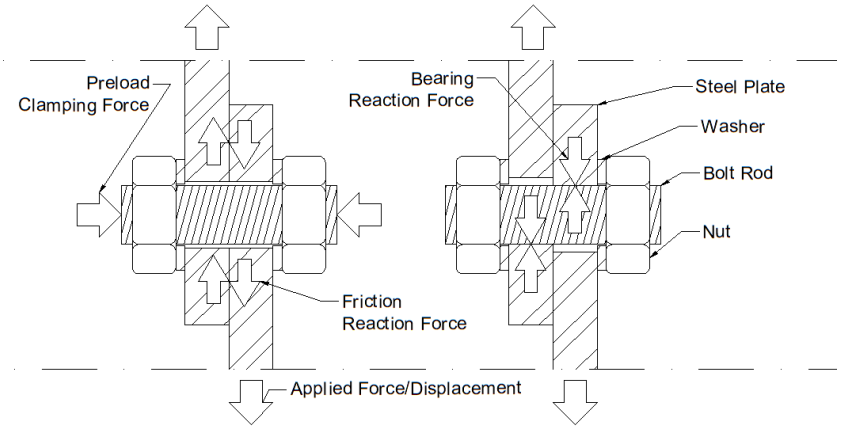

Figure 2.4 - Left) Friction grip connection; Right) Bearing connection

2.2.1 Loss of Preload

The clamping force in a HSFG bolted connection is the source of the friction resistance in the joint. This force is exerted by the bolt that has been preloaded by tightening the bolt in a controlled manner. The tightening methods used are described in EN 1090-2.

The loss of preload in the bolt is a major contributor to slip over time. The friction resistance diminishes due to the loss in clamping force, allowing slip to occur. The causes for this loss of preload can be categorized in two different ways: by the moment it occurs and whether the mechanism includes rotation of the bolt or not.

The initial loss of preload directly after tightening and the short term relaxation during the first 12 hours are mainly the consequence of embedding. To understand this process, the asperity of the surface must be understood. Eccles (2011) described this as the uneven roughness of the surface, which mostly consists of many asperities or small protrusions present on the surface. A simplified sketch of this is shown in Figure 2.5.

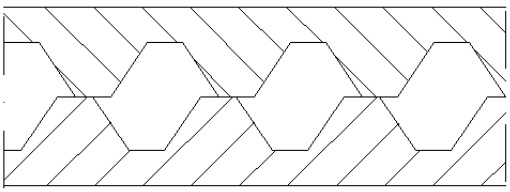

Figure 2.5 - Surface asperity

Eccles (2011) explained that when two surfaces come in contact with one another, the effective contact area consists of the tops of these asperities. When clamping these surfaces together, the asperities will fail plastically due to the high stress concentrations that exceed the yield strength of the material. This process continues during the preloading of the bolt and continues afterwards until a large enough area is reached for the stresses to fall below the yield strength. This process occurs in every single contact area including the treads. This is the major reason for the large loss of preload both directly and in the short term after preloading and plays a larger role for connections with more interfacing faying surfaces. The thickness and type of coating used also affect the loss of preload significantly. Experimental results described by Friede & Lange (2010, p. 290) showed that the loss of preload in a static situation due to embedding in the first 12 hours varied between 10% and 70% depending on the applied coating: the 10% loss was found when a hard coating of epoxy-zinc primer and epoxy-iron mica + polyurethane cover was used, while a loss of as much as 70% occurred when a thick coat of soft alkyd coating was used. Further factors affecting the short term relaxation were summed up by Abid et al. (2015, p. 44) as relaxation that "*occurs shortly, after the joint has been assembled or at least soon after it has been put into service, due to the number of reasons, such as bolt bending, soft parts (gasket), improper tooling and torquing, bolt quality, non-parallelism of flange joint surfaces, geometric variance and so on.*" Abid et al. (2015, p. 50) also noted that this short term relaxation could be compensated for by inducing a higher preload and retightening the bolts after a short period of time.

The long term relaxation as described by Abid et al. (2015, p. 44) "*is generally due to the stress relaxation and vibration loosening. Stress relaxation can be related to the creep, as this is substantial under high temperature applications.*" Eccles (2011) noted that, in addition to the specific stress relaxation, creep on its own also impacts the loss of preload in the long term. It was also noted by Eccles (2011) that embedding plays a role during long term relaxation. This was explained as the application of loads and displacements, especially cyclic ones, changing the locations of stress concentrations. This distorts the balance that is found over time causing more asperities to fail, the consequence being further plastic compression of the surface. Eccles (2011) also noted that two interfaces are especially important for self-loosening of the bolt, which are the thread contact areas and the bolt/nut to plate interfaces. Embedding at both interfaces reduces the rotational friction resistance of the bolt, which affects the self-loosening of the bolt. Research on the self-loosening of bolted connections due to vibrations was initially focussed on axial loading of the bolt such as by Goodier & Sweeney (1945) and by Sauer et al. (1950). Some of the earliest research that focussed on self-loosening due to perpendicular loading was conducted by Junker (1969). He concluded that it was not vibrations themselves that caused self-loosening, but the resulting relative displacements

between the bolt and nut threads and between the faying surfaces of the bolt and plate. This was explained as the bolt rotating due to the displacement of the connected plates perpendicular to the thread axis, resulting in the bolt head losing rotational friction resistance as soon as any small slip occurred in the connection. Under long term fatigue loading this process would repeat itself countless times resulting in the complete unloading of the bolt. It was thus also concluded that vibrations introduced perpendicular to the bolt axis caused a significantly higher loss of preload than axial loading.

To prevent this from occurring, self-locking bolts have been suggested and developed over the years in the form of specialized bolts and washers. More recent research by Pai & Hess (2002a, p. 599) attributed the initial loosening due to shear loading to localized slip in the thread contact areas. It was noted that due to this, loosening could start "*at roughly half the shear load required for complete head slip.*" Pai & Hess (2002b) furthered the research on this subject by producing a finite element model that demonstrated the process of loosening due to shear force. The influence that the type of coating has on self-loosening was concluded to be large by Friede & Lange (2010, p. 290), as it affected the rate of abrasion and further embedding over time.

2.2.2 Oversized Holes

Chen et al. (2014), Yang et al. (2018) and Kozma et al. (2019) all concluded that the low tolerance for deviation was the limiting factor for the use of demountable shear connectors. The nominal hole clearance can be increased to increase the deviation tolerance, but to what extents needs to be known. A larger nominal hole clearance also increases slip distance, which was demonstrated by Pavlović et al. (2013) to reduce the composite action and stiffness of steel-concrete composite beams. The definition of the nominal hole clearance as described in EN 1090-2 is the difference between the nominal hole diameter and the nominal bolt diameter. The different clearances from this norm can be seen in Table 1.

Table 1 - Nominal hole clearances for bolts (mm) according to EN 1090-2

Nominal bolt diameter d (mm)	**12**	**14**	**16**	**18**	**20**	**22**	**24**	**27 and over**
Normal round holes	1		2					3
Oversized round holes	3		4				6	8
Short slotted holes (on length)	4		6				8	10
Long slotted holes (on length)	1,5 d							

The question regarding the required nominal hole clearance was answered by Nijgh & Veljkovic (2020). They formulated a model to determine the required nominal hole clearance for steel-concrete composite floor systems. This was achieved by considering a significant number of deviations in both the geometry and the dimensions of both the composite floor system and the supporting structure. Based on these influence factors, an equation was set up that gave the total deviation from the nominal position for both the bolt holes and the embedded demountable shear connectors. This was combined with probability studies on the correct installation of connectors to complete the model. This model was applied on the case-study of a multi-storey carpark using composite floors. These floors were based on a design proposed by Nijgh et al. (2019). The results Nijgh & Veljkovic (2020, p. 494) found showed the need for significantly oversized holes with a nominal hole clearance varying between $12{,}7\ mm$ and $22{,}6\ mm$.

When comparing the required nominal hole clearances given by Nijgh & Veljkovic (2020) to those documented in EN 1090-2 it shows that these larger dimensions have yet to be formally included in the Eurocodes. A novel use of long open slotted holes that exceeded the dimensions given in EN 1090-2 was proposed by Husson (2008, p. 141), a sketch of which is shown in Figure 2.6. Herein long open slotted holes were used in HSFG connections to the benefit of wind tower construction. These novel connections were compared to similar connections with normal holes. The results showed a slight reduction of 4% in slip resistance when compared to the normal holed connection. This novel connection was further explored by Heistermann (2011) who placed the focus on possible bolt types to be used and the loss of preload in this connection. Further research on this proposed connection was conducted by Heistermann et al. (2013, p. 233). The design of slip resistant joints in both the Eurocodes and American design codes were reviewed and the viability of their application on connections with long open slotted holes was tested. The test data for connections with long open slotted holes showed a small increase of $1{,}5\%$ in preload loss over connections with normal holes during the first 12 hours. The average friction coefficient suffered a reduction of about 5% which was far less than the reduction factors used in the design codes. Most significant was the conclusion that the use of long open slotted holes had a smaller impact than several other factors in joint design, such as the type of joint, the bolt size and the coating used. A more recent study on friction connections in slotted holes was conducted by Dörre et al. (2022, p. 153-154) wherein a number of interesting conclusions were found. Of note were the reduced slip resistance in HSFG connections with slotted holes and the lack of influence that eccentric bolt placement in the hole had on the load-bearing capacity of the connection. A point that was of particular interest to this thesis was the conclusion that the reduction in slip resistance due to a slotted hole could be completely negated by placing a cover plate over the hole to increase the area of interaction.

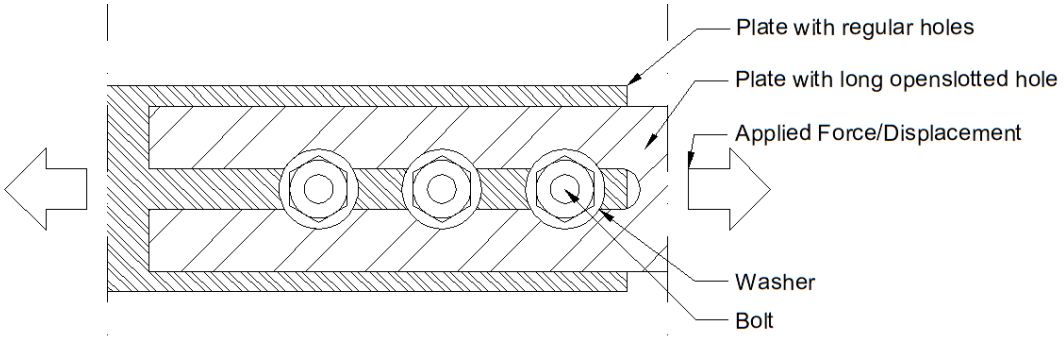

Figure 2.6 - Principle sketch of a connection with a long open slotted hole

2.3 CONCLUSION

A number of conclusions can be drawn from the existing literature. Further development of demountable shear connectors is currently limited by the small deviations allowed for both connector and hole placement. Oversized holes are proposed to compensate for this, but such holes diminish stiffness and composite action of the deck. The currently preferred solution for this problem is the use of resin injected bolts, rather than HSFG bolted connections. Resin injected bolts exhibit inferior performance under fatigue loading and require more time on site during construction when compared to HSFG bolted connections. Novel variations of resin based injection materials have been proposed which exhibit superior mechanical behaviour over regular resin injection material. These still require more time on site during construction and produce extra waste during deconstruction.

While oversized holes are defined in EN 1090-2, the required nominal hole clearance to meet the tolerance requirements exceeds the dimensions documented. The lack of research on such significantly oversized holes shows a gap in the current knowledge on the subject. A related subject which has received more attention in recent years is the use of slotted holes. Although of interest to give an initial idea on the behaviour of significantly oversized holes, it also shows the need for test results in such specific cases as the design codes are lacking in these situations. With this knowledge both the reason for this research subject and the gap to be filled could be defined.

The use of significantly oversized holes in demountable shear connectors is required for further progress in their development. Where resin injected bolts are a solution, the use of HSFG bolted connections would provide a shorter construction time and less waste when reused. Due to the lack of research data on such significantly oversized holes in HSFG bolted connections, their implementation is limited. Testing the viability of such connections could be the start of development progress on this method and eventual implementation in the future.

3 CONNECTION DESIGN

3.1 PROPOSED CONNECTION

Design of the proposed connection started with a principle connection. This connection could be described as a central plate with a significantly oversized hole and two outer plates with normal bolt holes as seen in Figure 3.1a. This design was the most basic version of a double lap joint that included a significantly oversized hole. A single lap connection was the next step to better simulate the nature of a demountable shear connector. This design incorporated a single cover plate as seen in Figure 3.1b. To decrease the number of parts that had to be replaced each test and further simulate the use in demountable shear connectors, the choice was made to implement extra cover plates in both designs as seen in Figure 3.1c and d. This removed the need to replace multiple large plates each test due to abrasion of the faying surfaces. The choice was made to use simple cover plates instead of large disc springs. The use of disc springs would lower the required thickness of the cover elements, but the difficulty of acquiring custom disc springs prohibited their use for this thesis. If used on a larger scale, they would be preferred over cover plates due to the lower thickness and the ability to prevent moisture from infiltrating the joint. The previous two designs were combined into the final design seen in Figure 3.1e for two major reasons. Firstly, the single lap design was not possible due to the limitations of the cyclic loading machine available. Secondly, the time limitation on the thesis made it preferable to increase the amount of test data collected per test. This final design addressed both problems: it approached the behaviour of a single lap joint more than a regular double lap joint and it provided double the test data compared to design c.

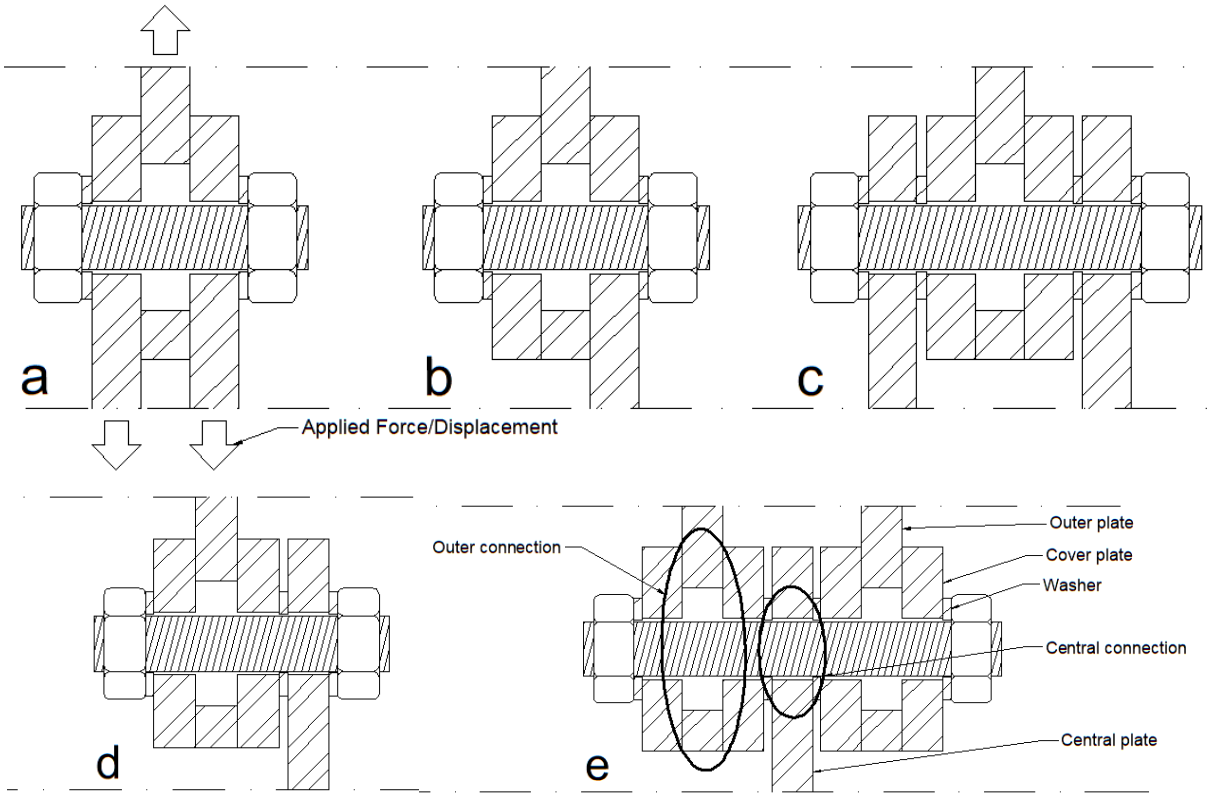

Figure 3.1 - Connection designs: a) Original double lap design; b) Original single lap design; c) Second double lap design; d) second single lap design; e) Final design

The next step was the choice of materials and parts that would be predefined constants. The steel grade used for the plates would be S355, mirroring the high strength steel used in steel bridges. The chosen bolt type of M27 was chosen based on related research on the use of prefab FRP bridge decks being conducted concurrently with this thesis. EN 1993-1-8 requires the use of either grade 8.8 or 10.9 bolts when preloaded in a slip resistant connection. This design code additionally stipulates slip resistance at ULS when oversized holes are used. The choice was made to use grade 10.9 bolts due to their higher preload capacity and use in related research. The appropriate coating of the plates was based on questions answered by Rijkswaterstaat and Akzonobel. Both noted that Interzinc22, an inorganic zinc rich silicate primer, is a common coating used for steel parts in bridge construction. The plates were coated in a $60\ \mu m$ thick layer of Interzinc22. The last constant was the use of disc springs on the outside of the connection. These were chosen to represent the use of larger disc springs instead of cover plates if the connection were to be used in practice. They would additionally provide a more constant preload in the bolt and would reduce self-loosening of the bolt during the cyclic tests as a consequence of loss of preload in the bolt. Based on DIN 6796, these M27 disc springs are flattened at a force of $230\ kN$ and provide appropriate resistance at differing amounts of deformation.

With these constants known and the general design of the connection completed, the next step could be taken. The nominal hole clearance in the design was based on the results found by Nijgh & Veljkovic (2020). The choice was made to define the hole diameter of the significantly oversized holes as roughly double the bolt diameter. The thought process behind this was that if no significant problems occurred in connections with such oversized holes, connections with a lower nominal hole clearance could be assumed to be also possible without problems. Based on this method the hole diameter was set at $60\ mm$ for M27 bolts, resulting in a nominal hole clearance of $33\ mm$. With the hole diameter defined, the initial dimensions of the plates could be determined. Both the inner and outer plates were initially set at a width of $100\ mm$ based on the flange width of larger steel girder types. The cover plates were then defined as $100\ mm$ by $100\ mm$ plates to keep symmetry and provide ease of assembly. The width of the outer plates was later increased to $140\ mm$ to provide space for the attachment of measuring equipment.

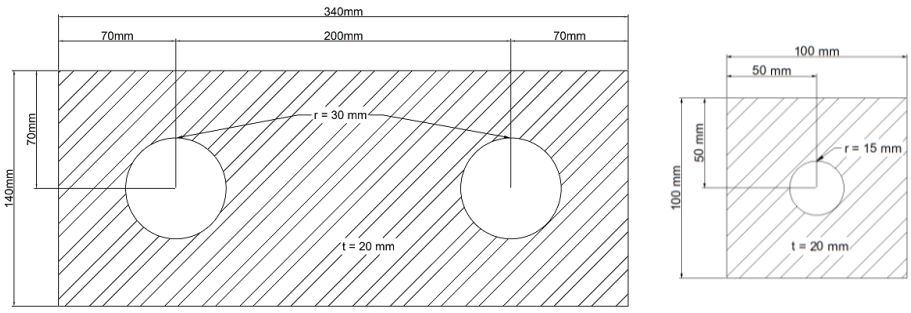

Figure 3.2 - Left) Outer plate; Right) Cover plate

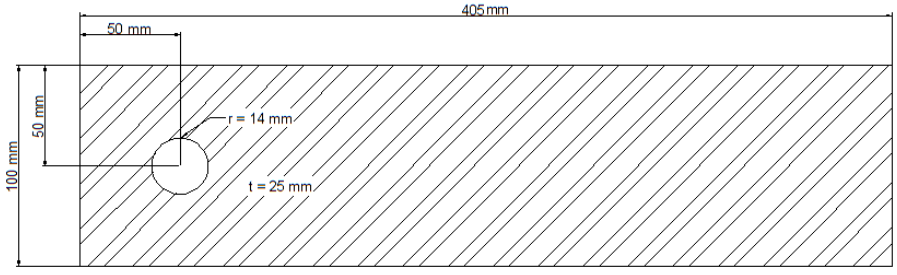

Figure 3.3 - Central plate

Before further dimensions could be defined, the applied loads needed to be known. These would depend on the method of loading during testing. The connection would be loaded both statically and cyclically. The static tests consisted of loading until the slip load was reached. For this test it was important for full slip to occur before failure in other parts such as shear failure of the bolt. The first step was the calculation of the applied preload of the bolt. The parts were designed based on the design preload given in EN 1993-1-8 for the bolt grade used. When using this preload, the plate thicknesses would be designed for the highest possible slip resistance in the connection, which in turn allowed for all lower slip resistances to be used if needed. The resulting preload for the bolts was calculated to be $321{,}3\ kN$. Based on this preload the total slip resistance of the outer connections, consisting of the interactions between the cover plates and the outer plates, was calculated to be $323{,}7\ kN$ which when halved resulted in $161{,}8\ kN$ per connection. The slip resistance in the central connection, consisting of the interactions between the inner washers and the central plate, was calculated as a double lap friction connection and resulted in a slip resistance of $190{,}4\ kN$. This meant that slip would occur in the central connection before the outer connections. As such, both the shear resistance of the bolt and the bearing resistance of the central plate needed to be larger than this value. A thickness of $25\ mm$ was used for the central plate, since this was the maximum thickness that the clamps of the cyclic loading machine could handle. With this the shear resistance of the bolt and the bearing resistance of the central plate were $183{,}6\ kN$ and $396{,}9\ kN$ respectively. The maximum shear force that the bolt had to bear was the slip resistance of a single outer connection. Comparing the results showed that the shear resistance of the bolt of $183{,}6\ kN$ was larger than the slip resistance of the outer connection of $161{,}8\ kN$. The bearing resistance of the central plate of $396{,}9\ kN$ also exceeded the total slip of the outer connections of $323{,}7\ kN$. Both connections had some breathing room in case the slip resistances were larger than expected (see appendix A for calculations).

The cyclic loading of the connection could then be defined based on the chosen dimensions. A load range and a frequency were required to check the possibility of fatigue damage in the connection. In the interest of time and the scope of this thesis, a single frequency of $10\ Hz$ was chosen up to one million cycles per test. The loading range consisted of the highest positive and lowest forces applied to the connection and their difference. The applied loading range was based on the results found in the related work of Gribnau (2021, p. 67-68). In this work the fatigue loading of shear connectors was investigated for a hybrid steel-FRP bridge design. The external loads and spans used were based on calculations of the traffic loading of the approach bridge Nieuw Vossemeer, where the maximum fatigue shear force ranges occurred at the end supports of the bridge spans. The different force ranges were expressed in R-ratios. This value was equal to the highest force divided by the lowest force in the force range. According to the results, the highest force range of $62\ kN$ occurred at an R-ratio between -0,5 and 0 with an occurrence frequency of roughly 1 million cycles. It was noted that this force range could increase with the addition of extra spans to the bridge.

Based on this information the chosen force range for the tests would be $65\ kN$. This would closely resemble the collected load data. In addition, a negative R-ratio of -0,1 was chosen to comply with the results found by Gribnau (2021) and to place the focus on the larger loads. Using this R-ratio, a minimum and maximum force of respectively $-5\ kN$ and $+60\ kN$ were chosen. As two such connections would be loaded simultaneously, the central plate would bear double the load. This resulted in a force range of $130\ kN$ ranging from -10 kN to $+120\ kN$ being applied to the central plate. The maximum applied force of $120\ kN$ did not exceed the $190{,}4\ kN$ slip resistance of the central connection. Based on this it was not deemed necessary to check if the fatigue shear resistance of the bolt was sufficient. Using this force range, the fatigue resistances of the connections were

checked. The choice was made to make the outer plates $20\ mm$ thick for possible future experiments with different assemblies and higher load levels. Based on equations from EN 1993-1-9 both the central connection and the outer connections would suffer no fatigue damage when loaded by this force range (see appendix A for calculations).

The final dimension to be determined was the thickness of the cover plates. Deformation of the cover plates was a problem due to the large hole the plates needed to span and the high preload in the bolt. Different thicknesses of cover plates were tested using the Finite Element Model of chapter 4. This resulted in a thickness of $20\ mm$ to be chosen.

3.2 Control Connection and Regular Connection

In addition to the proposed connection, two more connections were designed. Both were based on the parts designed for the proposed connection. Both a control connection and a regular HSFG bolted connection were designed as seen in Figure 3.4. The control connection was nearly identical to the proposed connection with the hole diameter of the outer plates as the single difference as shown in Figure 3.5. The goal of this connection was to document the effects this single change could have on the slip behaviour and the loss of preload in the bolt. The regular connection served to compare the performance of the proposed novel connection to a connection that is proven and better documented.

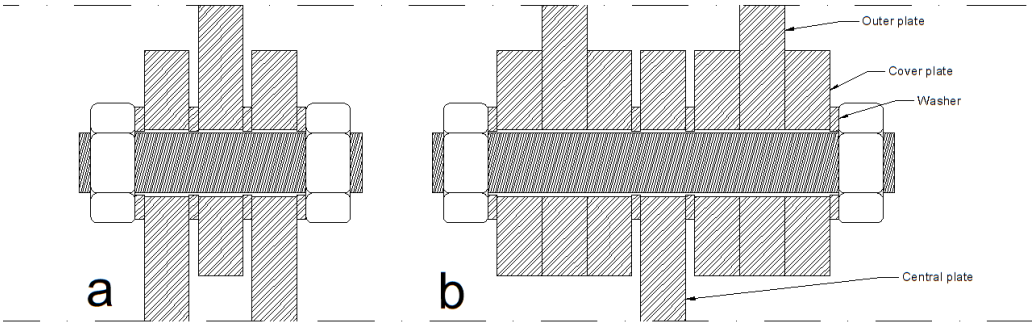

Figure 3.4 - Connection designs: a) Regular connection; b) Control connection

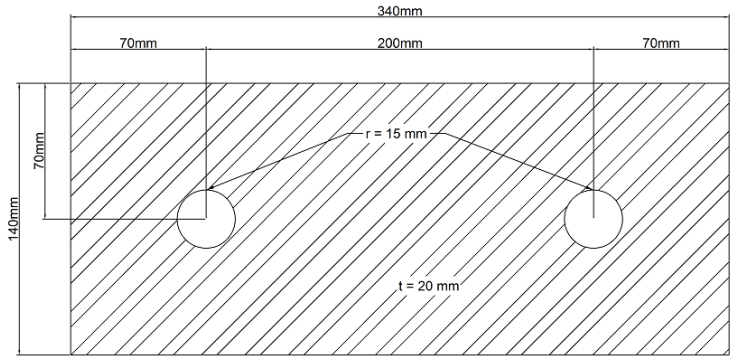

Figure 3.5 - Outer plate with regular holes

4 FINITE ELEMENT ANALYSIS

4.1 GEOMETRY, BOUNDARY CONDITIONS, MATERIALS AND INTERACTIONS

A Finite Element Model (FEM) was built to determine the required thickness of the cover plates and to conduct numerical analysis of the slip tests. Three models were built, one for each connection that would be tested under fatigue loading. A difference between the designs used for the experimental tests and the Finite Element Models is the lack of disc springs in the latter. Prior to this, three versions of the proposed connection were built with different thicknesses of the cover plates. The dimensions of the modelled parts were almost entirely the same as the designed parts in Chapter 3. The exceptions were the outer plates and central plate. The outer plates had a single hole rather than two and the central plate was shorter as shown in Figure 4.1. A second hole was not needed to simulate the behaviour of the connections and in this simulation there was no practical need for the central plate to be longer. The hexagonal bolt nuts used were standard M27 nuts of $22\ mm$ thick and the washers used had an outer diameter of $49\ mm$, an inner diameter of $28\ mm$ and a thickness of $4\ mm$. The bolt rod for the proposed and control models was $240\ mm$ long and the rod for the regular model was $160\ mm$ long.

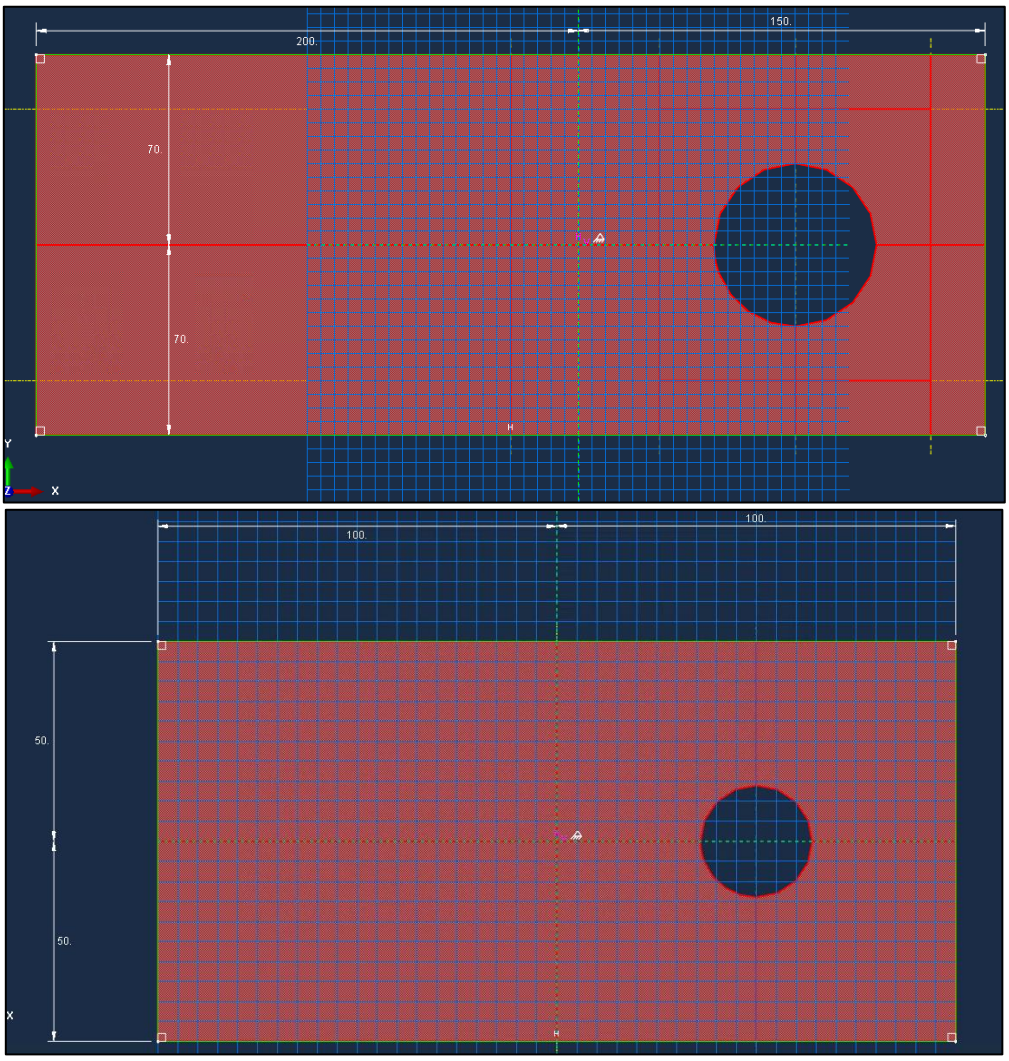

Figure 4.1 - Top) Dimensions outer plates; Bottom) Dimensions central plate

The proposed and control FEMs consisted of a single central plate, two outer plates, four cover plates, four washers, two bolt nuts and a single bolt rod as shown in Figure 4.2. Symmetry boundary conditions were applied to the ends of the outer plates which restricted displacement in x-direction and rotation in both y and z directions. The nodes at the end the of the central plate were coupled to a reference point (RP-1) and a positive displacement in x direction was applied to this reference point. This displacement was applied as a smooth step. The node displacements in x-direction of the outer plates and cover plates were measured at the red encircled meeting points between datum cell edges of the cover plates and outer plates. These were then subtracted to determine the slip of the outer and inner cover plates individually.

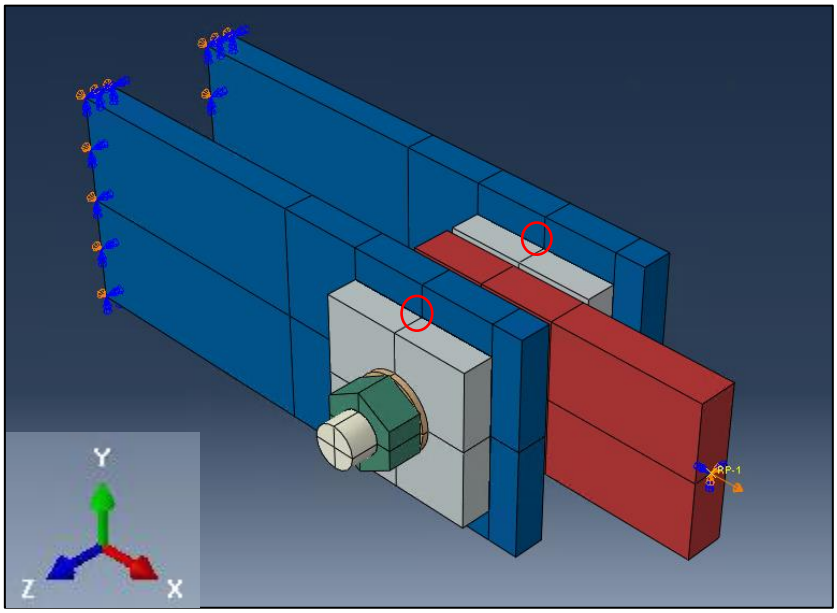

Figure 4.2 - Overview of proposed and control models

The regular connection, as shown in Figure 4.3, had the same boundary conditions. The slip was measured using the same method, but in this case between the washers and outer plates as marked by the red circle.

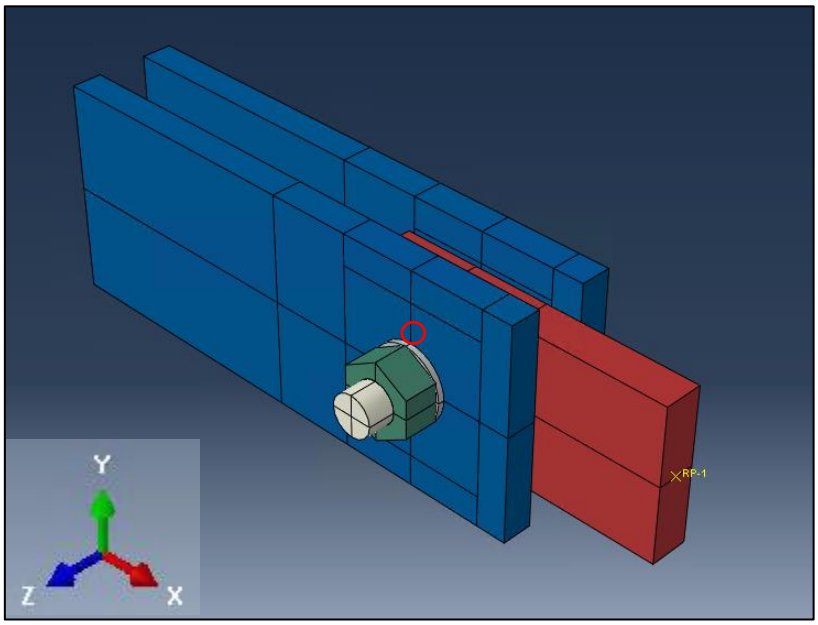

Figure 4.3 - Overview of regular model

The material used for the steel plates was S355. It was elastic isotropic with a Young's Modulus (E) of $200\ GPa$, a Poisson's ratio (ν) of $0{,}3$ and a mass density of $7{,}87\ g/cm^3$. The plastic yield was set to isotropic hardening and the yield stresses were set to $355\ N/mm^2$ at a plastic strain of 0 and $490\ N/mm^2$ at a plastic strain of $0{,}18$. The bolts were grade 10.9 bolts and elastic isotropic with an E-modulus of $210\ GPa$, a Poisson's ratio (ν) of $0{,}3$, a mass density of $7{,}87\ g/cm^3$ and a linear orthotropic thermal expansion coefficient of $0{,}0033$ in the axial direction. The thermal expansion coefficients in the other directions were set to $1E^{-12}$ to make them irrelevant. The plastic yield was set to isotropic hardening and the yield stresses were set to $900\ N/mm^2$ at a plastic strain of 0 and $1000\ N/mm^2$ at a plastic strain of $0{,}18$ for the ultimate tensile stress.

The method used to induce the preload in the bolt was a point of interest. Two ways to achieve the preload were possible, either by applying a load or by reducing the bolt length. The reduction of bolt length was chosen as it more closely represented the real method of tightening the bolt. This reduction of length was reached by applying a temperature field to the area of the bolt between the nuts as shown in Figure 4.4. The magnitude of this field was set to -1 and the reduction of length was then applied through a smooth step function with different amplitudes depending on the connection and applied preload as shown in Table 2. This would induce the intended clamping force to generate the friction force.

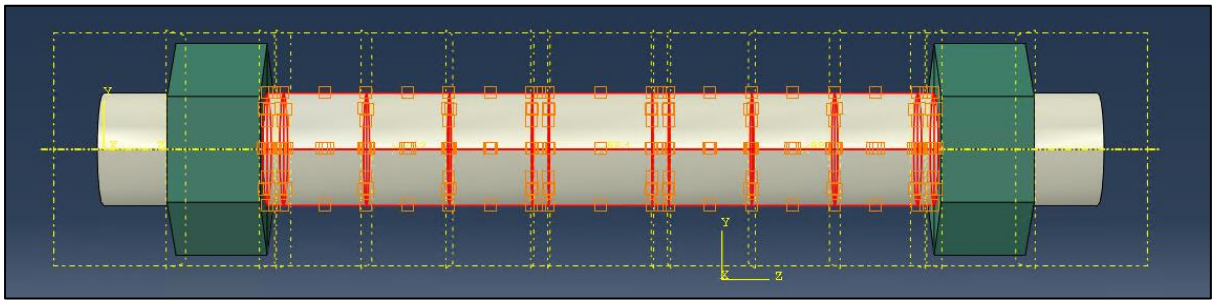

Figure 4.4 - Temperature field bolt shaft

Table 2 - Amplitudes for smooth step amplitude preloading of the bolt

Preload	Proposed ($10mm$)	Proposed ($15mm$)	Proposed ($20mm$)	Control	Regular
$200\ kN$	x	x	1	0,82	1
$321\ kN$	19,6	2,65	1,64	1,35	1,63

All contact surfaces in the models were given a friction coefficient of $0{,}4$ to take the coating into account based on EN 1993-1-8. This was implemented as an Isotropic Penalty formulation for the tangential behaviour and Hard contact for the normal behaviour. To allow for the bolt rod to induce a clamping force on the connection, the inside area of the nuts was connected to the bolt rod using tie constraints.

4.2 FINITE ELEMENT MESH

The program used was Abaqus due to its availability and the experience that members of the thesis committee already had with it. Eight-node linear solid elements (C3D8) were used for all parts. An overall mesh size of $5\ mm$ was used for all plates. The mesh of these plates was reduced to $1\ mm$ with curvature correction at the hole edges as shown in Figure 4.5 and Figure 4.6. The elements in between the outer edges and the hole edge were reduced to $1\ mm$ using a single bias. This reduction in mesh size increased the accuracy at the important interfaces. A side view of both outer plates is shown in Figure 4.7.

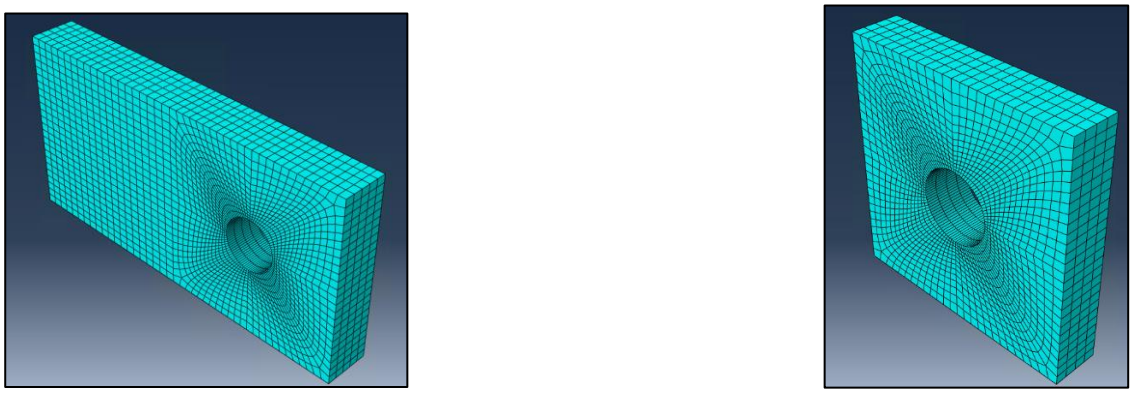

Figure 4.5 - Left) Mesh of central plate; Right) Mesh of cover plate

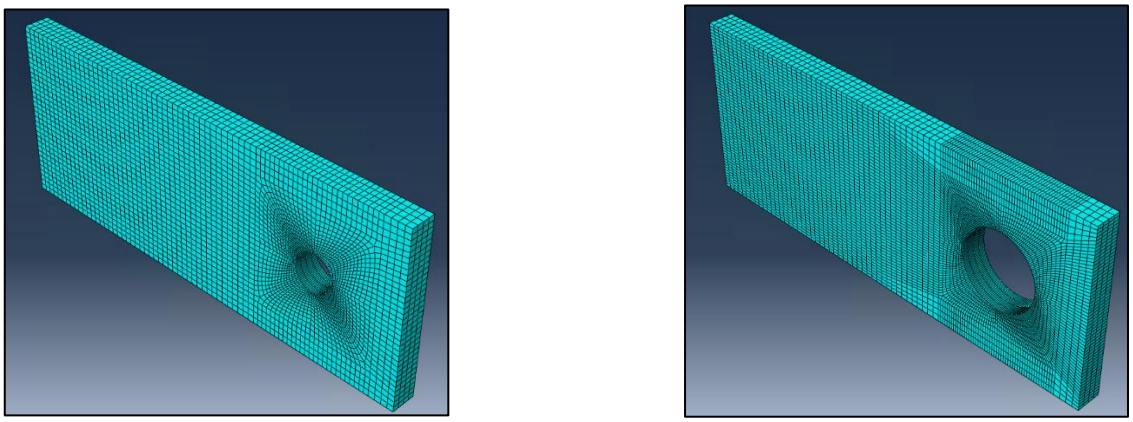

Figure 4.6 - Outer plate mesh: Left) Control/Regular; Right) Proposed

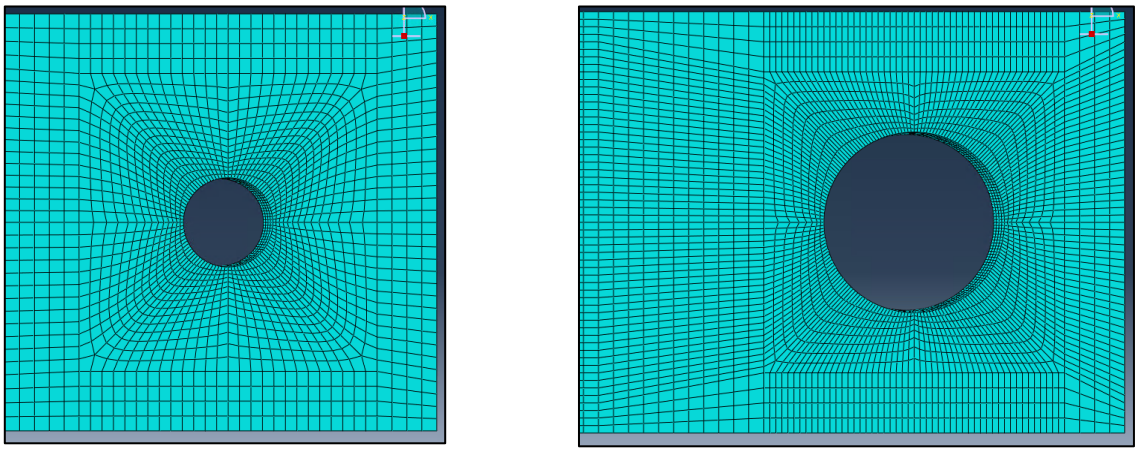

Figure 4.7 - Outer plate mesh: Left) Control/Regular; Right) Proposed

The meshes of the cover plates were mirrored on the central and outer plates. On the outer plates this was accomplished using partition cells as shown in Figure 4.8. These similar meshes were chosen to improve the friction interaction between these parts.

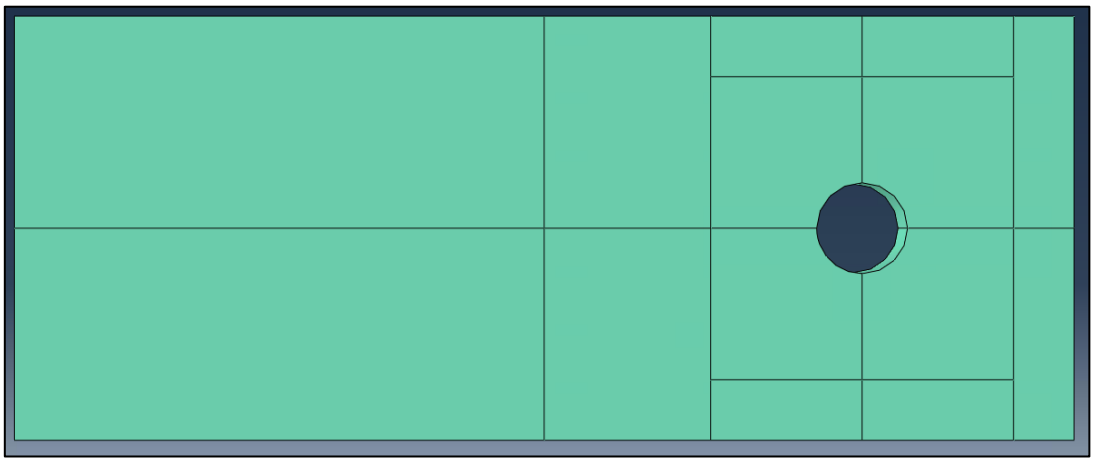

Figure 4.8 - Partition cells in outer plates.

The washers and nuts all used a mesh size of $3\ mm$ as shown in Figure 4.9. The mesh of the nuts was reduced to 2 mm with curvature correction at the hole edge to improve the quality. The washer did not need this. The bolt rod shown in Figure 4.10 used an overall mesh size of $3\ mm$ with curvature correction at the outer edges.

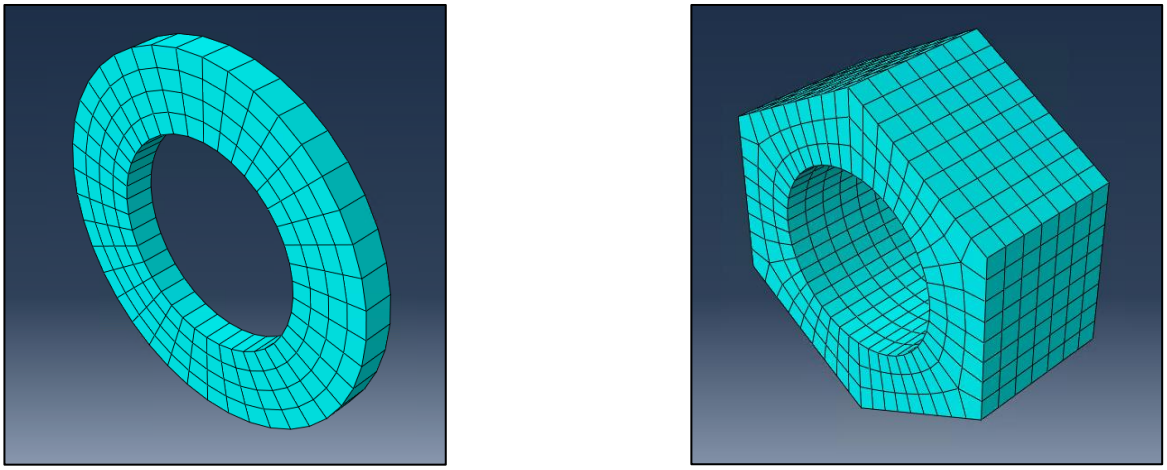

Figure 4.9 - Left) Washer mesh; Right) Bolt nut mesh

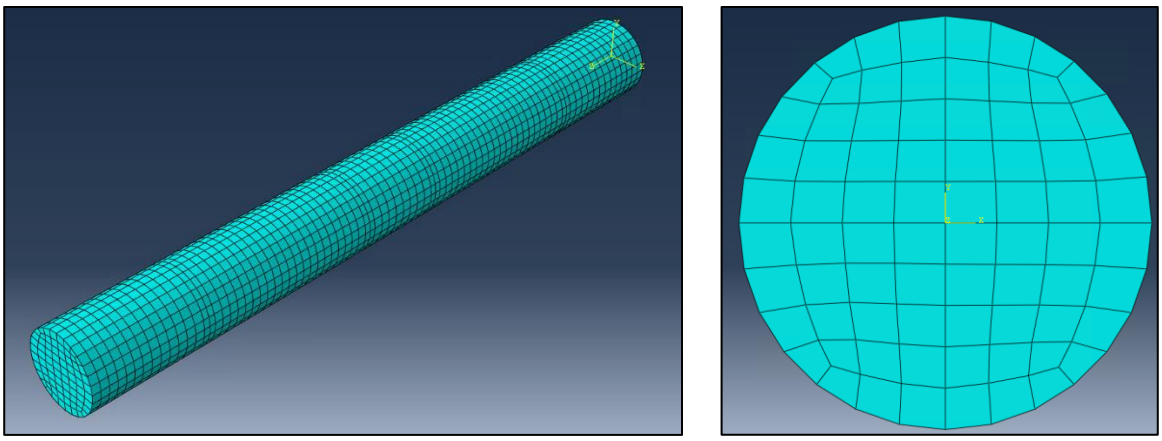

Figure 4.10 - Bolt rod mesh

4.3 ANALYSIS, LOADING STEPS AND QUASI-STATIC CONFIRMATION

The model was supposed to simulate friction interactions between plates. Of the solving methods, Abaqus/Explicit has shown a better performance of solving contact problems over the implicit method. This method was originally developed to model high-speed impacts, where inertia played a significant role. Due to this inertia effect, the time increment needed to be small to provide stable results. Consequently, the number of increments needed to be large, which translated in a long running time for the analysis. Due to their very nature quasi-static processes take a long time to progress, which is not economical to simulate. If these processes are accelerated too much, the simulation turns into a dynamic one rather than quasi-static. This results in the simulation of quasi-static processes being a balancing act between economical solving times and accurate results when Abaqus/Explicit is used (Massachusetts Institute of Technology, n.d.c).

To compensate for this shortcoming, mass scaling was used. To calculate the displacements per time step the Abaqus/Explicit solving method propagates forces that are out of equilibrium "*as stress waves between neighbouring elements while solving for a state of dynamic equilibrium*" (Massachusetts Institute of Technology, n.d.c). The speed of these waves c_d is dependent on the Young's Modulus E and the material density ρ of the material, and can be expressed in the equation $c_d = \sqrt{E/\rho}$ for linear elastic materials with a Poisson's ratio of zero. This results in a higher material stiffness having a higher wave speed (Massachusetts Institute of Technology, n.d.a). Mass scaling artificially increases the density of the material and in turn decreases the wave speed (Massachusetts Institute of Technology, n.d.b). If the minimum stable time increment is taken into account as expressed in $\Delta t = L_e/c_d$ where L_e is the characteristic element length, the benefits of mass scaling become clear (Massachusetts Institute of Technology, n.d.b). The lower wave speeds increase the minimum stable time increment which in turn reduces the number of steps needed to run an analysis.

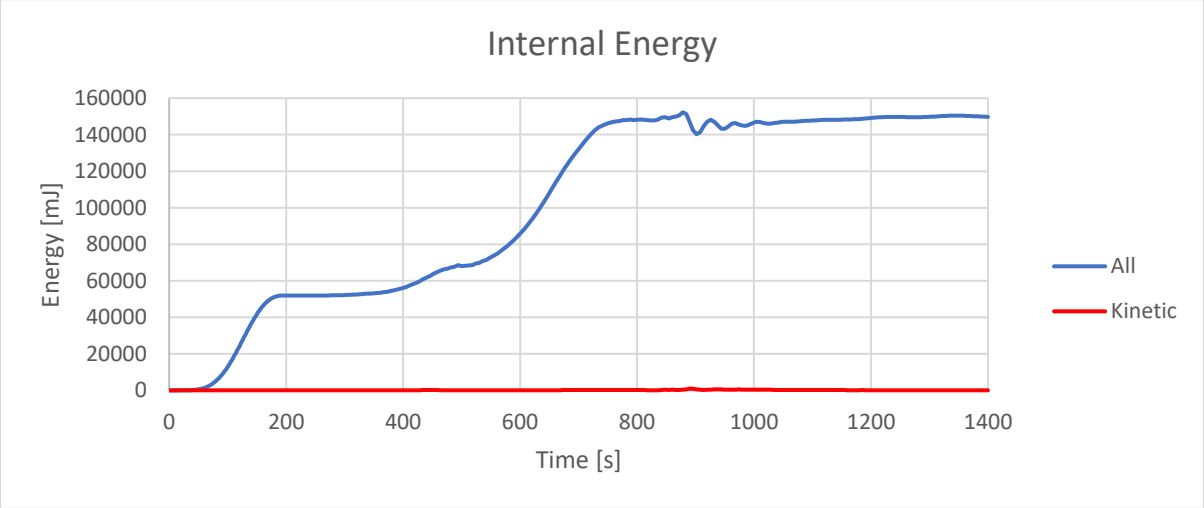

Figure 4.11 - Internal energy during Finite Element Analysis

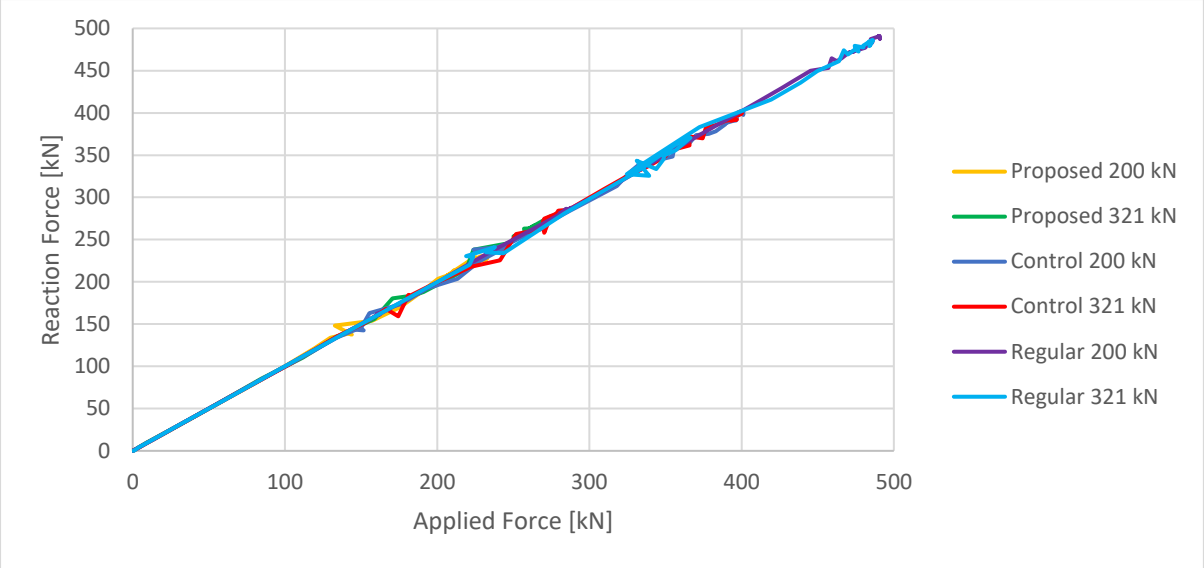

Figure 4.12 - Applied/Reaction force comparison during step 2

Each Finite Element Model was tested twice, once with a preload of $200\ kN$ as used during the fatigue experiments and once using a preload of $321\ kN$ based on EN 1993-1-8. The analysis consisted of two steps, a first preloading step and a second displacement step. During the first step the bolt rod was shortened and the preload clamping force was induced. This step was given a duration of 200 seconds with a target time increment of $0{,}01\ s$ for mass scaling. The second step had a duration of 1200 seconds during which the central plate was displaced by $5\ mm$. The target time increment for mass scaling during this step was $0{,}001\ s$. To confirm the analysis to be quasi-static, two tests were conducted. The kinetic energy in the model was compared to the total energy in the model to rule out dynamic behaviour. Secondly the applied force at the central plate was compared to the total reaction force at the ends of the outer plates to ensure that no waves or pulses affected the results. Both of these comparisons are plotted in Figure 4.11 and Figure 4.12. The graphs show that the kinetic energy is insignificant compared to the total energy and that the applied and reaction forces almost completely the same during the second step. At certain points small disturbances occur, their infrequent nature makes identifying the influence these disturbances have on the results easy. Their size is also small enough to not significantly influence the results.

4.4 Results and Analysis

4.4.1 Cover plate thickness

Finite Element Analysis of the preloading of the bolt was conducted with cover plates of $10\ mm$, $15\ mm$ and $20\ mm$ thick. The preload used in all three analysis was the design preload of $321\ kN$. The inside area of the bolt hole was used to measure the deflection of the cover plates. The deflections of the nodes, as shown in Figure 4.13, were measured and the average was used for the results. Large displacements of this area would negate the benefits of a friction connection and cause significant damage during cyclic loading due to the mechanical locking of the cover plates in the outer plate.

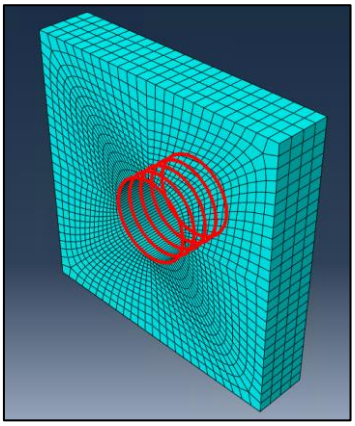

Figure 4.13 - Nodes used to measure deflection

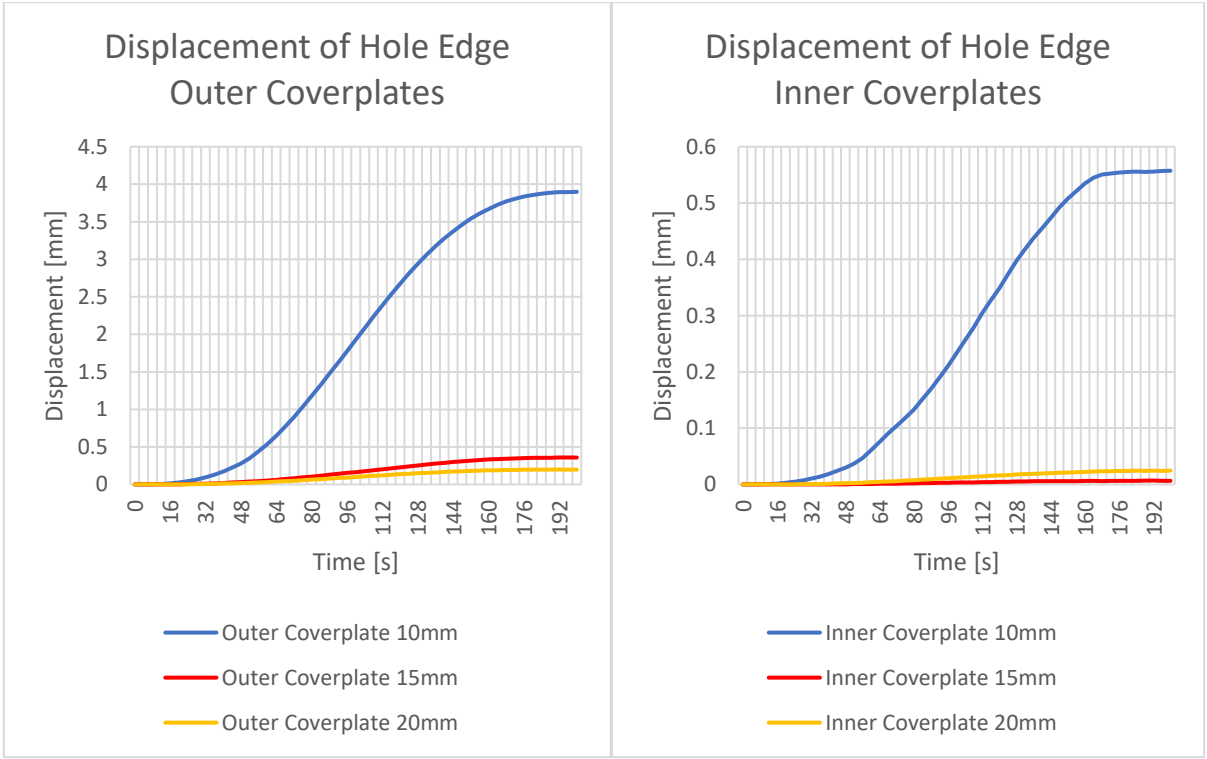

Figure 4.14 - Time-Displacement graphs of the cover plates during preloading

The graphs in Figure 4.14 show a significant reduction of displacement when comparing the $10\ mm$ thick plates to the $15\ mm$ and $20\ mm$ thick plates. The differences between $15\ mm$ and $20\ mm$ thick plates are significantly smaller. The difference in deflection of the inner cover plates of roughly $0{,}01\ mm$ to $0{,}02\ mm$ found between the $15\ mm$ and $20\ mm$ thick cover plates is small enough to not affect the results in a significant way. The difference between the $0{,}2\ mm$ and $0{,}4\ mm$ deflection of the outer cover plates found for respectively the $15\ mm$ and $20\ mm$ thick cover plates on the contrary could affect the results of the static FEA. Deflection of the outer cover plates could activate the resistance of these plates at an earlier moment in time during the proposed analysis than during the control analysis, falsely suggesting that friction resistance is present at that point.

The deformation of the cover plates is also shown visually in Figure 4.15. The large difference between the $10\ mm$ thick plates and the $15\ mm$ and $20\ mm$ thick plates is clear to see. The difference between the $15\ mm$ and $20\ mm$ thick plates is comparatively harder to discern.

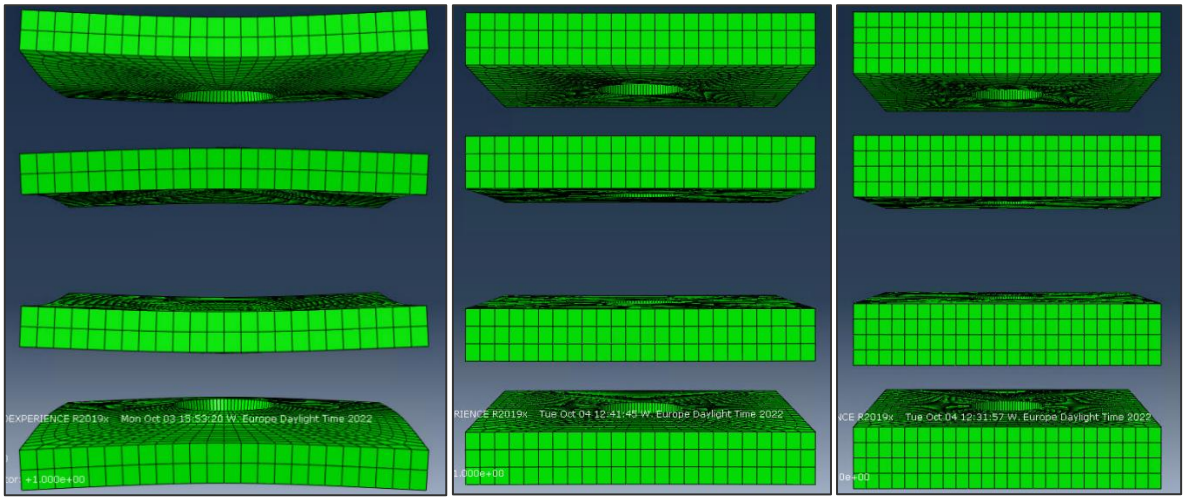

Figure 4.15 - Deflection of cover plates: Left) $10\ mm$*; Middle)* $15\ mm$*; Right)* $20\ mm$

Based on these results the thickness chosen was $20\ mm$. The $10\ mm$ thick plates exhibited intolerable deformation even at low preloads. Both the $15\ mm$ and $20\ mm$ thick plates showed tolerable deformation at all preload levels. Although the difference between the $15\ mm$ and $20\ mm$ thick plates was non-existent at low preloads, the smaller deformation of the $20\ mm$ plates at higher preloads gave a better guarantee of preserving the friction connection during the experiments and FEA.

4.4.2 Force-Displacement

Proposed connection

Both graphs in Figure 4.16 start with a similar course, where the central plate and inner washers are slipping relative to the inner cover plates. They split at roughly $0{,}25\ mm$ of slip where the slip resistance of this interface starts to be reached for the $200\ kN$ connection. Right after this point a dip is seen in the $200\ kN$ graph where the central plate comes in bearing contact with the bolt rod. This contact created a force wave during the analysis that is also seen in the graph comparing the applied and reaction forces. As such this dip will be interpreted as a plateau. After this point the inner and outer cover plates start slipping relatively to the outer plates until both cover plates are loaded in bearing. The bolt rod first makes contact with the inner cover plate before the outer cover plate due to the slight bending of the bolt rod. This occurs at roughly $1{,}5\ mm$ displacement and at this point the slip load of the outer connections is reached. The reaction force in the connections reduces afterwards as the final slip load is overcome and full head slip is reached. From this point the resisting force remains the same while the outer connections slip. The $321\ kN$ graph follows the same steps, but a higher load is required for each interface to start slipping resulting in an overall higher reaction force.

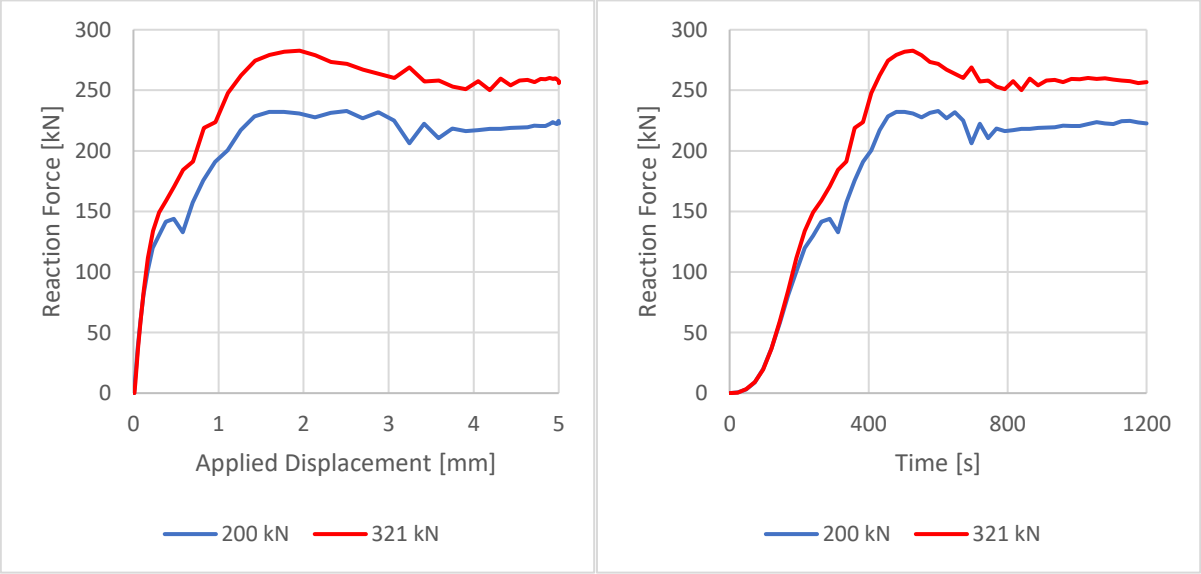

Figure 4.16 - Left) Proposed Force-Displacement graphs; Right) Proposed force graphs

Due to the early slip at $200\ kN$ preload, the bolt rod did not bend significantly and though the yield stress of $900\ N/mm^2$ of the bolt rod was reached, the ultimate tensile stress of $1000\ N/mm^2$ was not. The $321\ kN$ preloaded connection suffered more bending of the rod as shown in Figure 4.17 as a consequence of the higher slip resistance, but also did not reach the ultimate tensile stress in the bolt rod (See Appendix C for the full images).

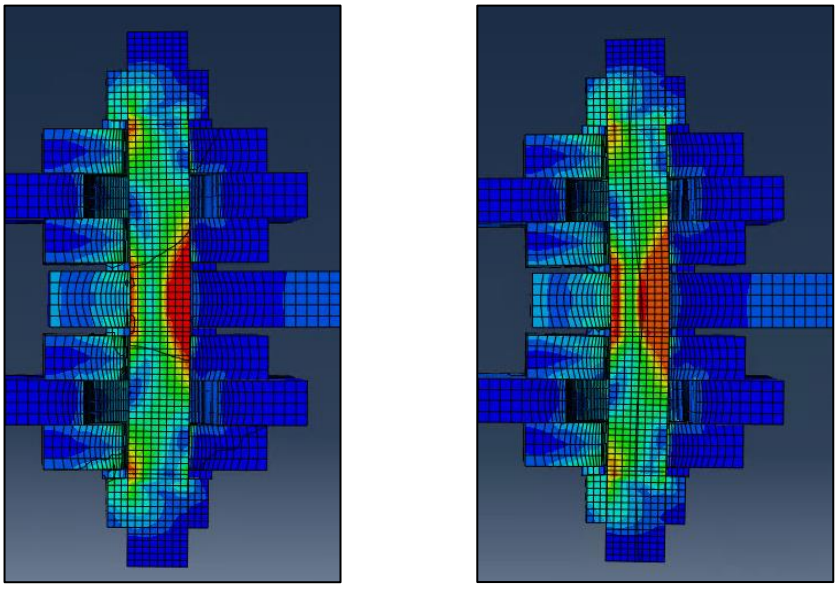

Figure 4.17 - Deformed proposed connections: Left) $200\ kN$ *preload; Right)* $321\ kN$ *preload*

Control connection

The initial steps of the control connections followed the same principles as the proposed connections. The central plate and inner washers would first slip relative to the inner cover plates until the inner cover plates started to slip as shown in the graphs of Figure 4.18. The smaller hole clearance of the outer plates make is so that rather than continually slipping, the outer plates are loaded in bearing at roughly $3\ mm$ of displacement.

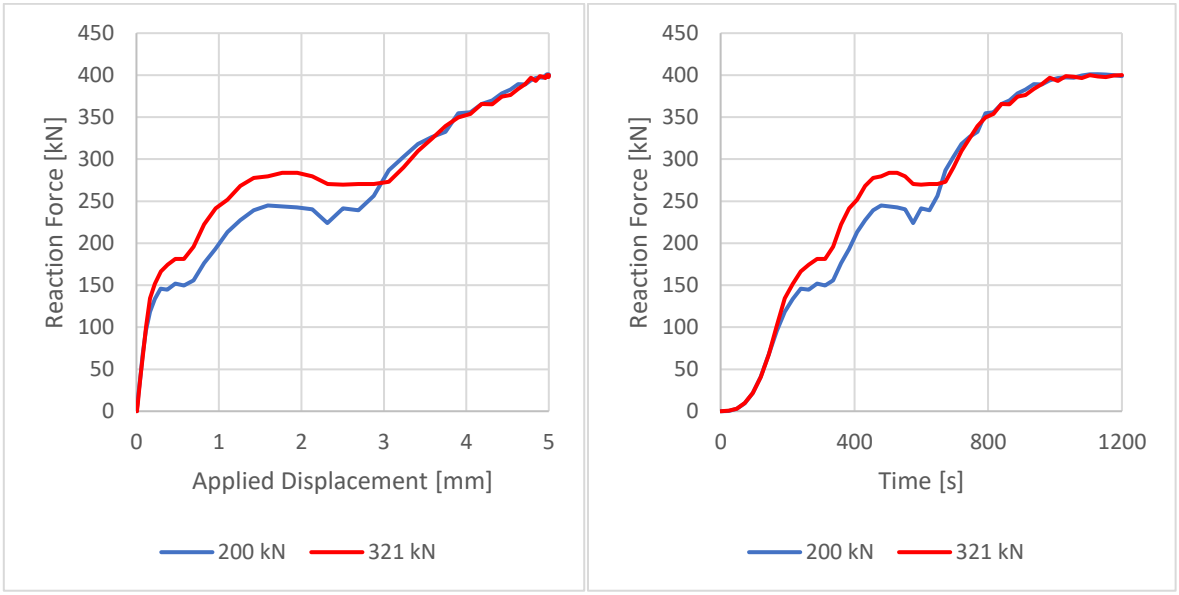

Figure 4.18 - Left) Control Force-Displacement graphs; Right) Control force graphs

After the outer plates are loaded in their bearing the full connection functions as a bearing connection. From this point on the plotted resistance is a result of bolt rod bending, as seen in Figure 4.19, as the ultimate tensile stress of the bolt rod is reached shortly after this point (See Appendix C for the full images). This is also gleamed from the graphs after $3\ mm$ of displacement, both graphs become almost identical as the preload no longer plays a role.

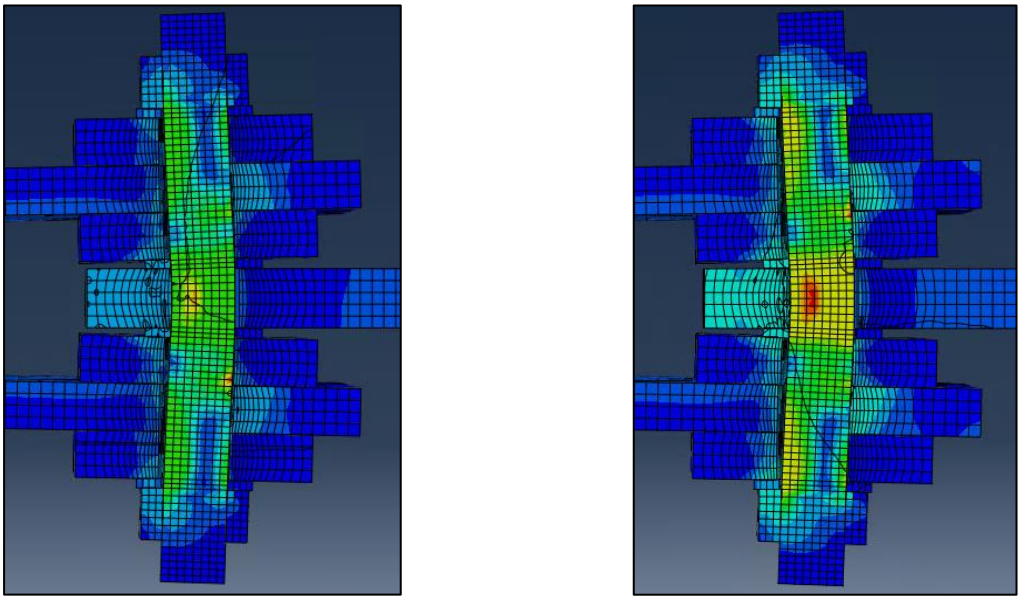

Figure 4.19 - Deformed control connections: Left) $200\ kN$ preload; Right) $321\ kN$ preload

Regular connection

The regular connections gave far clearer graphs as shown in Figure 4.20. The clear steps at both preloads show the force building up to the slip load of the weakest interface. The first plateau is the slipping of the central plate relative to the inner washers and the second plateau is the slipping of the central plate and all washers relative to the outer plates. At roughly $2{,}5\ mm$ the outer plates are loaded in bearing which is shown as an increase towards the third and final plateau. From this point onward the preload no longer plays a role. The final plateau is the consequence of bearing failure of the central plate. Due to the shorter clamping length, bending of the bolt rod played a smaller role in this connection as shown in Figure 4.21 (See Appendix C for the full images). The ultimate tensile stress of $1000\ N/mm^2$ in the bolt rod was not reached. The decline after a plateau is reached is far more profound in in the $321\ kN$ graphs due to the larger slip resistance present, which needs to be overcome for full head slip to occur.

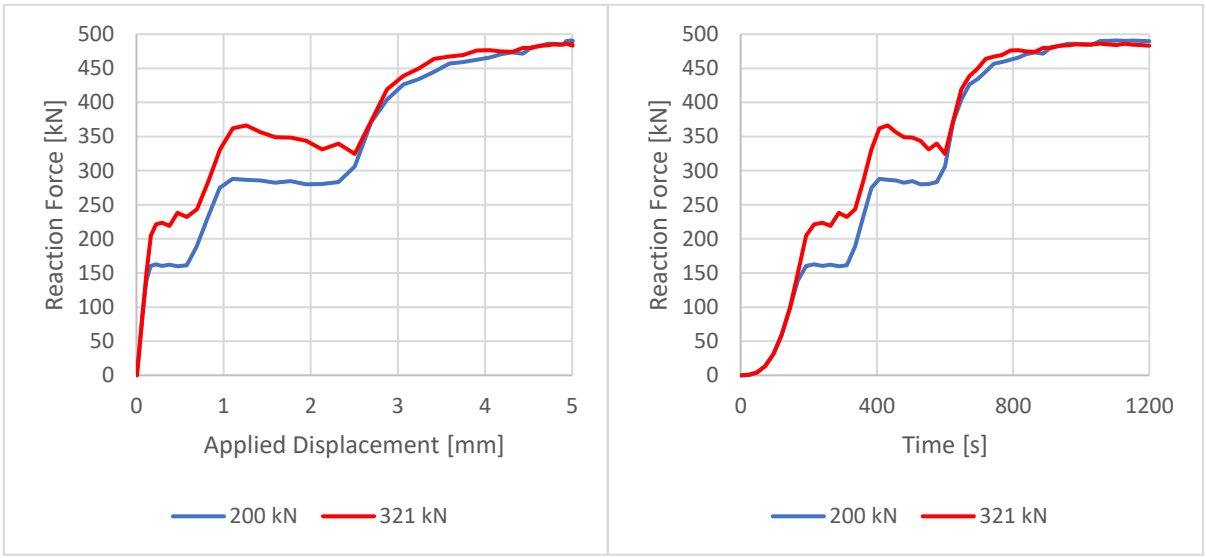

Figure 4.20 - Left) Regular Force-Displacement graphs; Right) Regular force graphs

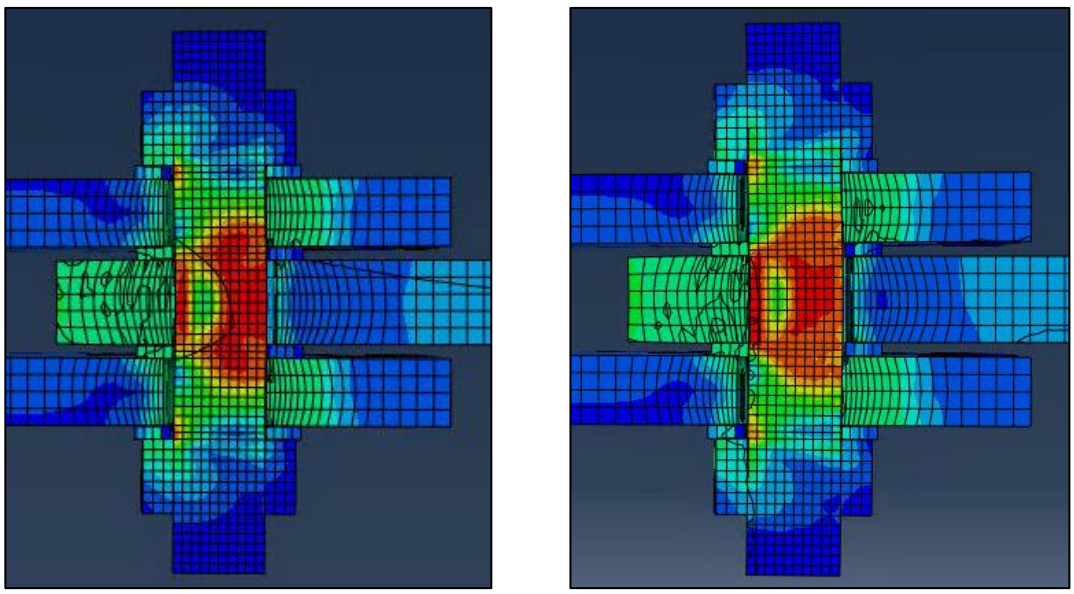

Figure 4.21 - Deformed regular connections: Left) $200\ kN$ preload; Right) $321\ kN$ preload

4.4.3 Slip and Slip Resistance

Proposed connection

The slip graphs of Figure 4.22 confirm the different slips of the inner and outer cover plates. It took 200 seconds before the slip load of the inner cover plates was reached and 400 seconds before the outer cover plates started slipping. This was due to the displacement being applied at the central plate and the inner cover plates in turn being subjected to displacements and forces before the outer cover plates. The initial slight slope of the graphs is a consequence of the cover plates slipping under influence of the friction the washers exert on them. The inflection point in each graph where the slip starts increasing more steeply is the point where the cover plates are loaded in bearing. This increased the maximum force that could be transferred between the central plate and cover plates. It is also the moment when the friction interface of the outer connections becomes the point of least resistance.

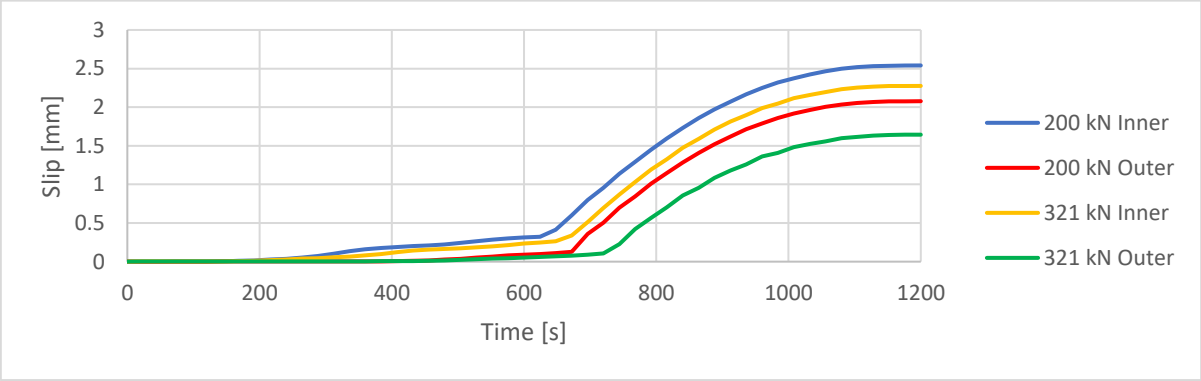

Figure 4.22 - Slip graphs proposed connection

The Force-Slip graphs of Figure 4.23 show that due to the force being focussed on the inner cover plates at the start, a lower applied force is needed for them to start slipping compared to the outer cover plates. The force needed for the outer cover plates to start slipping is the total slip resistance of both the inner and outer cover plates. This is also shown by the similar peaks of the inner and outer plates being separated by roughly $0{,}25\ mm$ and $0{,}20\ mm$ of slip for the $200\ kN$ and $321\ kN$ graphs respectively. This is the difference in slip between the inner and outer cover plates found at the inflection points of the slip graphs in Figure 4.22. After these peaks where the slip loads are reached, full head slip starts and the resistance of each connection reduces as both the inner and outer cover plates end up at the same friction resistance.

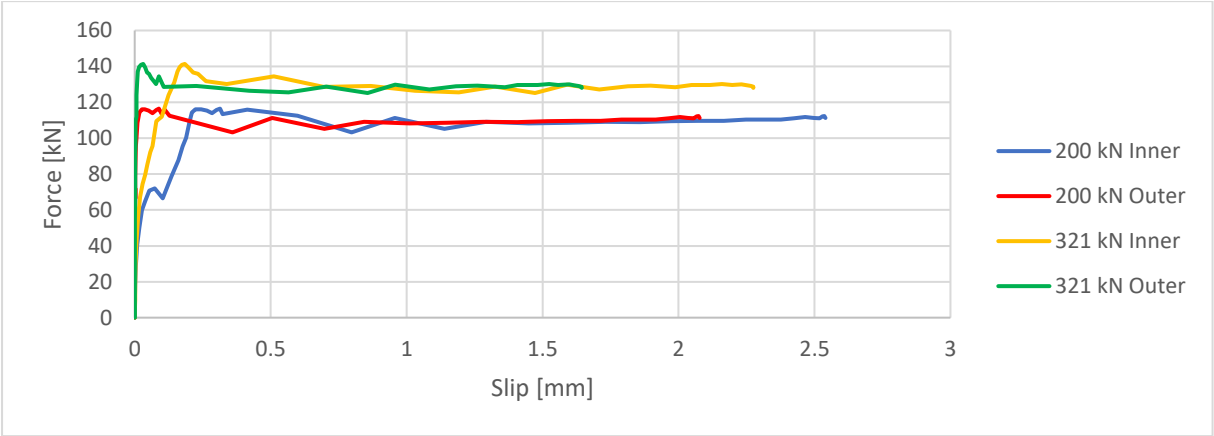

Figure 4.23 - Force-Slip graphs proposed connection; Force displayed is half of the applied force in the central plate

Control connection

The slip graphs of the control connection in Figure 4.24 show a large difference between in the inner and outer cover plates. The inner cover plates start slipping at 200 seconds and the outer cover plates at 400 seconds. Both due to the friction exerted on them by the washers. The normal sized holes in the outer plates cause bearing interaction to occur at roughly 640 and 670 seconds for the $200\ kN$ and $321\ kN$ connections respectively as shown in Figure 4.25. This prevents bearing interaction from occurring in the cover plates. The outer cover plates stop slipping after this point as they are no longer loaded due to bending of the bolt rod. The slip of the inner cover plates measured from this point on is a result of the increased friction force exerted by the inner washers due to compression as a result of bending of the bolt rod. This can be seen in the fully deformed state of the models as shown in Figure 4.26 where stress concentrations are present in the encircled parts of the inner washers.

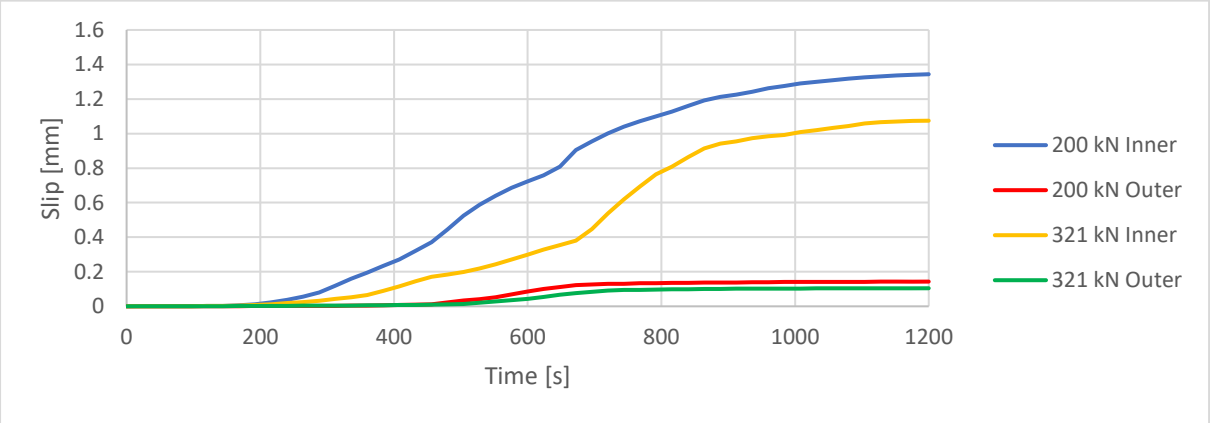

Figure 4.24 - Slip graphs control connection

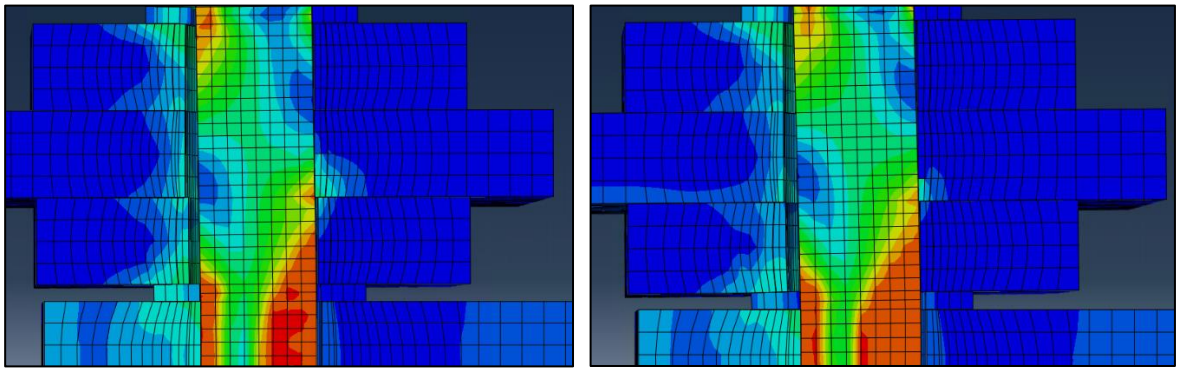

Figure 4.25 - Point where bearing interaction outer plates starts: Left) $200\ kN$; Right) $321\ kN$.

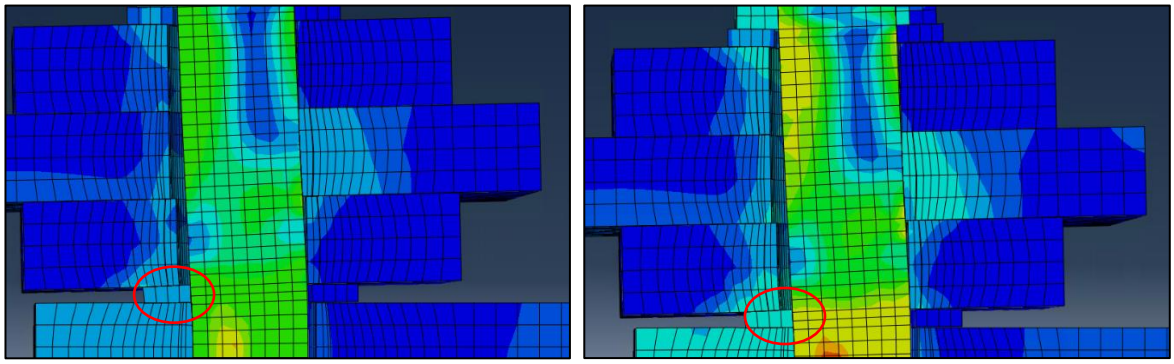

Figure 4.26 - Deformed state outer connection: Left) $200\ kN$; Right) $321\ kN$

The Force-Slip graphs of Figure 4.27 echo the observations of the slip graphs. The outer cover plates play no role after roughly $0{,}1\ mm$ slip and the force plotted for the inner cover plates after $0{,}4\ mm$ and $0{,}7\ mm$ of slip for the $200\ kN$ and $321\ kN$ connections respectively is a consequence of the bending of the bolt rod.

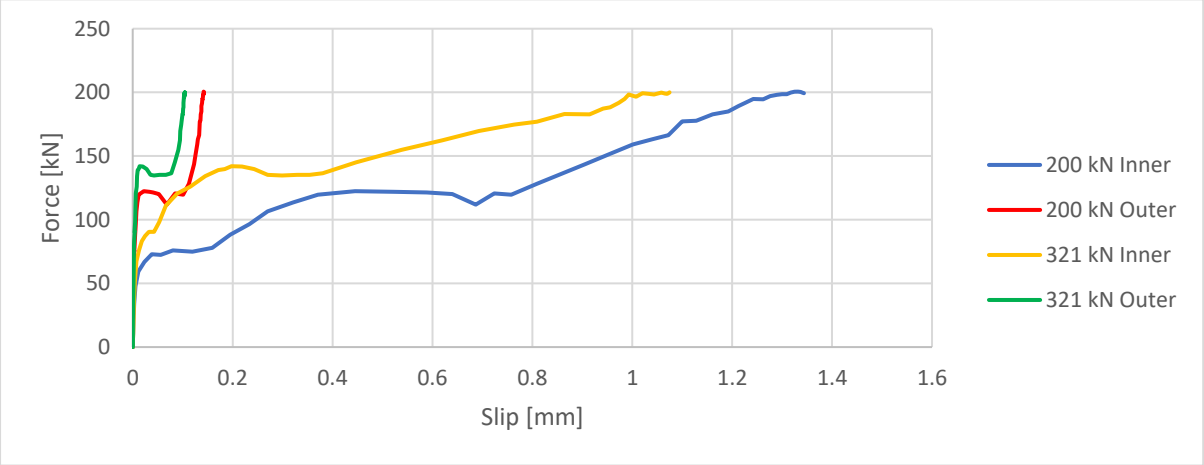

Figure 4.27 - Force-Slip graphs control connection; Force displayed is half of the applied force in the central plate

Regular connection

The graphs of Figure 4.28 show the same slip starting points for the washers as the cover plates of the other two connections at 200 second and 400 seconds for the inner and outer washers respectively. Both washers slip at a similar rate until 600 seconds where the outer plates are loaded in bearing. The outer washers stop slipping and the inner washers only slip as much as the bending of the bolt allows for. The shorter clamping length decreased the bending and in turn the difference in slip behaviour between the outer and inner washers, as shown in Figure 4.29.

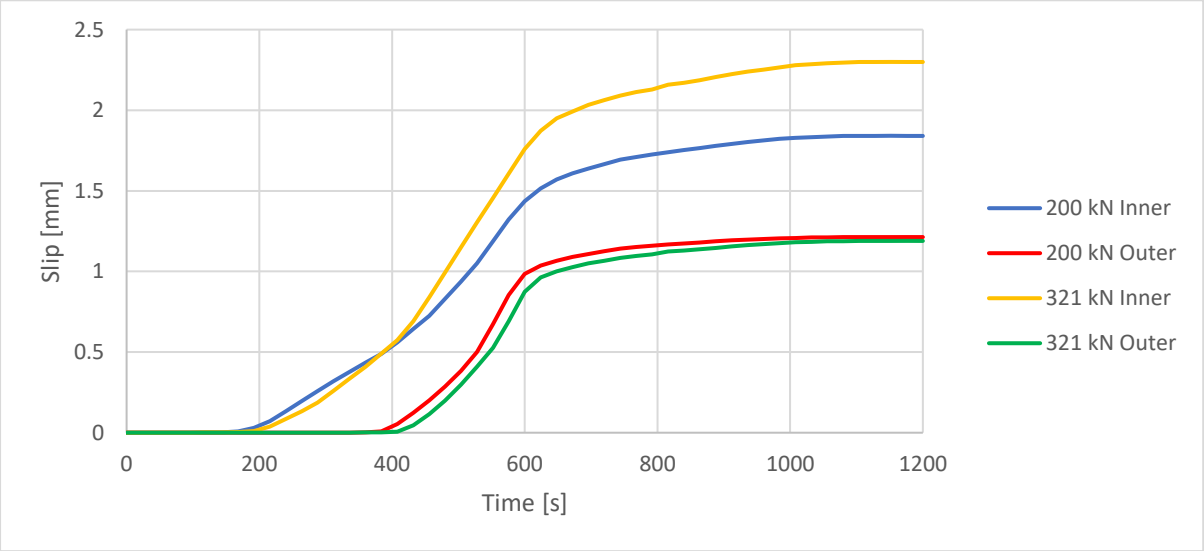

Figure 4.28 - Slip graphs regular connection

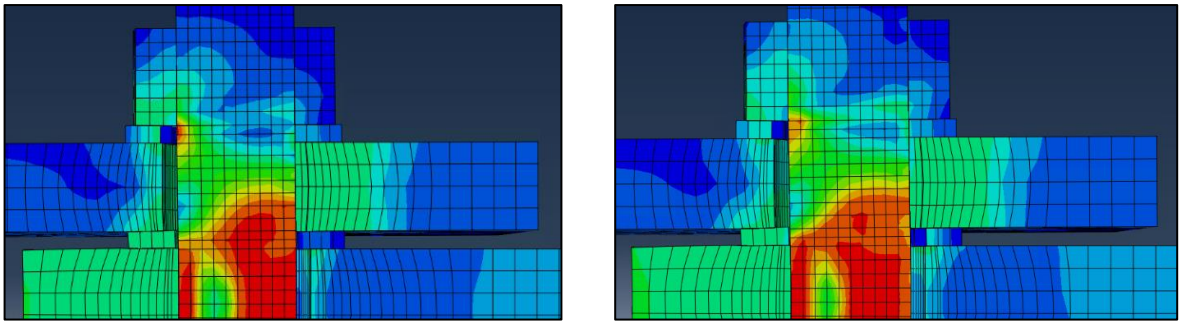

Figure 4.29 - Deformed state outer connection: Left) 200 kN; Right) 321 kN

The Force-Slip graphs of the regular connection in Figure 4.30 show the different steps clearer than the other two connections due to the lower number of interfaces and shorter clamping length. Each plateau signifies the maximum force that can be transferred between the central plate and outer plates. The first plateau is the slip load of the interface between the inner washer and central plate. This plateau ends at the point where the central plate is loaded in bearing, which allows for a higher force to be transferred between the central plate and the bolt. Directly after, the friction between the outer plate and outer washer is activated. The start of the second plateau is the point where the full slip load of the outer connection is reached. This can also be seen in the graph as the outer washers starting to slip at this force. This plateau ends once the outer plate is loaded in bearing.

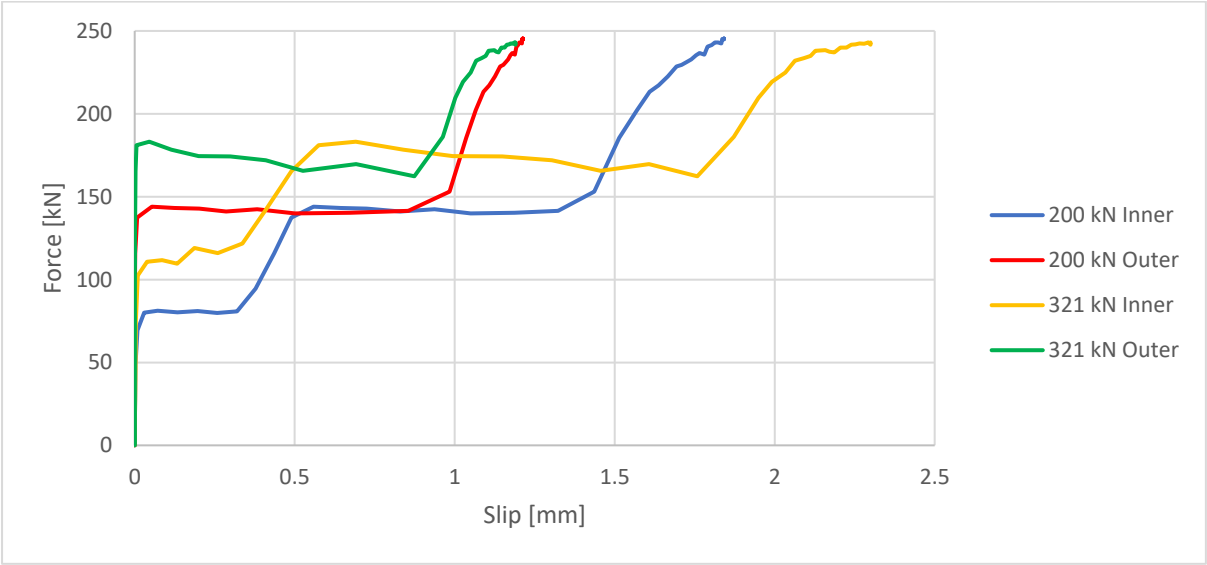

Figure 4.30 - Force-Slip graphs regular connection; Force displayed is half of the applied force in the central plate

4.5 Comparison and Conclusions

4.5.1 Force-Displacement and Stiffness

200 kN Preload

The Force-Displacement graphs of all three connections are plotted in Figure 4.31. The courses of the proposed and control graphs follow each other closely up to $2{,}5\ mm$ of applied displacement where the outer plates of the control connection are loaded in bearing. The graphs diverge at this point with the proposed graph continuing to slip in the outer connections with a constant reaction force. The reaction force of the control connection increased due to the bearing resistance of the central and outer plates and the bending of the bolt rod. The clear steps and plateaus found in the regular graph are obfuscated in the other two graphs by the larger number of interfaces and bending of the bolt rod due to the larger clamping length. Compared to the other two graphs, the regular connection shows an overall higher friction resistance force up to $2{,}5\ mm$ of applied displacement where the outer connections are loaded in bearing. The regular connection also performs better as a bearing connection than the control connection due to the shorter clamping length which does not allow the large amount of bending that the longer bold rod suffers.

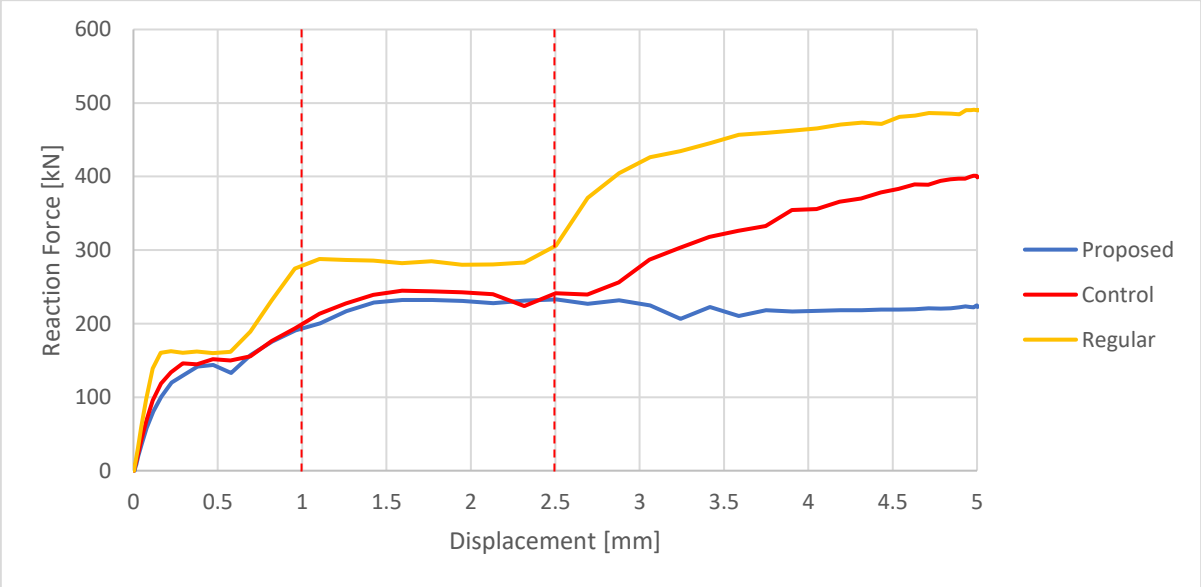

Figure 4.31 - Comparison of Force-Displacement graphs at 200 kN preload

In the interval between $1\,mm$ and $2{,}5\,mm$ displacement all three connections reached their maximum reaction forces prior to turning into full bearing connections. Figure 4.32 focusses on this interval, signified by the red dashed lines in Figure 4.31, to better visualize the differences between the graphs. The maximum reaction forces are $233\ kN$, $245\ kN$ and $288\ kN$ for the proposed, control and regular connections.

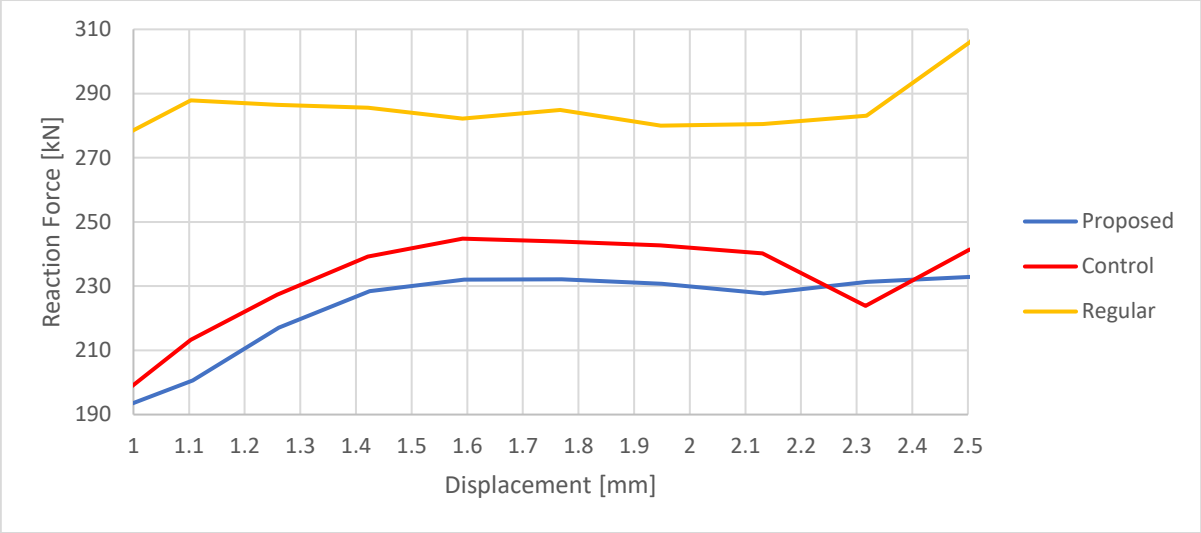

Figure 4.32 - Comparison of Force-Displacement graphs in the interval between $1\ mm$ and $2{,}5\ mm$ at $200\ kN$ preload

321 kN Preload

The Force-Displacement graphs of the connections with $321\ kN$ preload as shown in Figure 4.33 follow the same course as their respective $200\ kN$ graphs at higher reaction forces. The major difference is the overall higher value of the reaction forces. The differences between the proposed and control graphs are smaller, as a consequence of the higher preload reducing the influence of the difference in faying surface contact area.

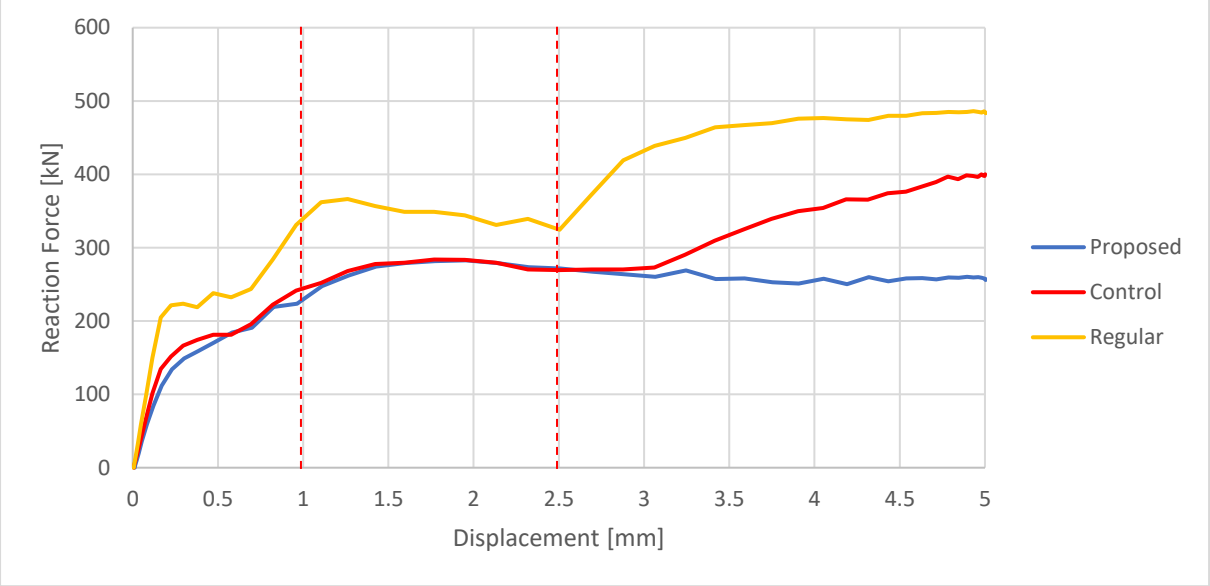

Figure 4.33 - Comparison of Force-Displacement graphs at $321\ kN$ preload

All three friction connections reached their maximum reaction force in the interval between $1\ mm$ and $2{,}5\ mm$ of applied displacement, as shown in Figure 4.34. This resulted in reaction forces for the proposed, control and regular connections of $283\ kN$, $284\ kN$ and $366\ kN$ respectively.

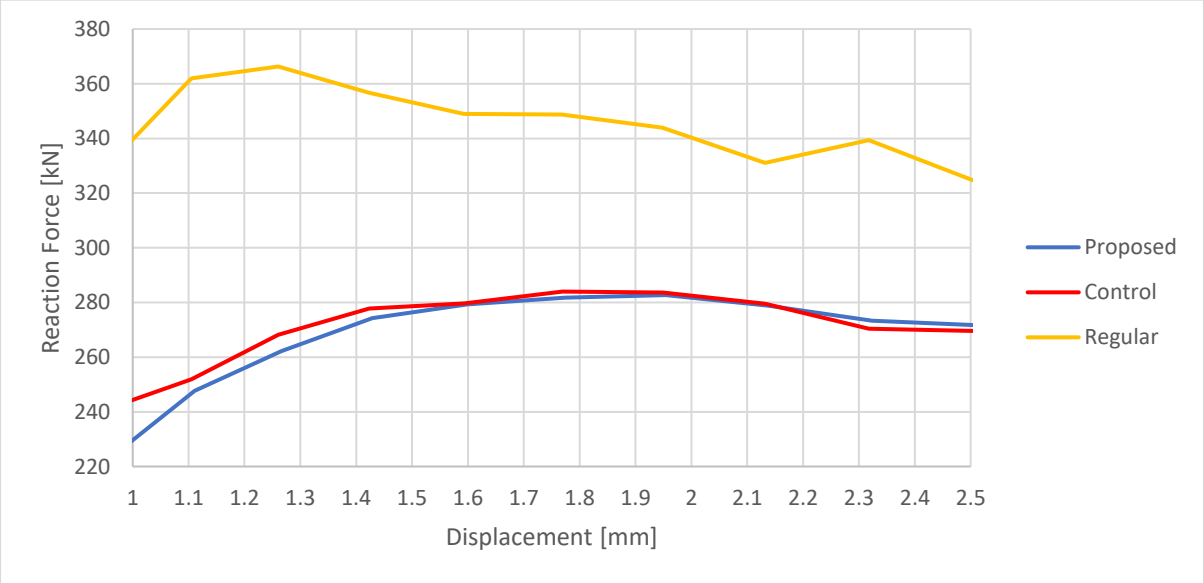

Figure 4.34 - Comparison of Force-Displacement graphs in the interval between $1\ mm$ and $2{,}5\ mm$ at $321\ kN$ preload

Overall Comparison

A number of observations are made based on the accumulated results in Table 3. The proposed connection benefits roughly $5\% - 6\%$ more from a higher preload than the control connection and the resistance of the regular connection increases relatively even more with an increase of $27{,}1\%$. When comparing the resistance of the control connection to the proposed connection it is noted that the difference between the two connections becomes smaller at higher preloads with a difference of $5{,}2\%$ at $200k\ kN$ preload and $0{,}4\%$ at $321\ kN$. The difference between the regular connection and the proposed and control connections on the contrary increases at higher preloads with $23{,}6\%$ and $17{,}6\%$ higher resistances at $200\ kN$ preload and $29{,}3\%$ and $28{,}9\%$ higher resistances at $321\ kN$ preload compared to the proposed and control connections respectively.

Table 3 - Comparison of connection resistance force

Connection type:	Proposed ($a = Prop$)	Control ($a = Con$)	Regular ($a = Reg$)
Max resistance at $200\ kN$ preload ($F_{R,max;(a);\ 200\ kN}$)	$233\ kN$	$245\ kN$	$288\ kN$
Max resistance at $321\ kN$ preload ($F_{R,max;(a);\ 321\ kN}$)	$283\ kN$	$284\ kN$	$366\ kN$
$100 * \frac{F_{R,max;(a);\ 321\ kN}}{F_{R,max;(a);\ 200\ kN}} - 100\%$	$+21{,}5\%$	$+15{,}9\%$	$+27{,}1\%$
$100 * \frac{F_{R,max;(a);\ 200\ kN/321\ kN}}{F_{R,max;(Prop);\ 200\ kN/321\ kN}} - 100\%$	X	$+5{,}2\%$ / $+0{,}4\%$	$+23{,}6\%$ /$+29{,}3\%$
$100 * \frac{F_{R,max;(Reg);\ 200\ kN/321\ kN}}{F_{R,max;(Prop);\ 200\ kN/321\ kN}} - 100\%$	X	X	$+17{,}6\%$ /$+28{,}9\%$

The derivative of the Force-Displacement graphs was taken to determine the stiffness of each connection (See Appendix B for the used graphs). The slope at the start of each graph was most important as this was still in the elastic domain. The applied preload did not affect the stiffness of the connections as the results from both preloads gave similar stiffness graphs. This resulted in the proposed and control connections having a relatively similar stiffness of roughly $850\ kN/mm$ and $950\ kN/mm$ respectively. The larger faying surfaces in the control connection increased its stiffness. The stiffness of the regular connection is roughly $1350\ kN/mm$ due to the shorter clamping length and lower number of interfaces.

4.5.2 Slip and Slip Resistance

200 kN Preload

Of note in the slip graphs of Figure 4.35 is that all three connections started slipping at roughly the same moment in time. The Inner cover elements (cover plates in the proposed and control connections and washers in the regular connection) at 200 seconds and the outer cover elements at 400 seconds. The force-slip graphs, as shown in Figure 4.36, of the inner cover elements all show the similar steps of reaching two distinct slip plateaus. The first plateau is the point of slip for only the inner cover elements, the second plateau is the point where the outer cover elements start slipping as well. This is also seen in the force-slip graphs of the outer cover elements which all start slipping at the force value of the second plateau of the inner cover elements, as clearly shown by the red dashed lines. This means that the force-slip graphs of the outer cover elements represent the friction resistance of the outer and inner cover elements combined. All three connections display a dip in friction resistance directly after reaching a plateau, this is the consequence of the slip resistance being overcome and full head slip starting during which the friction resistance is lower.

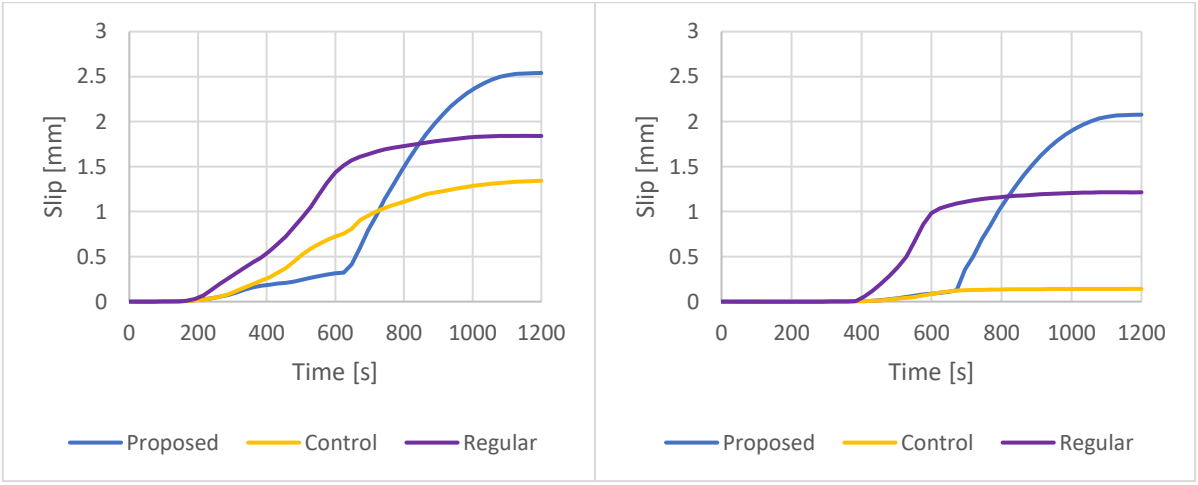

Figure 4.35 - Comparison of the inner (left) and outer (right) slip graphs of the cover elements at 200 kN preload

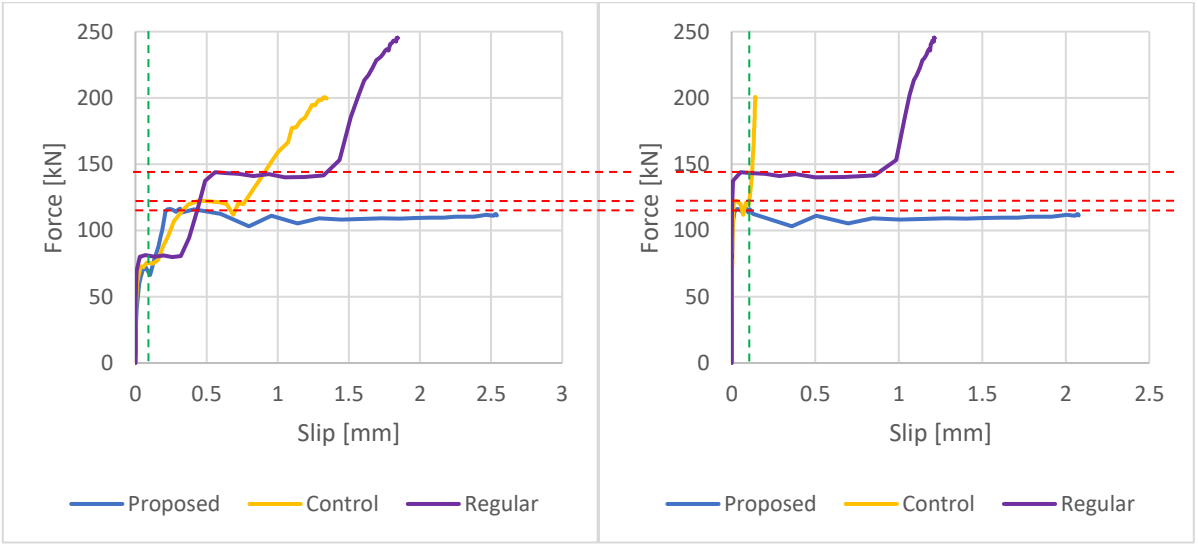

Figure 4.36 - Comparison of the inner (left) and outer (right) force-slip graphs of the cover elements at 200 kN preload

To better compare the slip loads of the connections, the force-slip graphs of the first $0{,}1\ mm$ of slip are plotted in Figure 4.37. This interval is indicated by the green dashed lines in Figure 4.36. This is the point where the first plateau is reached. The highest point of each of these graphs is taken as the slip load prior to full head slip starting, the results are found in Table 4.

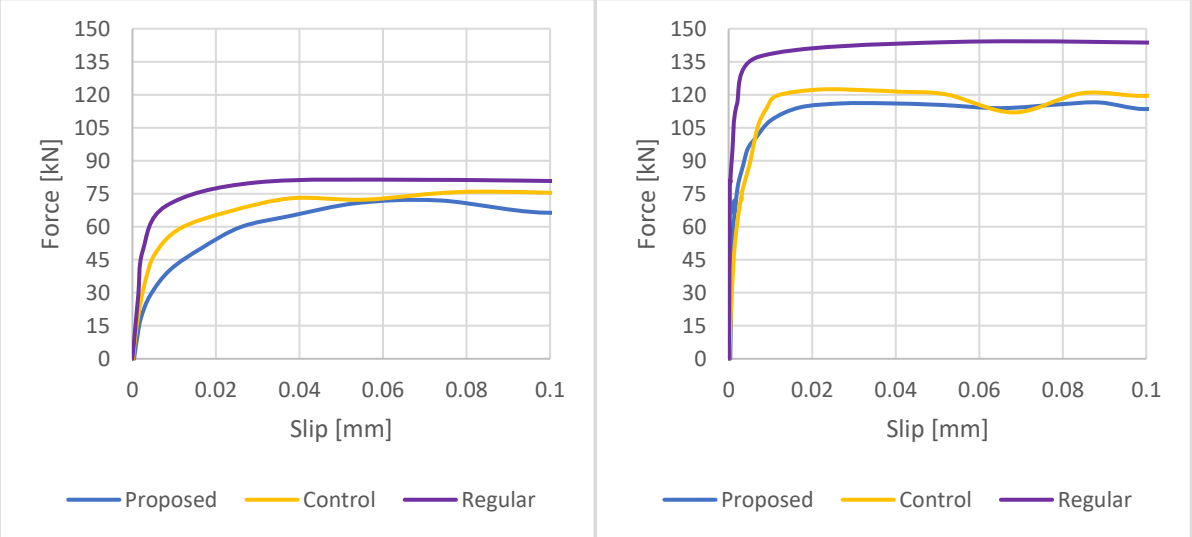

Figure 4.37 - Comparison of the force-slip graphs of the inner (left) and outer (right) cover elements at $200\ kN$ preload

Table 4 - Slip loads at $200\ kN$ preload

Connection	Slip load inner cover element	Slip load outer connection
Proposed	$72\ kN$	$116\ kN$
Control	$75\ kN$	$122\ kN$
Regular	$81\ kN$	$143\ kN$

321 kN Preload

Compared to the slip graphs at 200 kN preload, the slip graphs of Figure 4.38 show mostly similar behaviour, including the same starting points of slip. The force-slip graphs in Figure 4.39 show the difference between the slip load at the start of a plateau and the friction resistance during full head slip directly after more prominently than the connections with 200 kN preload did. The inner cover elements of the proposed and control connections also show a far more similar behaviour in the first 0,2 mm of slip. The same relationship between the force-slip graphs of the inner and outer cover elements is found as shown by the red dashed lines. The graphs of the outer cover element display the force-slip graph of the full outer connection.

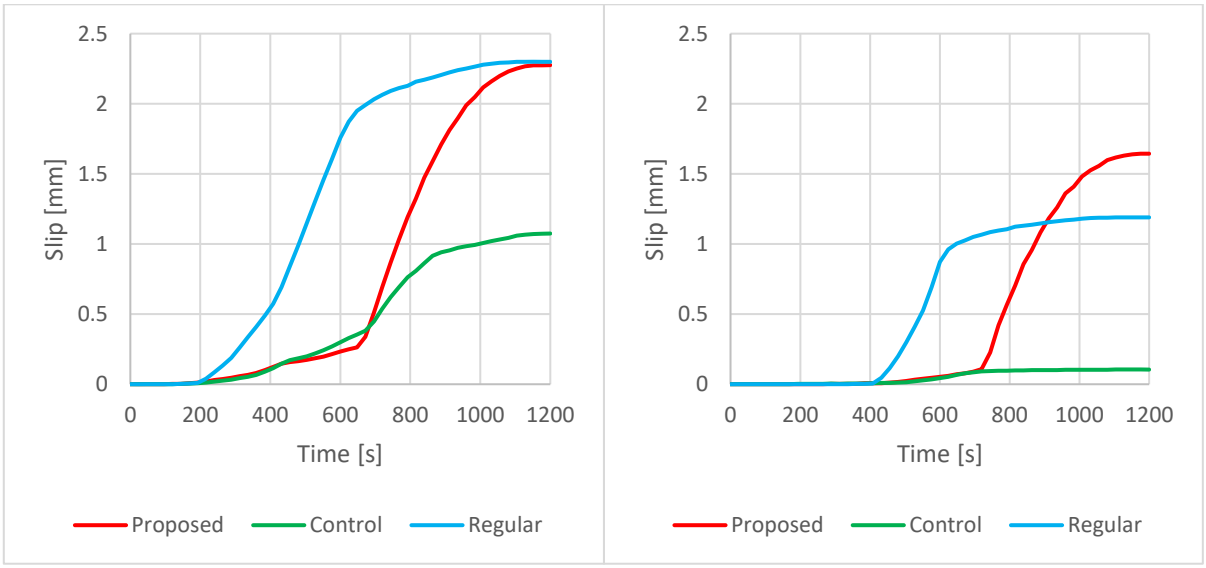

Figure 4.38 - Comparison of the inner (left) and outer (right) slip graphs of the cover elements at 321 kN preload

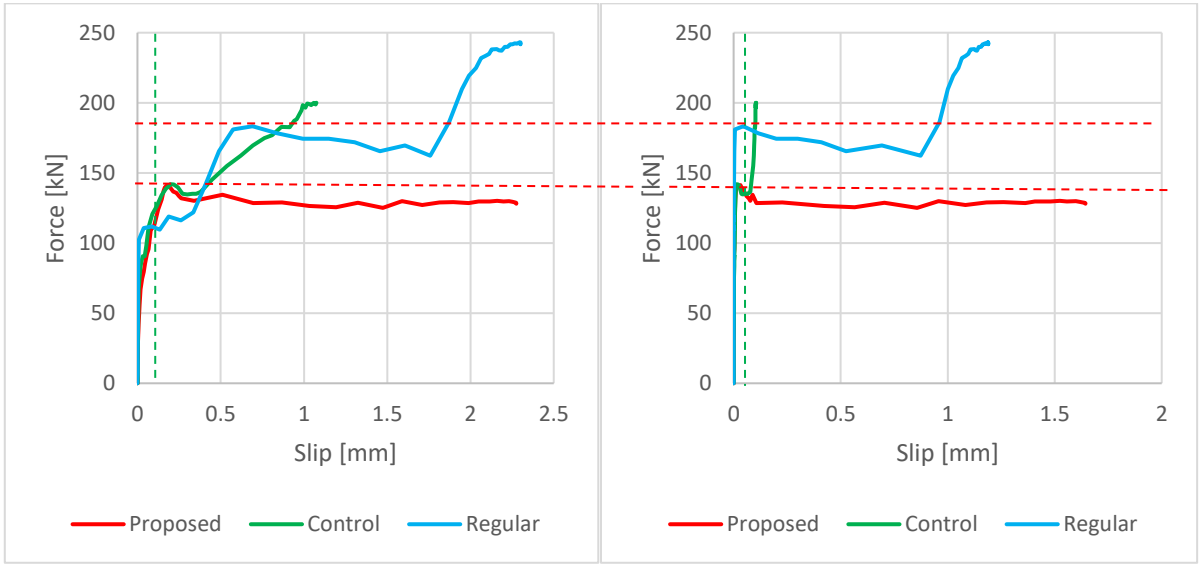

Figure 4.39 - Comparison of the inner (left) and outer (right) force-slip graphs of the cover elements at 321 kN preload

The force-slip graphs are focussed on the start of the graphs, indicated by the green dashed lines in Figure 4.39, and plotted in Figure 4.40 to determine the slip loads of the connections with $321\ kN$ preload. The graphs of the outer cover elements show the plateaus clearly, just like the regular graph of the inner cover element. The plateaus of the proposed and control graphs of the inner cover elements are harder to determine. In the control graphs it is seen that the higher preload increased the slip resistance of the inner cover element and activated the slip resistance of the outer cover element at an earlier point in time compared to the control connection with $200\ kN$ preload. This caused the slip between the central plate and inner washers relative to the inner cover elements to have to lowest friction resistance. Rather than the applied displacement being divided over all friction interfaces like in the connections with $200\ kN$ preload, a majority of the applied displacement is directly exerted on the central connection as slip. This caused the central plate to come in contact with the bolt rod at an earlier point of the simulation, ending the first slip plateau.

This same mechanism is present in the proposed connection, with a single difference. A first slip plateau is reached at a similar friction resistance as the control connection, as marked by the purple circles in the graphs. The proposed graphs display a third slip plateau, encircled in yellow in the graphs, between the first and second slip plateaus present in the control and regular graphs. This plateau is a consequence of the outer cover element slipping before the cover elements are loaded in bearing. This plateau will be ignored for the inner cover element as it is not the first slip load. The first plateau of the outer cover element will also be ignored due to the small slip length and it not being the slip load of the full outer connection. The slip loads of all connections are noted in Table 5.

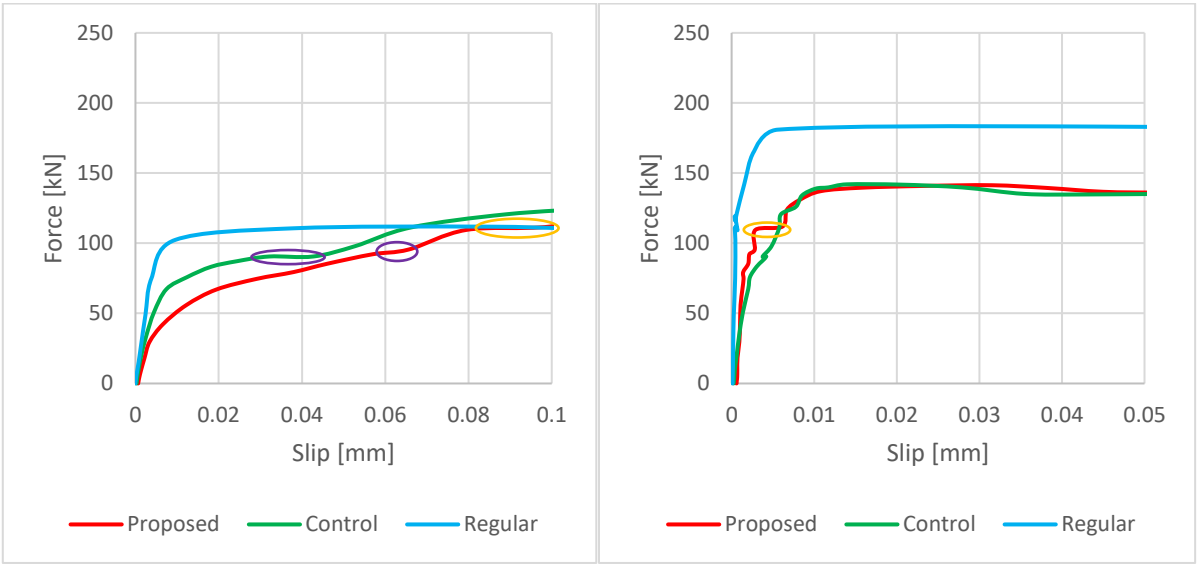

Figure 4.40 - Comparison of the force-slip graphs of the inner (left) and outer (right) cover elements at $321\ kN$ preload

Table 5 - Slip loads at $321\ kN$ preload

Connection	Slip load inner cover element	Slip load outer connection
Proposed	$92\ kN$	$141\ kN$
Control	$90{,}5\ kN$	$142\ kN$
Regular	$112\ kN$	$183\ kN$

Overall Comparison

All of the slip loads found using the Finite Element Analysis are listed in Table 6, as well as the calculated slip resistance of each connection. Comparing the found slip loads of the full outer connections to the slip resistances shows that the calculations are too conservative at $200\ kN$ preload and that they overestimate the slip load of the connections at $321\ kN$ preload.

Table 6 - Comparison of slip loads and slip resistances

Connection	Preload	Slip load inner cover element	Slip load outer connection	Slip resistance based on EN 1993-1-8
Proposed	$200\ kN$	$72\ kN$	$116\ kN$	$100{,}3\ kN$
	$321\ kN$	$92\ kN$	$141\ kN$	$161{,}8\ kN$
Control	$200\ kN$	$75\ kN$	$122\ kN$	$118{,}5\ kN$
	$321\ kN$	$91\ kN$	$142\ kN$	$190{,}4\ kN$
Regular	$200\ kN$	$81\ kN$	$143\ kN$	$118{,}5\ kN$
	$321\ kN$	$112\ kN$	$183\ kN$	$190{,}4\ kN$

The differences in slip load between the connections are noted in Table 7, based on which a number of observations are made. In all three connections the slip load of the inner cover element benefitted more from a higher preload than the full outer connections. This is also shown by the increase in the percentage of the slip load of the inner cover element as a part of the slip load of the full outer connection. The difference in slip load between the proposed and control connections decreases at higher preloads, as shown by the $+4{,}2\%$ and $+5{,}2\%$ slip load differences at $200\ kN$ preload and the $-1{,}1\%$ and $+0{,}7\%$ differences at $321\ kN$ preload of the inner cover element and the full outer connection respectively when comparing the control connection to the proposed connection. The results in Table 7 show that the differences in slip load between the regular connection and the proposed and control connections become larger at higher preloads.

Table 7 - Differences in slip load

Connection type:	Proposed ($a = Prop$)		Control ($a = Con$)		Regular ($a = Reg$)	
Inner cover element / Full outer connection:	Inner	Outer	Inner	Outer	Inner	Outer
Slip load at $200\ kN$ preload ($F_{S;\,(a);\,200\ kN}$)	$72\ kN$	$116\ kN$	$75\ kN$	$122\ kN$	$81\ kN$	$143\ kN$
Slip load at $321\ kN$ preload ($F_{S;\,(a);\,321\ kN}$)	$92\ kN$	$141\ kN$	$91\ kN$	$142\ kN$	$112\ kN$	$183\ kN$
$100 * \frac{F_{S;\,(a);\,321\ kN}}{F_{S;\,(a);\,200\ kN}} - 100\%$	$+27{,}8\%$	$+21{,}6\%$	$+21{,}3\%$	$+16{,}4\%$	$+38{,}3\%$	$+28\%$
$100 * \frac{F_{S;\,(a);\,200\frac{kN}{321}kN}}{F_{S;\,(Prop);\,200\frac{kN}{321}kN}} - 100\%$	X	X	$+4{,}2\%$ / $-1{,}1\%$	$+5{,}2\%$ /$+0{,}7\%$	$+12{,}5\%$ /$+21{,}7\%$	$+23{,}3\%$ /$+29{,}8\%$
$100 * \frac{F_{S;\,(Reg);\,200\frac{kN}{321}kN}}{F_{S;(Prop);\,200\frac{kN}{321}kN}} - 100\%$	X	X	X	X	$+8\%$ /$+23{,}1\%$	$+17{,}2\%$ /$+28{,}9\%$
$100 * \frac{F_{S;\,(a);\,Inner;\,200\ kN/321\ kN}}{F_{S;\,(a);\,Outer;\,200\ kN/321\ kN}}$	$62{,}1\%$ / $65{,}2\%$		$61{,}5\%$ / $64{,}1\%$		$56{,}6\%$ / $61{,}2\%$	

5 EXPERIMENTS

5.1 PLANNING AND SETUP

The experiments consisted of a total of two short term relaxation tests and three cyclic tests. Both the proposed connection and control connections were subjected to a 24 hour period without loading after assembly to collect data on the short term relaxation. The regular connection was not subjected to this test due to the shorter clamping length used. With different clamping lengths used, the results would not have been comparable and thus not useful. All three connections were subjected to fatigue loading with a duration of one million cycles. The goal of these fatigue experiments was to collect data on the loss of preload and slip of the outer connections over its duration.

For the fatigue tests to occur, the connections had to be turned into test specimens. The parts designed prior had to be altered to fit the machine used and the intended test setup. The first step was mirroring the connections to end up with specimens that could be mounted in the machine used. The length of the central plates was chosen based on the required space needed for measuring equipment to be attached and the length of the clamps of the machine. The clamps of the machine had a depth of $85\ mm$ and the space intended for measuring equipment was set at $200\ mm$ for ease of access. The outer plates were kept shorter to keep the overall length of the specimen under $1\ m$ for ease of handling during the experiments. The space between the cover plates was kept large enough for smaller measuring equipment to be installed. The resulting specimens are shown in Figure 5.1.

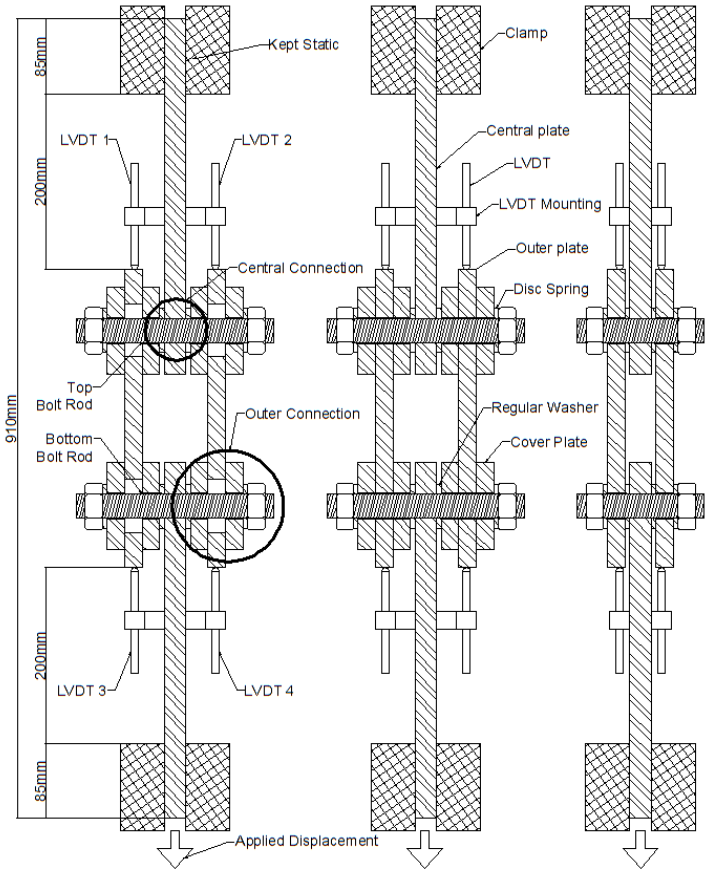

Figure 5.1 - Specimen setup: Left) Proposed specimen; Middle) Control specimen; Right) Regular specimen

With the specimens designed, the loads to be applied were the next step. The connections were designed with a preload of $321\ kN$ in mind, but due to uncertainty of the possibility of inducing this preload it was lowered to $200\ kN$. This also affected the applied force range. The initial plan was for a total force range of $130\ kN$ to be applied, which ranged from $-10\ kN$ to $+120\ kN$. This force range was altered for several reasons. The first factor was that the slip resistances in the specimens were reduced due to the lower preload. The initial slip resistance of $190{,}4\ kN$ was reduced to $118{,}5\ kN$ if the surface conditions of the washers were assumed to be similar to the coated plates. If the washers were taken as worse surface conditions, the slip resistance was reduced further to $89\ kN$. With a maximum applied force of $120\ kN$ during the fatigue tests, it was guaranteed for the central connection to slip. The central plate itself could withstand this without significant damage, but the bolt rod would not survive the fatigue test for the full one million cycles (see appendix A for calculations). The second factor was the changing of load direction during cyclic loading. If full slip would occur in the central connection for any reason, the bolt would be hitting the hole edges at a high frequency. This would produce an extremely loud noise and damage both the bolt and the central plate. This would mandate the termination of the test and in turn increase the time needed for the experiments.

To compensate for these factors the applied loading was changed. Rather than a minimum load of $-10\ kN$, a minimum load of $+5\ kN$ was chosen. The specimen would constantly be in tension and if full slip would occur in the central connection, the bolt would be pulled against a single side of the hole. To prevent full slip from occurring in the central connection, the maximum force was reduced to $+60\ kN$. Even in the worst case, this load was $29\ kN$ lower than the slip resistance of the central connection.

Although the central plates were reused and only a single set of cover plates was ordered, an effort was still made to minimise the difference in conditions for the tests of the proposed and control specimens. During the first fatigue test, which was the proposed specimen, a part of the cover plate coating was damaged as shown in Figure 5.2. By flipping the cover plates over for the control test, both sides would still interact with mostly undamaged faying surfaces.

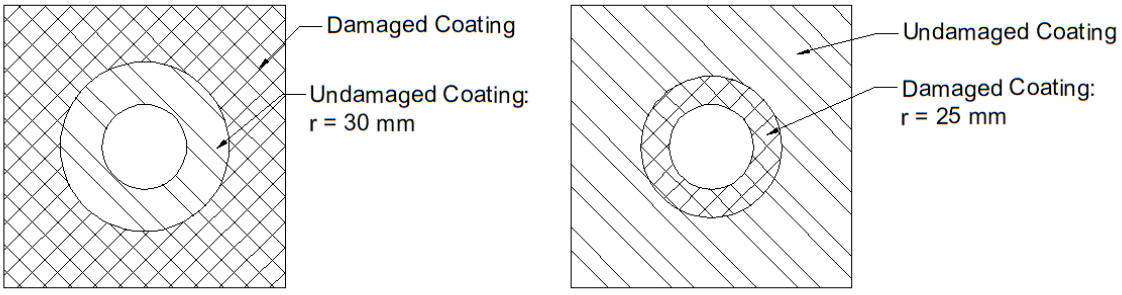

Figure 5.2 - Damage to the coating after proposed fatigue test: Left) Inside cover plate; Right) Outside cover plate

After the first test this plan was abandoned due to the significant damage the disc springs did to the outer surfaces of the cover plates as shown in the left picture of Figure 5.3. The accumulated coating at the edges of where the disc springs were located would have influenced the results of the control test more than the partially embedded coating layers.

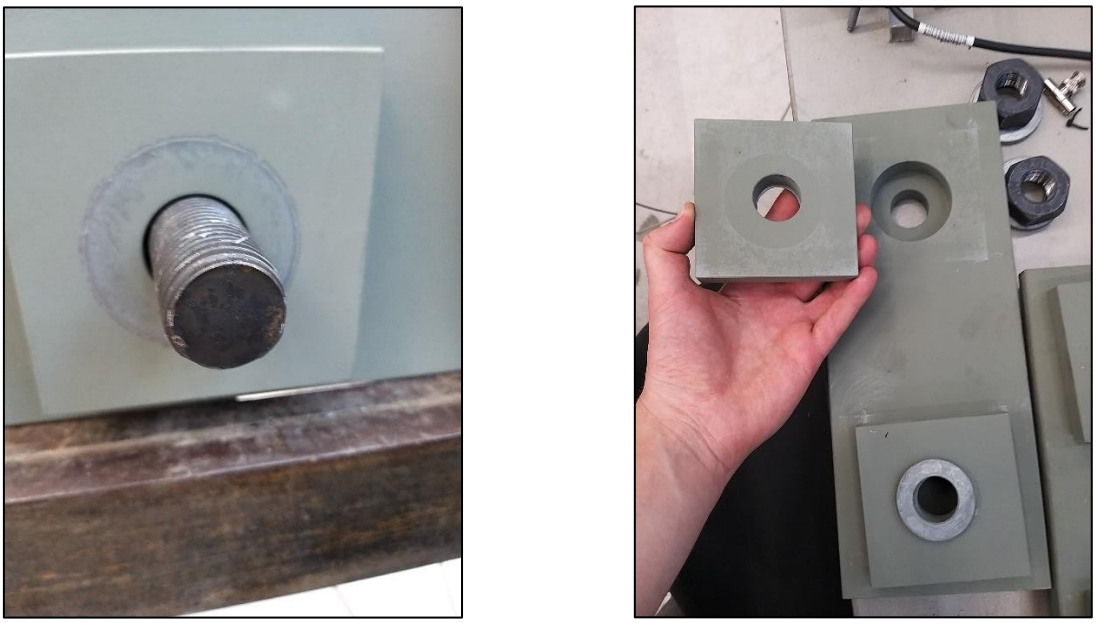

Figure 5.3 - Left) Damage to outside cover plates due to disc springs; Right) Damage to inside cover plates

With all of the preparations planned for, the next step was to define the measuring tools used during the experiments. The cyclic loading machine used recorded the applied load and displacement to induce the load. Strain gauges were placed inside the bolt rods to measure the preload. These were calibrated beforehand for loads around $200\ kN$. The last measurement tools used were the LVDTs, four of them were attached to the central plates to measure the relative displacement of the outer plates compared to the central plates. Both the strain bolt and LVDTs are shown in Figure 5.4 and the LVDTs' placement is shown in Figure 5.1.

Figure 5.4 - Left) LVDT; Middle) Strain bolt; Right) LVDT support assembly

5.2 PROCEDURE

Before the assembly of the specimen started, the Dowty Rotel cyclic loading machine had to be set to the correct height to fit the specimen as seen in Figure 5.5. This was accomplished with the use of the hall's overhead crane.

Figure 5.5 - Setting up the Dowty Rotel cyclic loading machine

Afterwards, the assembly of the specimen was started. A forklift was used as a working surface during the assembly. Steel plates with a thickness of $20\ mm$ were used to support the central plates to keep the holes of the different plates in line, as seen in the left picture of Figure 5.6. To keep the specimen in place during the preloading of the bolts, an assembly was used to clamp it to the fork as shown in the right picture of Figure 5.6. The preloading of the bolts went in alternating steps of $50\ kN$ between the two bolts, as not to overload a single side. After each bolt reached $200\ kN$ they were retightened once more due to the fast initial loss of preload directly after preloading. This process is shown in the right picture of Figure 5.6. This process was not properly adhered to during the assembly of the proposed specimen, where only the top bolt rod received this last retightening.

Figure 5.6 - Left) Specimen assembly; Right) Preloading of the bolts

With the proposed specimen assembled, it was left for 24 hours to gather data on the short term relaxation. After this period, the assemblies for the LVDTs were attached and the bolts were retightened to a preload of $200\ kN$. After this step, the specimen was hoisted into the cyclic loading machine using the overhead crane as shown in the left picture of Figure 5.7. With the specimen in place, the LVDTs could be placed in their support assemblies, shown in the right picture of Figure 5.7. With the specimen in place, the final preparations consisted of setting the safety measures for the machine and the final calibration of the measuring equipment. The machine was then turned on and the first fatigue test was started. The machine would displace the bottom of the specimen to induce the force that was set. The top of the specimen was kept static.

Figure 5.7 - Left) Moving the specimen; Right) Specimen placed in cyclic loading machine

After the fatigue test of the proposed specimen had concluded, the outer plates were removed and replaced by the outer plates of the control specimen. This time both bolts were preloaded the same way to prevent influencing the results. After the short term relaxation period the specimen was placed in the cyclic loading machine. During the process of moving the upper and lower clamps into place, the top clamp moved further than expected and pressed on the specimen in such a way that the top central plate was rotated noticeably. This forced the complete unloading and reloading of the top bolt rod to return the top central plate into the correct position.

After the control cyclic test had concluded, observations of the outer plates showed an unexpected interaction between the bolt rods and the plates. The bolt rods had interacted with the side of the hole and etched the threads into the steel damaging both the plates and the bolt rods as shown in Figure 5.8. The most likely cause was for the bolt rods to be supported by the outer plates during assembly and holding this placement during preloading.

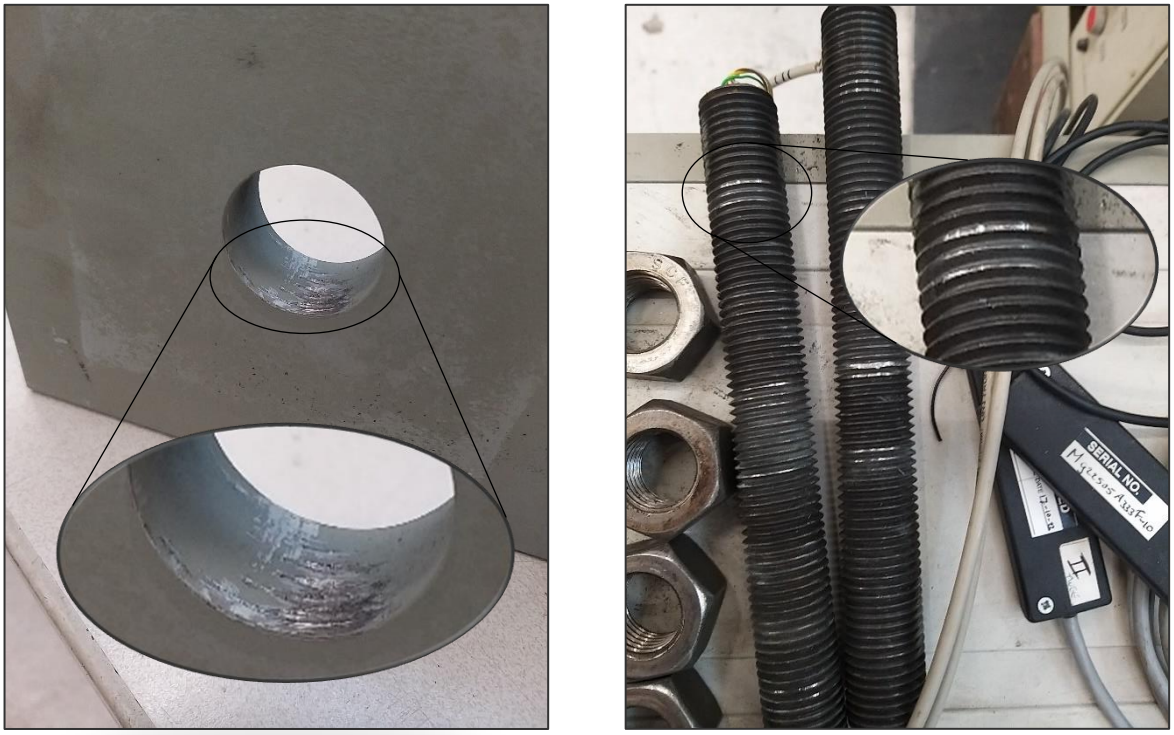

Figure 5.8 - Damage to plates (Left) and bolt rods (right) due to interaction

After the control test, the regular specimen was assembled by removing the cover plates and using the same outer plates as for the control specimen. The bolt rods were replaced with the shorter set meant for the regular specimen. No short term relaxation test was conducted with this specimen. To compensate for the initial loss of preload directly after preloading, the specimen was left for 15 minutes. After this period the bolt rods were retightened, after which the specimen was placed in the cyclic loading machine for the test to start. After the test was concluded, it was noticed that the bolt rods had once again etched their threads into the outer plates.

5.3 RESULTS

With all of the following results the outside influences during the tests were taken into account when reviewing them. In addition, all data presented here are the averaged results rather than the actual values. This was done to decrease the amplitude of the resulting graphs and make them more readable.

5.3.1 Loss of Preload

The first results were collected before the fatigue loading started. The 24 hour short term relaxation of the proposed and control specimens were recorded and are shown in Figure 5.9. All of the graphs showed the same steep decline at the start due to the initial loss of preload directly after preloading. A major influence factor on this behaviour was the embedding of the coated contact areas, which can be seen when comparing the proposed and control specimens. The control test was the second one conducted and all but two parts were used during the first test. This meant that a total of 10 coated interface surfaces were already partially embedded, and the reuse of the rods and nuts entailed the same for the thread contact areas. When comparing the top and bottom rods during each test, a problem was noticed in the results of the proposed specimen. During the assembly of this specimen the bottom rod was not tightened the same number of times as the top bolt rod, resulting in a larger loss to embedding at the start. Apart from the difference in value between the top and bottom rods, the shape of the graphs was nearly identical. The two rods of the control specimen in comparison showed nearly identical graphs in both value and shape. Based on this information it could be conjectured that had the bottom rod of the proposed specimen been retightened like the top rod was, that both graphs would have been nearly identical. In this light, an adjusted graph of the results of the proposed specimen was made by increasing all data values of the bottom rod by $5{,}8\ kN$. This was done for the purpose of comparing the different specimens. This graph is shown in Figure 5.10.

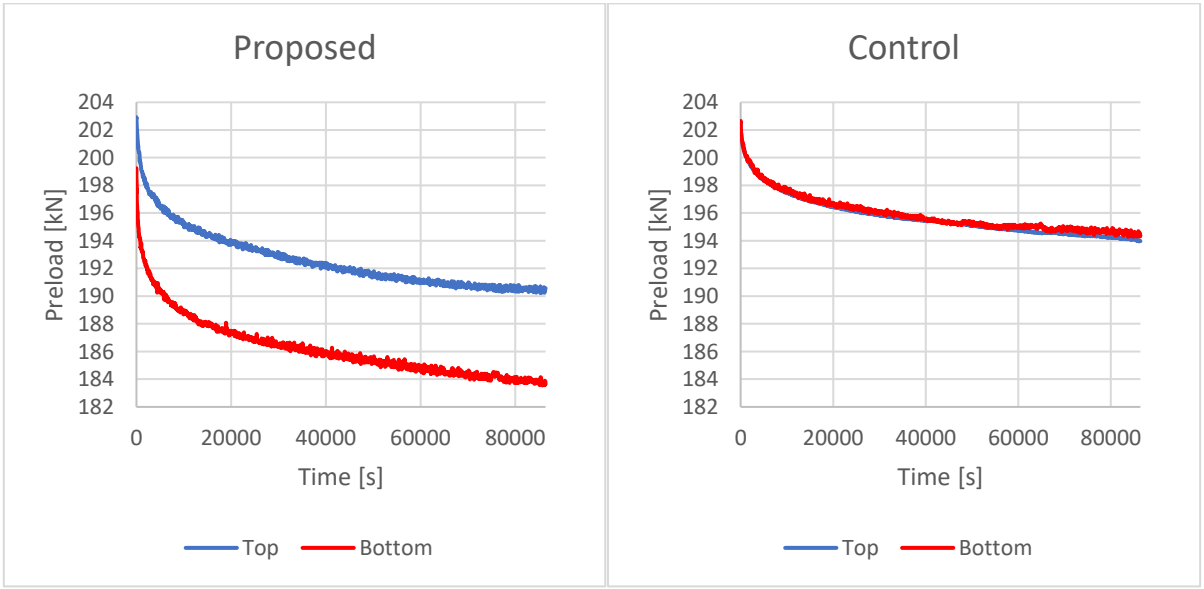

Figure 5.9 - Short term relaxation of the bolt rods

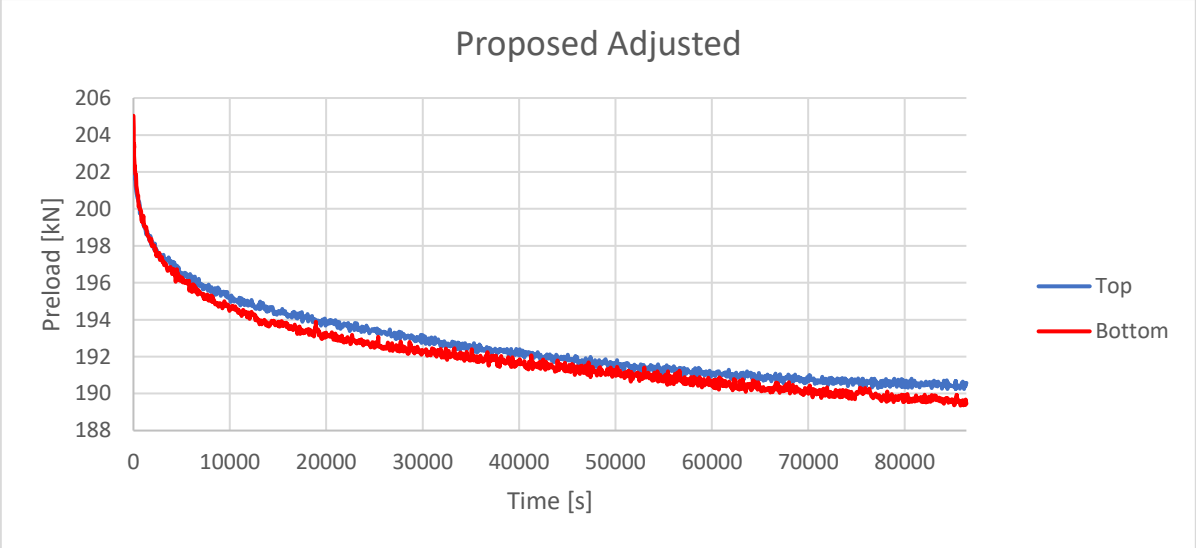

Figure 5.10 - Adjusted graph of proposed short term relaxation

The initial loss of preload after retightening the bolt rods was also present in the graphs of the preload during the fatigue tests, as shown in Figure 5.11 and Figure 5.12. An additional factor to consider was the bolt relaxation of the bolt rods. Although not reaching extremely high temperatures, the high frequency of loading caused the specimens to be at a higher temperature during the fatigue tests than during assembly. The influence this had on the total loss of preload is expected to be small and of no significance due to its influence being similar during all three tests.

Comparing the proposed short term relaxation graphs to the proposed graphs in Figure 5.11 shows a similar difference between the top and bottom graphs, which has the same cause. The reason for this was in part the uneven preloading applied when initially assembling the specimen. Even though both bolt rods were retightened to the same preload prior to fatigue loading, the amount of room that the bottom rod had for relaxation was larger than the top rod. This also meant that the bottom rod could start self-loosening before the top rod. The diverging graph shapes near the end may be a visualisation of this. Unlike the short term relaxation graph, this graph was not adjusted due to the difference in conditions between the top and bottom bolt rods during fatigue loading.

The second point of attention was the significant loss of preload of the control specimen's upper bolt rod. Most of the benefits gained during the initial 24 hour period were negated due to the complete unloading and reloading prior to the fatigue test. The bottom graph shows a far flatter curve than both the top rod and the proposed graphs. Two possible causes exist for this course. This was either a result of the near complete removal of embedding and self-loosening in the system or the etching of grooves into the side of the hole by the threads of the bolts and the subsequent partial connections that this formed. Another point was the significant amplitude present in the results of the bottom rod of this specimen. This may have been the result of the interaction between the bolt rod and hole edge of the outer plates. This interaction was also present in the top rod, but the graph did not show the same amplitude. This could have been a consequence of the lower preload. Due to the large differences in conditions between the top and bottom bolt rods it was not possible to adjust these graphs. The overall smaller loss of preload compared to the proposed specimen was, similar to the short term relaxation, also affected by the already partially compressed interfaces.

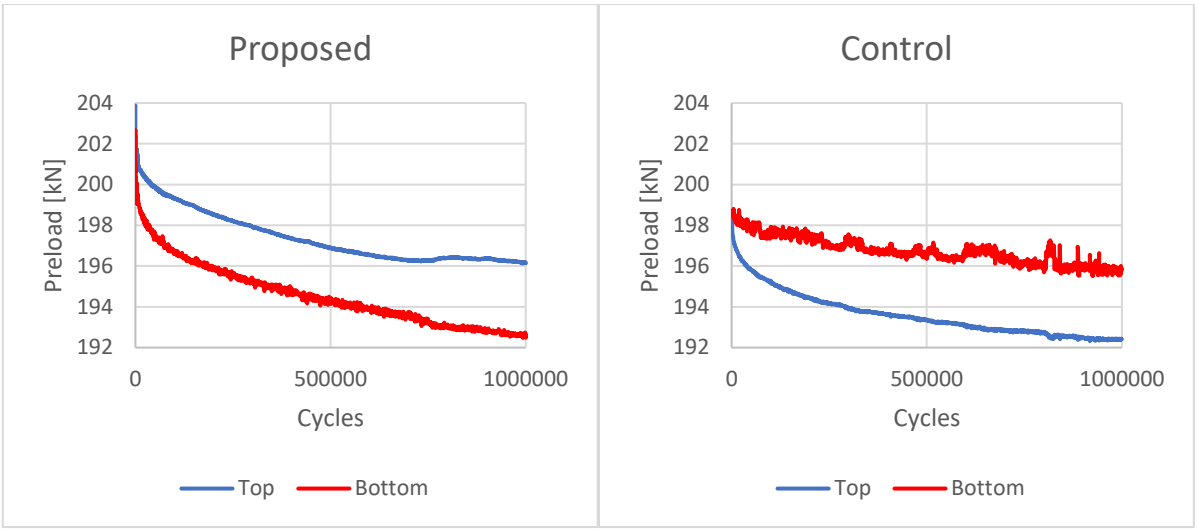

Figure 5.11 - Preload during fatigue tests

The third fatigue test conducted was the regular specimen. Due to the shorter clamping length used, the comparison of short term relaxation between this specimen and the first two was of less interest. As such, no 24 hour short term relaxation test was conducted with this specimen. This had to be considered when observing the preload results during the fatigue test. Where the first two specimens had 24 interfaces of which 14 were coated, the regular specimen had 16 of which only six were coated. This reduced the number of surfaces that could be compressed by eight, all of which were coated faying surfaces. This had a positive effect on the loss of preload. The shorter clamping length on the contrary had a negative effect on the loss of preload according to Nijgh (2016, p. 73) as shorter bolts lose comparatively more preload compared to longer bolts with the same diameter. Both rods interacted with the side of the holes, just like the control specimen. The large amplitude in the results could be attributed to this, as no other reason presented itself. The top bolt rod behaved as expected with a steep drop at the start and flattening out over time. The bottom rod's behaviour was more peculiar as it suddenly gained 2 kN of preload after 45000 cycles. Taking this as a problem with the strain gauge, the graph after this point was lowered by 2 kN to make it follow a more constant course. Both graphs are shown in Figure 5.12. The final observation when comparing both graphs is that both the top and bottom rod show an increase of preload around 600.000 cycles. The reason for this is unknown and could be an external factor.

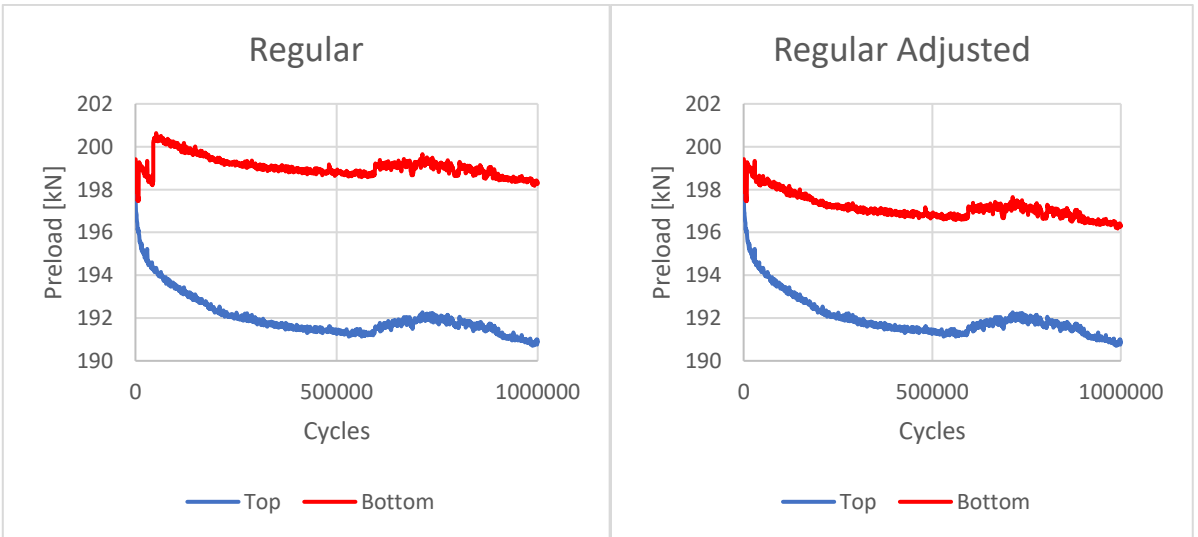

Figure 5.12 - Preload during fatigue tests

5.3.2 Slip

The cyclic loading machine applied displacements to the bottom of the specimen to induce the required loads, the average results of both are shown in Figure 5.13. When comparing the applied forces of all three specimens, the graphs show minimal differences. These differences are most likely the consequence of small unintended changes during the setup of the specimens in the machine. The displacements do show that the control specimen is a significant outlier. A larger displacement was apparently needed to induce the same forces. This is contradicted by the FEA results, which show similar stiffness' for the proposed and control connections. The cause for this can most likely be found in the damage of the parts used. With the exception of the outer plates, all parts used during the control test were already subject to fatigue loading as part of the proposed specimen. This damage to the faying surfaces reduced the overall stiffness of the specimen.

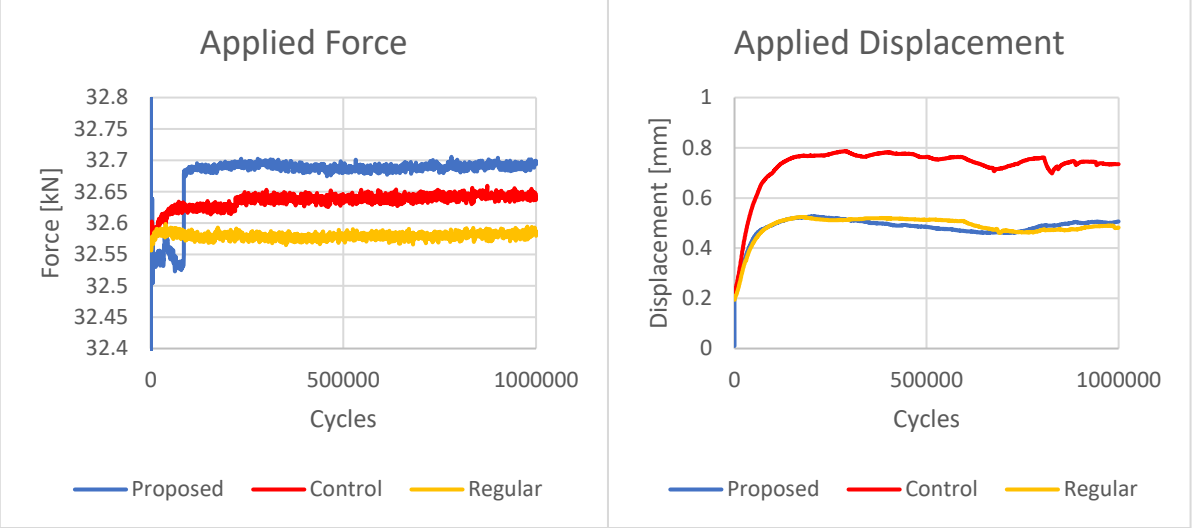

Figure 5.13 - Comparison of applied force and displacement by the machine

The final set of data that was collected were the relative displacements between the central plates and the outer plates. The raw results of the control specimen showed LVDT 2 as an outlier with a far larger displacement. This was the consequence of a problem with the LVDT itself and its results were thus not used. Both the raw data graphs and final graphs of the control test are shown in Figure 5.14.

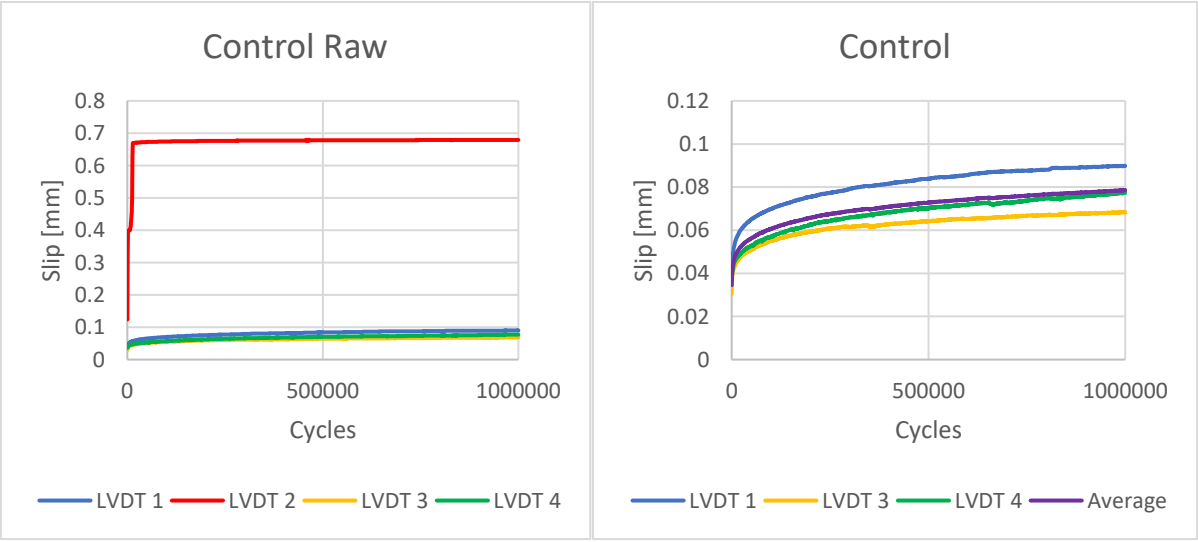

Figure 5.14 - Slip graphs of the control specimen

Looking at the results of each individual specimen in Figure 5.14 and Figure 5.15 it shows that overall the displacements of the LVDTs group together. In the control specimen all three LVDTs are roughly similar in value and course, with the exception of LVDT 1 which has a higher displacement. This is most likely the result of the faster loss of preload suffered by the top bolt rod. The same is the case for the regular specimen, apart from LVDT 1. The results of the proposed specimen clearly showed the dependence on preload for the friction resistance. LVDTs 3 and 4 suffered more slip due to the lower preload present in the bottom bolt rod. For better comparison an average displacement of each test was also plotted.

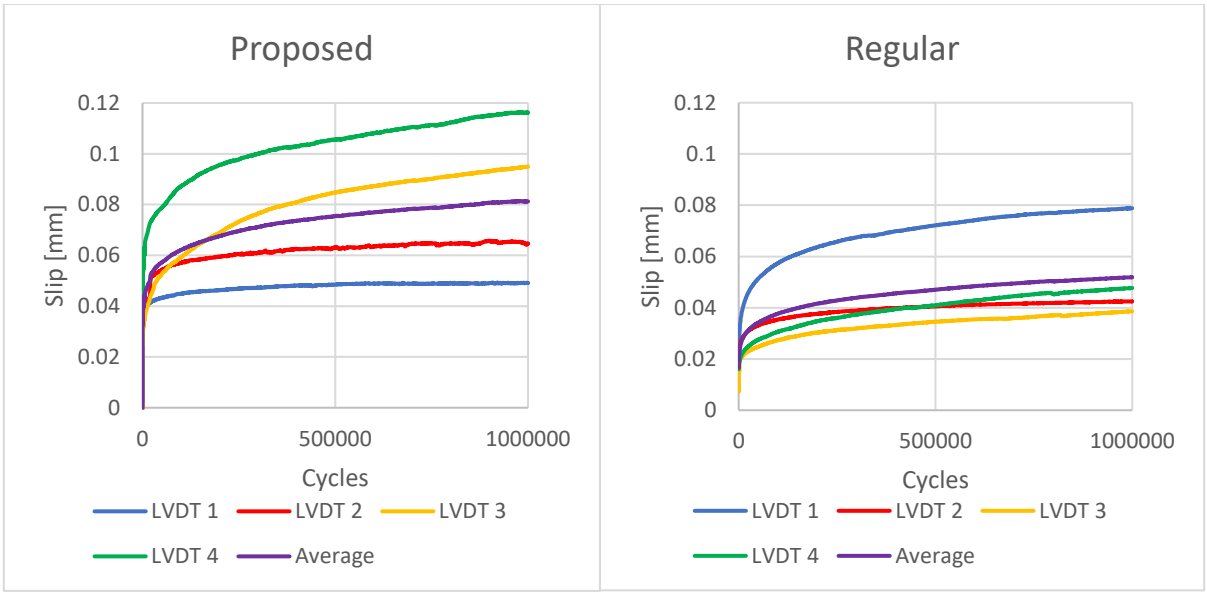

Figure 5.15 - Slip graphs

5.4 ANALYSIS AND CONCLUSIONS

5.4.1 Loss of Preload

Short Term Relaxation

The short term relaxation of both specimens prior to the fatigue tests, as shown in Figure 5.16, display similar graphs. Both rods exhibit the same difference between the specimens, a reduction of roughly $4\ kN$ at the end of the 24 hour period.

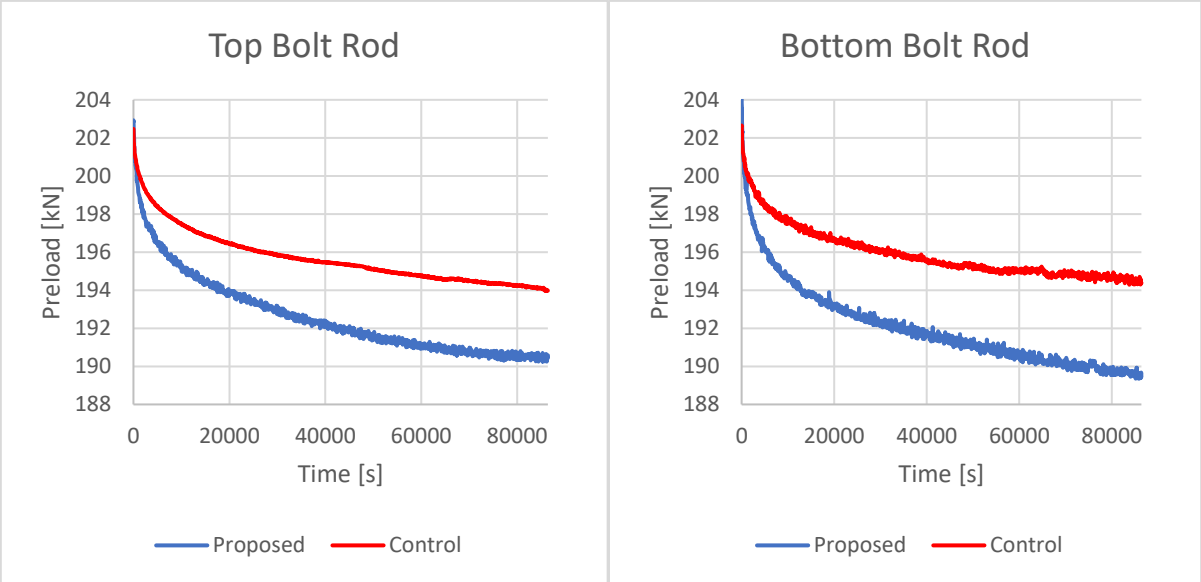

Figure 5.16 - Comparison of short term relaxation

To better compare the results, the preload of each bolt was expressed as a percentage of its respective starting preload and plotted (see Appendix B for these graphs). These values were averaged for each specimen and plotted in Figure 5.17. The average loss of preload was also plotted in the right graph for easier reading. The proposed connection lost 7% of its initial preload and the control connection lost 4%, a 3% difference between the two.

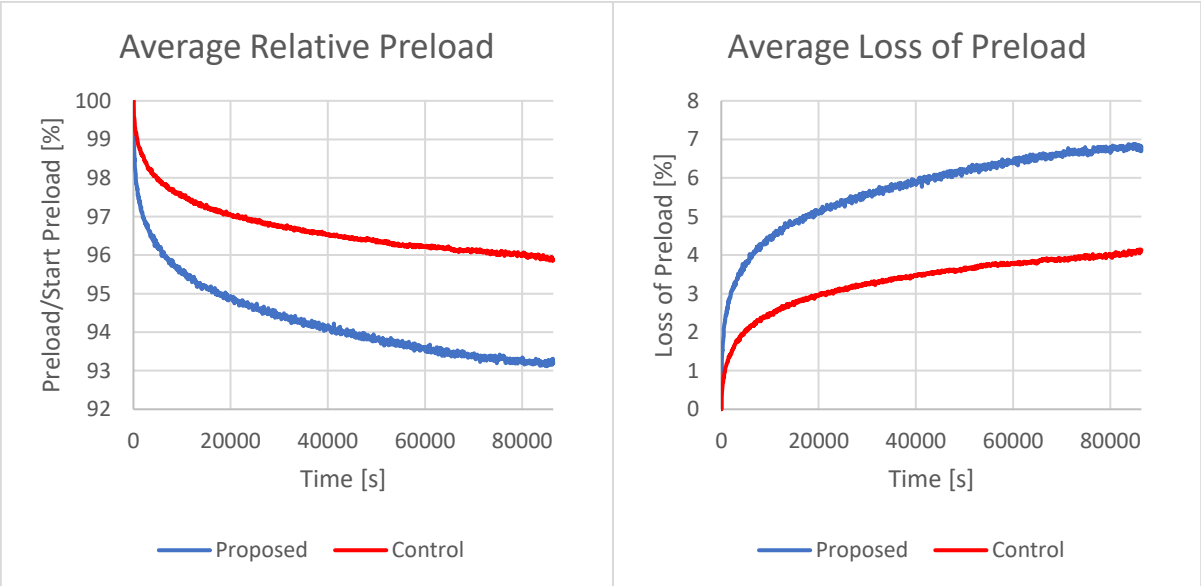

Figure 5.17 - Comparison of: Left) Average relative preload; Right) Average loss of preload

To visualize the difference in embedding, the length gain of each bolt rod was calculated and plotted (see Appendix B for these graphs). The average length gain per test and the difference between the tests is plotted in Figure 5.18. The proposed specimen gained roughly $10\ \mu m$ more length during the short term relaxation, about half of which was immediately at the start. This difference is in majority caused by the reuse of the same parts during the control test, causing the interfacing surfaces to be partially compressed at the start and in turn reducing the amount of embedding that was possible.

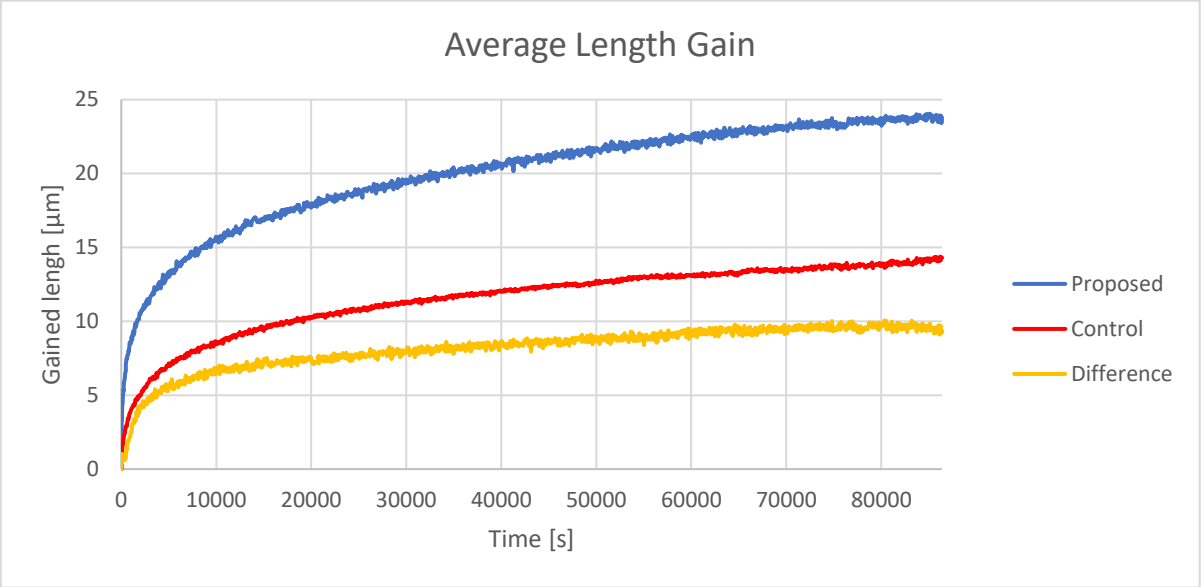

Figure 5.18 - Comparison of average length gain during short term relaxation

Both specimens had 14 coated interfacing surfaces, with a coating layer thickness of $60\ \mu m$. During the proposed test all of these surfaces were still fresh. At the start of the control test, 10 of these surfaces were already subjected to short term relaxation and fatigue loading, resulting in thinner coating layers. To put this in perspective, doubling the coating thickness can increase preload loss due to embedding by 60% (Friede & Lange, 2010, p. 290). The coated area that was partially compressed at the start of the control test was 55% of the total coated interface area in the connection. The reduction of coated interface area due to the use of larger holes was only 20% (See Appendix A for calculations).

Loss of preload during fatigue loading

When plotting the preload graphs of all three specimens in the same coordinate system, as shown in Figure 5.19, the differences in starting conditions stand out. This makes it more difficult to properly compare the results. To solve this the preloads of all bolts are expressed as a percentage of their respective starting preload and plotted in in Figure 5.20.

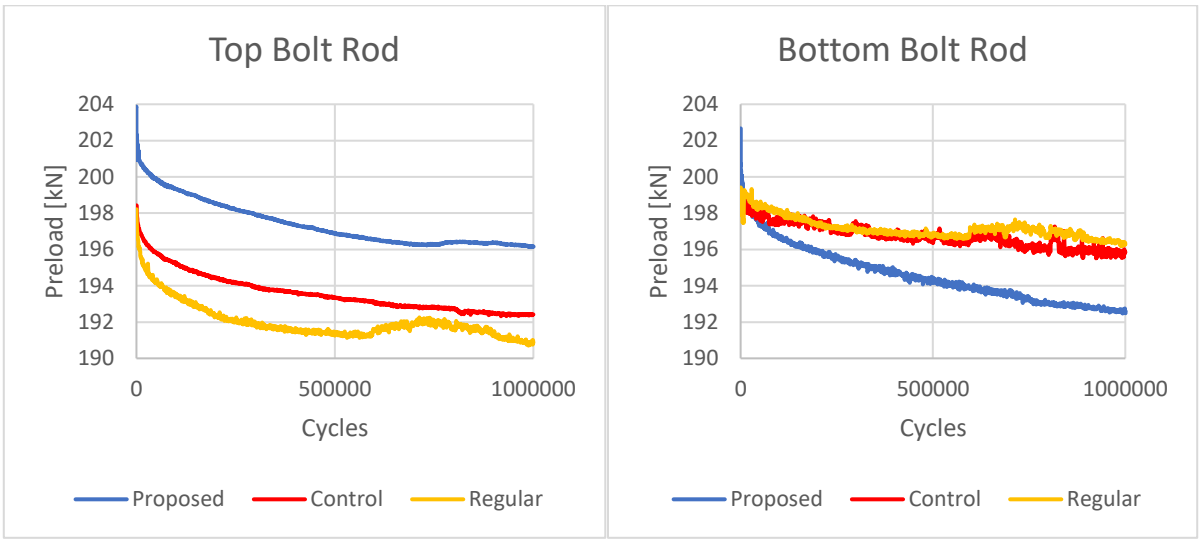

Figure 5.19 - Comparison of preload during fatigue tests

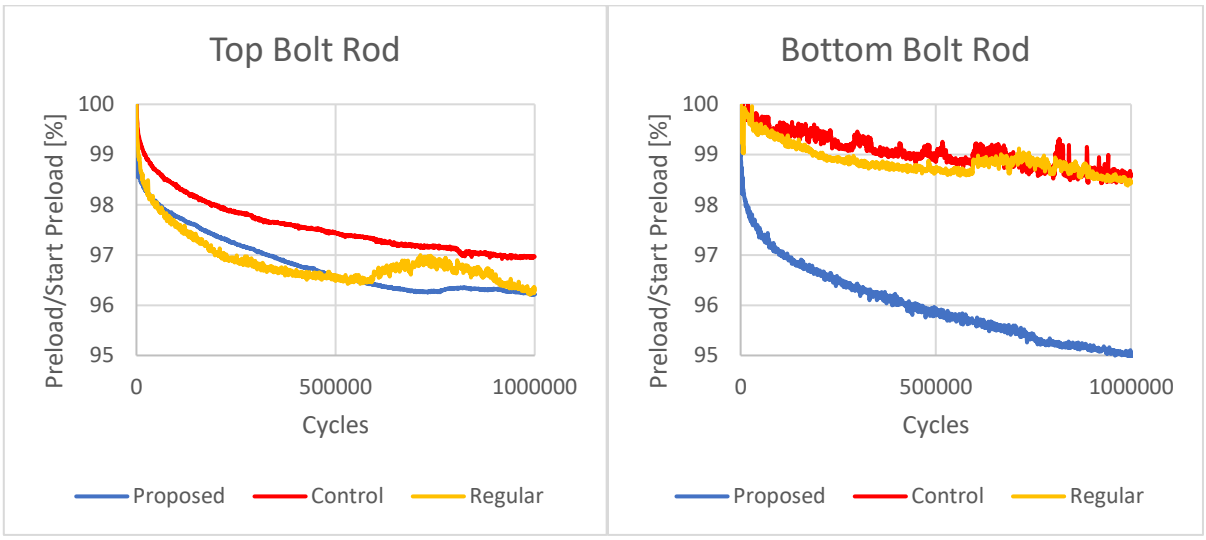

Figure 5.20 - Comparison of relative preload during fatigue tests

Looking at the bolts individually, it shows that for the top bolt rod all three graphs follow a similar course and lose a very similar percentage of their starting preload. The differences are less than a percent between all three specimens. The bottom bolt rod on the contrary shows a large difference between the control and regular graphs and the proposed graph. Two of the possible influences for this variation are relaxation and interaction between the bolt rod and bolt hole. The first is the different amounts of space for relaxation the specimens had. The reuse of parts during the control test reduced the possible space for relaxation compared to the proposed test. The regular specimen had inherently less space for relaxation due to its lower number of interfacing surfaces. The second possibility is the interaction between the bolt rods and bolts holes that the control and regular specimens had. The threads of the bolt rods etched grooves into the side of the holes and inserted themselves in these grooves, creating a weak partial connection of sorts. This second possible

influence was also present at the top bolt rod, but this did not result in similar results. The point of force application may be the reason. The machine applied the displacement at the bottom of the specimens, resulting in the bottom connections needing to transfer this load to the top before those were activated. The larger amplitudes of the bottom results may also be a consequence of this. More experiments are needed to confirm this.

To come to a conclusion and properly compare the three connections, the average of both bolt rods was taken as shown in Figure 5.21. The loss of preload was also plotted in Figure 5.22. The control and regular specimens lost roughly $2{,}2\%$ and $2{,}6\%$ respectively of their initial preload during the fatigue tests. The proposed connection lost about $4{,}4\%$ of its initial preload, which is approximately 2% more than the other two connections. This is a small difference when taking the favourable conditions during the control and regular tests into account.

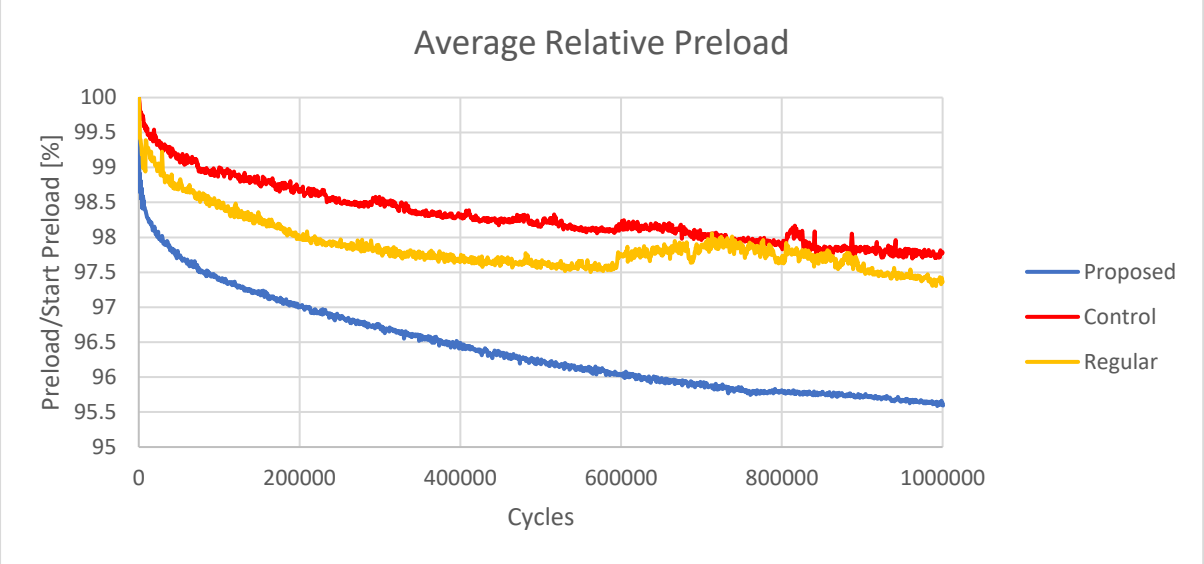

Figure 5.21 - Comparison of average relative preload during fatigue tests

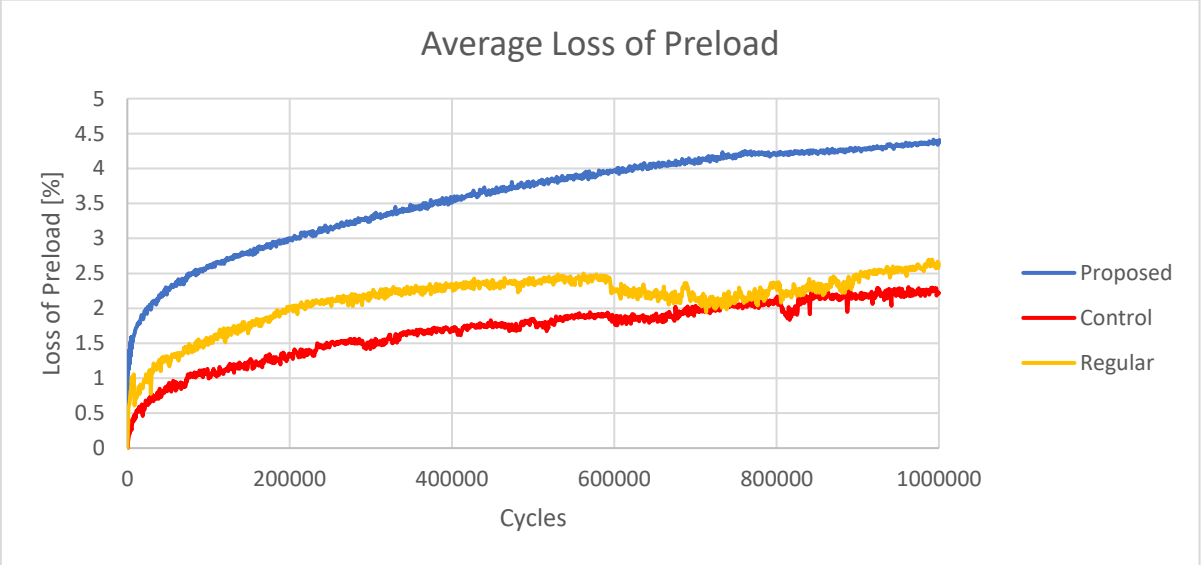

Figure 5.22 - Comparison of average loss of preload during fatigue tests

5.4.2 Slip

The average slip of each specimen was used, the graphs of which are shown in Figure 5.23, to minimize the impact of unwanted influences. When analysing these results it should be taken into account that the displacements measured were the relative displacements of the outer plates compared to the central plates. This means that these results are also affected by slip in the central connection. The proposed and control specimens had more interfaces compared to the regular specimen and as a result were influenced more by this problem. Looking at the graphs shows that the proposed connection suffered a bit more slip than the control specimen. This difference between the $0{,}081\ mm$ slip of the proposed specimen and the $0{,}078\ mm$ slip of the control specimen is $0{,}003\ mm$ at the end of the tests. A larger difference is found between the slip of these two specimens and the $0{,}052\ mm$ slip of the regular specimen. This ends up at a difference of $0{,}029\ mm$ and $0{,}026\ mm$ slip between the regular specimen and the proposed and control specimens respectively.

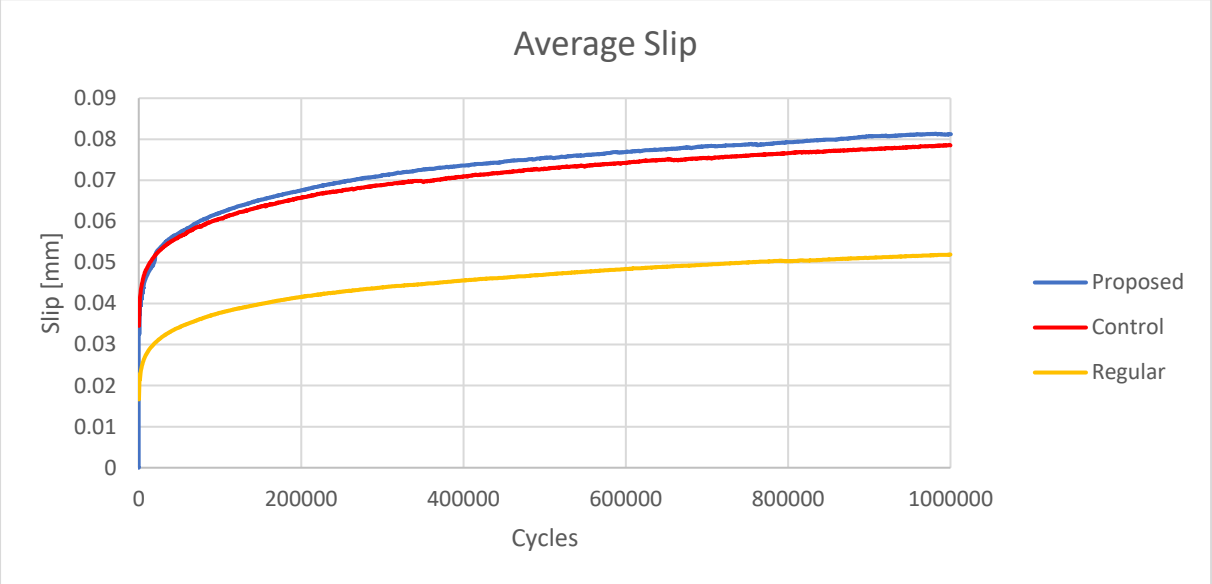

Figure 5.23 - Comparison of average slip during fatigue tests

6 CONCLUSIONS AND RECOMMENDATIONS

6.1 CONCLUSIONS

The impact that the bolt hole size and nominal hole clearance have on the slip and relaxation behaviour of High Strength Friction Grip bolted connections was studied in this thesis. To achieve this, a proposed novel HSFG bolted connection with significantly oversized holes was designed. This design included cover plates to span the large holes. Two more connections were designed, a control connection that was identical to the proposed connection with the exception of using normal sized holes instead of significantly oversized holes and a regular HSFG bolted connection that had normal sized bolt holes and did not have cover plates. These three connections were subjected to Finite Element Analysis and experimental tests. The collected data was used to form the following conclusions.

6.1.1 Conclusions on the static slip behaviour of the connections based on numerical results

The static slip behaviour of all three connections was simulated using Finite Element Models made in Abaqus. The results of the Finite Element Analysis are used to form conclusions on this behaviour.

- The joint friction resistance of the proposed, control and regular connections increased by $21{,}5\%$, $15{,}9\%$ and $27{,}1\%$ respectively when comparing the $321\ kN$ preload case to the $200\ kN$ preload case.
- The slip load of the outer connections in the proposed, control and regular connections increased by $21{,}6\%$, $16{,}4\%$ and 28% respectively when comparing the $321\ kN$ preload case to the $200\ kN$ preload case. These increases mirror the respective increases in joint friction resistance and signify that these joint friction resistance increases are caused by the increase in slip load in the outer connections as a consequence of the higher preload.
- The differences between the control and regular connections show that the use of thick cover plates and by extent a larger clamping length and an increased number of faying surfaces reduces the slip load of the outer connection by $17{,}2\%$ and $28{,}9\%$ at $200\ kN$ and $321\ kN$ preload respectively. This is a consequence of the longer bolt rod bending more and the increased number of faying surfaces that can slip. These detrimental influences increase the difference by $11{,}7\%$ when the preload is increased by $121\ kN$. These influences cause the slip load of the control connection to be nearly 30% lower than the regular connection at design preloads, which is a significant reduction.
- The smaller faying surface area as a consequence of the larger bolt holes in the proposed connection reduces the slip load of the outer connection by $5{,}2\%$ and $0{,}7\%$ at $200\ kN$ and $321\ kN$ preload respectively. It is concluded that this difference is reduced by $4{,}5\%$ when the preload is increased by $121\ kN$ and more importantly, that the difference is nearly zero at design preloads.

- The numerical force-displacements graphs were also differentiated to calculate the stiffness of the connections prior to plastic deformation occurring. This resulted in approximate values of the initial stiffnesses, which are $850\ kN/mm$, $950\ kN/mm$ and $1350\ kN/mm$ for the proposed, control and regular connections respectively. The difference in stiffness between the proposed and control connections shows that the smaller faying surfaces reduced the stiffness of the connection by roughly 10%. The difference in stiffness between the control and regular connections shows that the introduction of the cover plates, and thus a larger clamping length and additional interfaces reduced the stiffness of the connection by roughly 30%.
- When comparing the slip loads of the outer connections found using numerical analysis to the slip resistances calculated using EN 1993-1-8 it is concluded that at $200\ kN$ preload the design calculations underestimate the slip resistance of the connections and at $321\ kN$ preload the design calculations overestimate the slip resistance of the connections.

6.1.2 Conclusions on the loss of preload in the connections based on previous research and experimental results

The experimental results of the preload in the bolt rods was measured during a 24 hour short term relaxation test and during a cyclic fatigue loading test. A major influence factor that is taken into account is the reuse of parts with damaged coating layers caused by the control specimen tests.

- From existing research it is known that the thickness of the coating layer plays a major role in the loss of preload, as a doubling of the coating thickness can increase the loss of preload due to embedding by as much as 60% (Friede & Lange, 2010, p. 290).
- The reuse of parts with damaged and partially embedded coating layers during the control tests provided these tests with beneficial conditions by reducing the coating thickness of 55% of the coated interface areas before they started (See appendix A for calculations).
- The use of larger holes reduced the coated interface areas by 20% (See appendix A for calculations).
- Based on these points it is expected that the influence of larger bolt holes is of a smaller magnitude than the influence of the damaged coating.
- The lack of cover plates in the regular specimen meant that the number of $60\ \mu m$ thick coating layers was reduced from 14 to six. This meant that the total thickness of the clamped coating layers was reduced from $840\ \mu m$ to $360\ \mu m$, a reduction of 57%. Based on this it is expected for the regular specimen to have a smaller loss of preload compared to the other two specimens.

Short term relaxation:

- The proposed and control specimens lost respectively $15\ kN$ and $7\ kN$ of preload during short term relaxation. Due to both unwanted influences and different starting preloads it is beneficial to express the loss of preload as a percentage of the initial preload present in the bolts. This results in the proposed specimen losing 7% preload and the control specimen losing 4%.
- Taking both the results and the conditions into account it is concluded that the 3% increase in the loss of preload of the proposed specimen compared to the control specimen is predominantly caused by the difference in coating thickness.

- Based on this it is expected for the larger bolt holes to increase the loss of preload during short term relaxation by roughly 1%.
- To confirm these conclusions, new experiments that exclude differences in coating thickness are needed.

Loss of preload during fatigue loading:

- Comparison of the results is difficult due to the large differences in starting preloads and conditions during the experiments. To compensate for this the preload losses are expressed as a percentage of the starting preload. This results in the proposed specimen losing $4{,}4\%$ of its preload and the control and regular specimens losing $2{,}2\%$ and $2{,}6\%$ respectively.
- Comparing the proposed specimen to the control and regular specimens results in respectively $2{,}2\%$ and $1{,}8\%$ more preload loss. Taking the favourable conditions of these specimens compared to the proposed specimen into account shows that these differences are largely caused by the difference in total clamped coating thickness present in the connections.
- Based on this it is expected for the larger bolt holes to increase the loss of preload during fatigue loading by less than 1%.
- New experiments that use undamaged parts are needed to confirm this conclusion.

6.1.3 Conclusions on the fatigue slip behaviour of the connections based on experimental results

The experimental results of the slip in the connections were measured by documenting the relative displacement of the outer plates compared to the central plates during fatigue loading tests of the specimens consisting of 1 million cycles with a force range of $+2{,}5\ kN$ to $+30\ kN$ per connection. This means that slip and displacement at other points of the test specimens influenced the results.

- The displacement results of the four LVDTs that measure the slip in the four outer connections were averaged for each specimen. This results in the proposed and control specimens suffering $0{,}081\ mm$ and $0{,}078\ mm$ of slip respectively. The regular specimen received $0{,}052\ mm$ of slip.
- The resulting differences are an increase of $0{,}003\ mm$ slip when comparing the proposed specimen to the control specimen and an increase of $0{,}026\ mm$ when comparing the control specimen to the regular specimen.
- The lower slip of the regular specimen compared to the proposed and control specimens is in majority caused by the smaller number of interfaces in the connection. This is clearly shown by the $0{,}026\ mm$ slip difference between the regular and control specimens which only differ by the presence of the cover plates in the control specimen.
- If the measuring conditions and the difference in preload conditions are considered when comparing the proposed specimen to the control specimen, the difference of $0{,}003\ mm$ will be further reduced. The fatigue slip behaviour of the proposed and control specimens is thus nearly identical under these conditions.
- To confirm that these specimens behave identical in all fatigue loading situations, experiments at different load ranges are required.

6.1.4 Conclusions on the viability and application of the connections

Based on the collected data and previous conclusions the following can be concluded regarding the viability and application of the connections:

- The $200\ kN$ preload present in the bolts during the fatigue tests must be considered when comparing the slip results of the proposed and control specimens. The numerical FEA results show that the static slip behaviours of the proposed and control connections become nearly identical at the design preload of $321\ kN$. Based on this information and the small difference in fatigue slip found, it is expected for the fatigue slip behaviour of the proposed and control specimens to be nearly identical when design preloads are applied. It can thus be concluded that the bolt hole size has nearly no influence on the static and fatigue slip behaviour of HSFG bolted connections that include cover plates.
- The comparisons of preload loss between the proposed and control specimens showed that during both short term relaxation and fatigue loading, the influence of the larger holes increased the loss of preload by less than 1%. Based on this, it is concluded that the hole size has nearly no impact on the loss of preload in a HSFG bolted connection with cover plates.
- Based on these results it is concluded that the use of significantly oversized bolt holes in HSFG bolted connections with cover plates is viable and does not impact the slip behaviour or loss of preload under static or fatigue loading in a significant way.
- The comparison in static and fatigue slip behaviour of the control and regular connections reveals the negative influences of the use of thick cover plates. The FEA numerical results show a 30% decrease in both the slip load and stiffness of the connection when implementing thick cover plates. The experimental test results indicate a 50% increase in slip under fatigue loading when thick cover plates are used. It is concluded based on these results that an alternative for thick cover plates is needed if HSFG bolted connections are to be used in bolted connections with significantly oversized holes.
- An alternative to thick cover plates that removes their detrimental influences is the use of large disc springs. These disc springs would need to have an outer diameter of roughly three times the bolt diameter to span the hole and provide a large enough faying surface. The use of these disc springs has several benefits. Disc springs would not need and extra washer between the disc spring and the bolt nut, which reduces the clamping thickness and number of interfaces. The reduced clamping thickness also reduces the required clamping length.

6.2 RECOMMENDATIONS

With the knowledge that the slip behaviour and the loss of preload of the proposed connection is nearly identical to the control connection under the used static and fatigue conditions, it is viable for more experiments to be conducted under different loading conditions to confirm these initial conclusions and more precisely quantify the influence of the hole size on the slip behaviour and the loss of preload.

Regarding the viability of the proposed connection compared to regular HSFG bolted connections, it is recommended to conduct experimental research on specimens that use large disc springs rather than thick cover plates.

The following recommendations consist of lessons learned from the conducted experiments, specific new experiments to confirm or rule out certain influences and alternative and improved test setups to prevent the problems that happened during the experiments from occurring in future experiments (see Appendix D for small recommendations specific to the use of the existing specimens).

6.2.1 General recommendations

Embedding of interfacing surfaces and especially coated surfaces influenced the results significantly due to the lower magnitude of the influences that were the focus of this research. It is thus preferred for each test specimen to be comprised of new and unused parts to prevent any damage incurred during an experiment from influencing subsequent tests.

It is unknown how much influence the location of the load application had on the results of the experiments. It is recommended to document this for any future experiments. Based on the results it can be concluded if the point of force application was the culprit or if noise in the strain gauge was the cause.

Similarly, to what extent the interactions between the bolt rods and hole edges influenced the results of the control and regular tests is unknown. It is advised to conduct an experiment to confirm this and for all future experiments to centre the bolt rods during preloading.

As the conclusions in this thesis regarding the static slip behaviour of the connections are based on numerical analysis, it is recommended to confirm these conclusions using experimental tests.

6.2.2 Recommended test setups

Improvements can be made to the measuring setup used in this thesis. The main difference in setup from the tests conducted in this thesis is the method of measuring slip. The slip that was measured in the conducted experiments is significantly influenced by slip of the central connection and the numerous interfaces present. To negate these influences the difference in displacement between the outer plates and cover plates needs to be known, rather than the difference in displacement between the central plate and outer plates. Three options are presented here to accomplish this.

The first option will be to place LVDTs on the outer plates and record the displacement of the cover plates relative to the outer plates, as shown in the left and middle drawings of Figure 6.1. This will negate the influence of slip in other interaction planes. A downside is the space required to place the LVDTs.

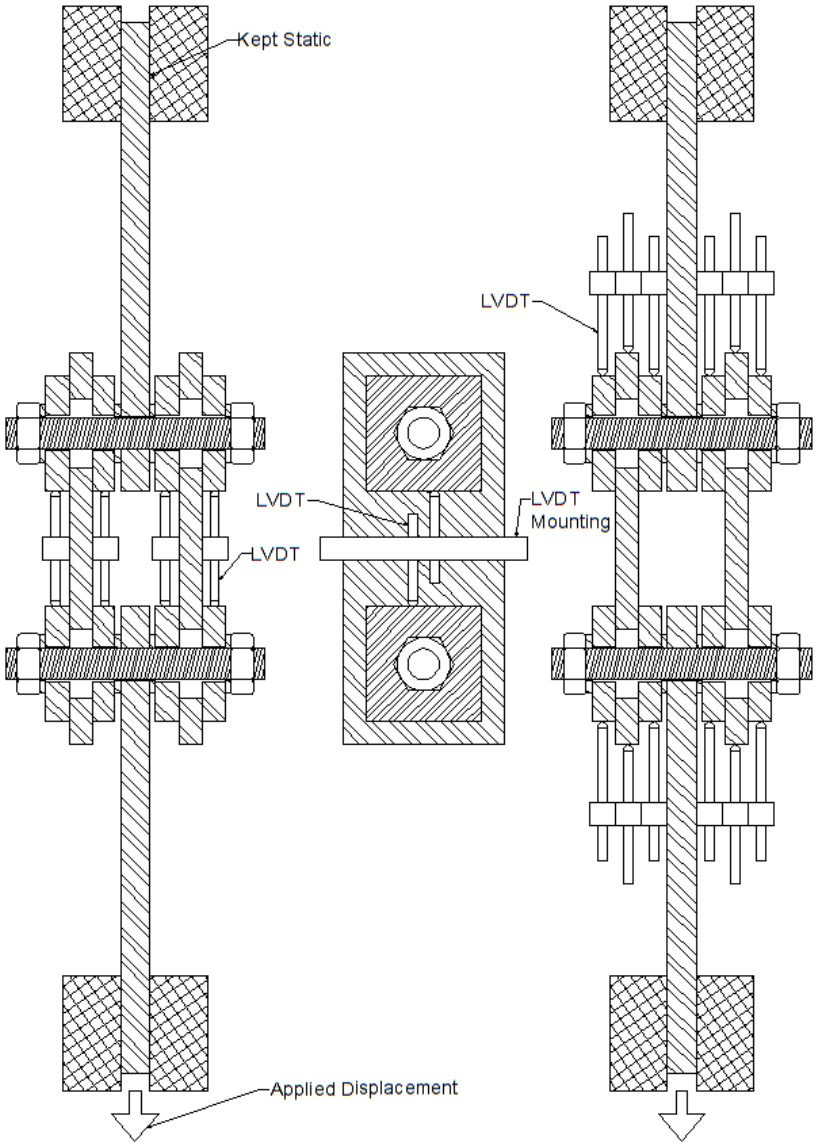

Figure 6.1 - Proposed measuring setups: Left) Option 1; Middle) Sideview option 1; Right) Option 2

The second option keeps the LVDTs that measure the relative displacement between the central plate and outer plates and adds two more LVDTs per outer connection. These will measure the relative displacement between the central plate and both cover plates individually. With this data the slip of each individual cover plate can be determined. The setup for this option is shown in the right drawing of Figure 6.1. The main downside of this setup is the number of LVDTs needed.

A third option is to use Three-Dimensional Digital Image Correlation (3D-DIC) using cameras rather than LVDTs. This is accomplished by observing an applied dot pattern on the side of the test specimen using two cameras. The resulting data are evaluated by correlating the images using a specialised program. The slip of the cover plates can be extracted from this evaluated data.

When comparing all three options, the third one is preferable due to its more accurate results. In the case that DIC is not possible, the first option is preferable due to the lower number of LVDTs required and more direct collection of data. A problem with this setup for the existing specimens is a lack of space. There is not enough space in between the cover plates for the placement of LVDTs on the outer plates. For this reason, the use of the second option is required for the existing specimens if DIC is not available.

Different test setups will broaden the knowledge on the proposed connections behaviour. The choice for the used connection design was in the interest of gathering the most results in a short time. A non-symmetrical design will better simulate the application of the proposed connection as a shear connector. A symmetrical design with the tested connection in the centre will provide more accurate results due to the lack of outside interference and the direct measuring of the relative displacement of the cover plates compared to the central plate. A sketch of both connections is shown in Figure 6.2.

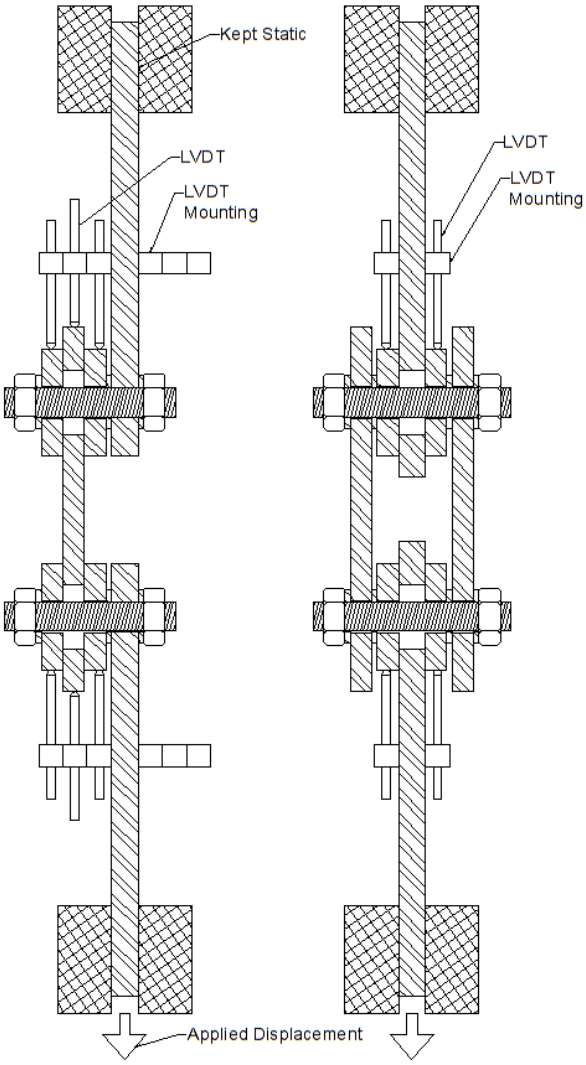

Figure 6.2 - Alternative test specimens: Left) Non-symmetrical design; Right) Single central connection design

Whereas the experiments in this thesis made use of cover plates and disc springs, preference for future experiments goes towards large disc springs. It will make for a better comparison between the proposed specimen and the regular specimen. A sketch of this proposed change is shown in Figure 6.3 next to a sketch of the regular specimen. Due to the relatively thin disc springs, the preferred method to measure the slip is 3D-DIC.

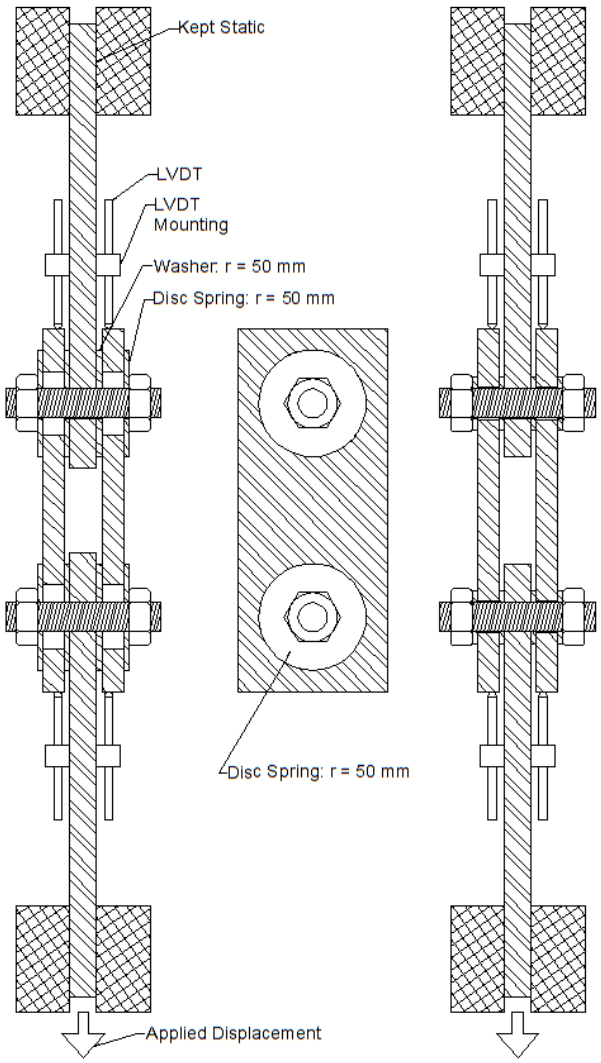

Figure 6.3 - Left) Specimen with large washers and disc springs; Middle) Side view of this specimen; Right) Regular specimen

BIBLIOGRAPHY

Abid, M., Khalil, M. S., & Wajid, H. A. (2015). AN EXPERIMENTAL STUDY ON THE RELAXATION OF BOLTS. *IIUM Engineering Journal*, *16*(1). https://doi.org/10.31436/iiumej.v16i1.539

Chen, Y. T., Zhao, Y., West, J., & Walbridge, S. (2014). Behaviour of steel–precast composite girders with through-bolt shear connectors under static loading. *Journal of Constructional Steel Research*, *103*, 168–178. https://doi.org/10.1016/j.jcsr.2014.09.001

Correia, J. A. F. D. O., Pedrosa, B. A. S., Raposo, P. C., De Jesus, A. M. P., dos Santos Gervásio, H. M., Lesiuk, G. S., da Silva Rebelo, C. A., Calçada, R. A. B., & da Silva, L. A. P. S. (2017). Fatigue Strength Evaluation of Resin-Injected Bolted Connections Using Statistical Analysis. *Engineering*, *3*(6), 795–805. https://doi.org/10.1016/j.eng.2017.12.001

Cullimore, M. S. G. (1982). Fatigue of HSFG Bolted Joints: Effects of Design Parameters. *IABSE Reports*, *37*, 715–723. https://doi.org/10.5169/seals-28974

Dallam, L. N. (1968). High Strength Bolt Shear Connectors -Pushout Tests. *ACI Journal Proceedings*, *65*(9). https://doi.org/10.14359/7511

Dedic, D. J., & Klaiber, W. F. (1984). High strength bolts as shear connectors in rehabilitation work. *Concrete International*, *6*(7), 41–46. https://www.concrete.org/publications/internationalconcreteabstractsportal/m/details/id/15012

Dörre, M., Glienke, R., Schwarz, M., & Henkel, K. (2022). Slip resistance of bolted joints with slotted holes. *Materialwissenschaft Und Werkstofftechnik*, *53*(2), 139–155. https://doi.org/10.1002/mawe.202100206

Eccles, B. (2011). *Bolt Science*. Retrieved from Self-Loosening of Threaded Fasteners: https://www.boltscience.com/pages/self-loosening-of-threaded-fasteners.pdf

Friede, R., & Lange, J. (2010). *Loss of preload in bolted connections due to embedding and self loosening*. Institut for Steel Structures and Material Mechanics, Technische Universität Darmstadt, Germany. http://www.labciv.eng.uerj.br/sdss2010/files/sdss_rio_2010_4_15.pdf

German Institute for Standardization. (2009). *Conical spring washers for bolted connections* (DIN 6796). https://www.en-standard.eu/din-6796-conical-spring-washers-for-bolted-connections/

Goodier, J. N., & Sweeney, R. J. (1945). Loosening by vibration of threaded fastenings. *Mechanical Engineering*, *67*(12), 798–802. https://archive.org/details/sim_mechanical-engineering_1945-12_67_12/page/n1/mode/2up

Gribnau, K. (2021, June). *Shear force in bolted connections for hybrid steel-FRP bridges: Due to traffic, temperature and fatigue loading* (Thesis). Delft University of Technology. http://resolver.tudelft.nl/uuid:a6250270-77b4-4ee3-9495-fc1aeac84813

Hawkins, N. M. (1987). Strength in shear and tension of cast-in-place anchor bolts. *American Concrete Institute, ACI Special Publication*, *SP-103*, 233–255. https://www.concrete.org/publications/internationalconcreteabstractsportal/m/details/id/1677

Heistermann, C. (2011). *Behaviour of pretensioned bolts in friction connections : towards the use of higher strength steels in wind towers* (Licentiate dissertation). Luleå tekniska universitet. http://urn.kb.se/resolve?urn=urn:nbn:se:ltu:diva-17672

Heistermann, C., Veljkovic, M., Simões, R., Rebelo, C., & Simões da Silva, L. (2013). Design of slip resistant lap joints with long open slotted holes. *Journal of Constructional Steel Research*, *82*, 223–233. https://doi.org/10.1016/j.jcsr.2012.11.012

Husson, W. (2008). *Friction connections with slotted holes for wind towers* (Licentiate dissertation). Luleå tekniska universitet. http://urn.kb.se/resolve?urn=urn:nbn:se:ltu:diva-17866

Junker, G. H. (1969). New Criteria for Self-Loosening of Fasteners Under Vibration. *SAE Transactions*, *78*, 314–335. https://www.jstor.org/stable/44563013

Kozma, A., Odenbreit, C., Braun, M., Veljkovic, M., & Nijgh, M. (2019). Push-out tests on demountable shear connectors of steel-concrete composite structures. *Structures*, *21*, 45–54. https://doi.org/10.1016/j.istruc.2019.05.011

Kwon, G., Engelhardt, M. D., & Klingner, R. E. (2010). Behavior of post-installed shear connectors under static and fatigue loading. *Journal of Constructional Steel Research*, *66*(4), 532–541. https://doi.org/10.1016/j.jcsr.2009.09.012

Massachusetts Institute of Technology. (n.d.-a). *Definition of the stability limit*. Retrieved 1 December 2022, from https://abaqusdocs.mit.edu/2017/English/SIMACAEGSARefMap/simagsa-c-ovwdefinition.htm

Massachusetts Institute of Technology. (n.d.-b). *Mass scaling*. Retrieved 22 September 2022, from https://abaqus-docs.mit.edu/2017/English/SIMACAEGSARefMap/simagsa-c-qsimasscaling.htm

Massachusetts Institute of Technology. (n.d.-c). *Quasi-Static Analysis with Abaqus/Explicit*. Retrieved 22 September 2022, from https://abaqus-docs.mit.edu/2017/English/SIMACAEGSARefMap/simagsa-m-Quasi-sb.htm

Netherlands Standardization Institute. (2006). *Eurocode 3: Design of steel structures - Part 1-8: Design of joints* (NEN-EN 1993-1-8:2006). https://www.nen.nl/en/nen-en-1993-1-8-2006-en-44903

Netherlands Standardization Institute. (2006). *Eurocode 3: Design of steel structures - Part 1-9: Fatigue* (NEN-EN 1993-1-9:2006). https://www.nen.nl/en/nen-en-1993-1-9-2006-en-44905

Netherlands Standardization Institute. (2006). *Design of composite steel and concrete structures - Part 1-1: General rules and rules for buildings* (NEN-EN 1994-1-1:2005). https://www.nen.nl/en/nen-en-1994-1-1-2005-en-64948

Netherlands Standardization Institute. (2018). *Execution of steel structures and aluminium structures - Part 2: Technical requirements for steel structures* (NEN-EN 1090-2:2018). https://www.nen.nl/en/nen-en-1090-2-2018-en-247888

Nijgh, M. P. (2016, October). *Loss of preload in pretensioned bolts* (Thesis). Delft University of Technology. http://resolver.tudelft.nl/uuid:4776e217-d7b7-4122-8e36-61ab7ed8c672

Nijgh, M. P. (2017, April). *New Materials for Injected Bolted Connections: A Feasibility Study for Demountable Connections* (Thesis). Delft University of Technology. http://resolver.tudelft.nl/uuid:089a5c6f-3c28-4c58-9b5a-34138bf2be86

Nijgh, M. P., Gîrbacea, I. A., & Veljkovic, M. (2019). Elastic behaviour of a tapered steel-concrete composite beam optimized for reuse. *Engineering Structures*, *183*, 366–374. https://doi.org/10.1016/j.engstruct.2019.01.022

Nijgh, M. P., & Veljkovic, M. (2020). Requirements for oversized holes for reusable steel-concrete composite floor systems. *Structures*, *24*, 489–498. https://doi.org/10.1016/j.istruc.2020.01.021

Nijgh, M. P., Xin, H., & Veljkovic, M. (2018, September). Non-linear hybrid homogenization method for steel-reinforced resin. *Construction and Building Materials*, *182*, 324–333. https://doi.org/10.1016/j.conbuildmat.2018.06.111

Ollgaard, J. G., Slutter, R. G., & Fisher, J. W. (1971). Shear Strength of Stud Connectors in Lightweight and Normal-Weight Concrete. *Engineering Journal*, *8*, 55–64. https://www.aisc.org/Shear-Strength-of-Stud-Connectors-in-Lightweight-and-Normal-Weight-Concrete

Pai, N., & Hess, D. (2002a). Experimental study of loosening of threaded fasteners due to dynamic shear loads. *Journal of Sound and Vibration*, *253*(3), 585–602. https://doi.org/10.1006/jsvi.2001.4006

Pai, N., & Hess, D. (2002b). Three-dimensional finite element analysis of threaded fastener loosening due to dynamic shear load. *Engineering Failure Analysis*, *9*(4), 383–402. https://doi.org/10.1016/s1350-6307(01)00024-3

Pavlović, M., Marković, Z., Veljković, M., & Buđevac, D. (2013). Bolted shear connectors vs. headed studs behaviour in push-out tests. *Journal of Constructional Steel Research*, *88*, 134–149. https://doi.org/10.1016/j.jcsr.2013.05.003

Satasivam, S., Feng, P., Bai, Y., & Caprani, C. (2017). Composite actions within steel-FRP composite beam systems with novel blind bolt shear connections. *Engineering Structures*, *138*, 63–73. https://doi.org/10.1016/j.engstruct.2017.01.068

Sauer, J. A., Lemmon, D. C., & Lynn, E. K. (1950). Bolts: How to prevent their loosening. *Machine Design*, *22*(8), 133–139. https://archive.org/details/sim_machine-design_1950-08_22_8/mode/2up

Suwaed, A. S., & Karavasilis, T. L. (2020). Demountable steel-concrete composite beam with full-interaction and low degree of shear connection. *Journal of Constructional Steel Research*, *171*, 106152. https://doi.org/10.1016/j.jcsr.2020.106152

Wijesiri Pathirana, S., Uy, B., Mirza, O., & Zhu, X. (2016). Flexural behaviour of composite steel–concrete beams utilising blind bolt shear connectors. *Engineering Structures*, *114*, 181–194. https://doi.org/10.1016/j.engstruct.2016.01.057

Xin, H., Nijgh, M., & Veljkovic, M. (2019, February). Computational homogenization simulation on steel reinforced resin used in the injected bolted connections. *Composite Structures*, *210*, 942–957. https://doi.org/10.1016/j.compstruct.2018.11.069

Yang, F., Liu, Y., Jiang, Z., & Xin, H. (2018). Shear performance of a novel demountable steel-concrete bolted connector under static push-out tests. *Engineering Structures*, *160*, 133–146. https://doi.org/10.1016/j.engstruct.2018.01.005

Zhou, A., & Keller, T. (2005). Joining techniques for fiber reinforced polymer composite bridge deck systems. *Composite Structures*, *69*(3), 336–345. https://doi.org/10.1016/j.compstruct.2004.07.016

APPENDIX A. HAND CALCULATIONS

Design calculations based on EN 1993-1-8 and EN 1993-1-9.

Design calculations using a preload of $321\ kN$

Design preload force bolt:

- Grade 10.9: f_{ub} $= 1000\ N/mm^2$
- M27: A_s $= 459\ mm^2$
- Preload: $F_{p;C} = 0{,}7 * f_{ub} * A_s$ $= 321{,}3\ kN$

Design slip resistance outer plates:

- Bolt in oversized hole: k_s $= 0{,}85$
- Friction coefficient: μ $= 0{,}40$
- Number of surfaces: n $= 4$
- Safety factor: γ_{M3} $= 1{,}35$
- Slip resistance: $F_{s;Rd} = \frac{k_s * n * \mu}{\gamma_{M3}} * F_{p;C}$ $= 323{,}7\ kN$
- Slip resistance per connection: $F_{s_{Rd}} = \frac{323{,}7}{2}$ $= 161{,}8\ kN$

Design slip resistance central plate:

- Bolt in regular hole: k_s $= 1{,}00$
- Friction coefficient: μ $= 0{,}40$
- Number of surfaces: n $= 2$
- Safety factor: γ_{M3} $= 1{,}35$
- Slip resistance: $F_{s;Rd} = \frac{k_s * n * \mu}{\gamma_{M3}} * F_{p;C}$ $= 190{,}4\ kN$

Bolt shear resistance:

- Completely threaded rod: α_v $= 0{,}5$
- Safety factor γ_{M2} $= 1{,}25$
- Shear resistance: $F_{v;Rd} = \frac{\alpha_v * f_{ub} * A_s}{\gamma_{M2}}$ $= 183{,}6\ kN$

Bearing resistance central plate:

- S355: f_u $= 490\ N/mm^2$
- Thickness: t $= 25mm$
- Hole diameter: d_0 $= 28mm$
- e_1 $= 50mm$
- e_2 $= 50mm$
- $\alpha_d = \frac{e_1}{3 * d_0}$ $= 0{,}60$
- $a_b = \min\left(\alpha_d; \frac{f_{ub}}{f_u}; 1{,}0\right)$ $= 0{,}60$
- $k_1 = \min\left(2{,}8\frac{e_2}{d_0} - 1{,}7; 2{,}5\right)$ $= 2{,}5$
- Bearing resistance: $F_{b,Rd} = \frac{k_1 * \alpha_b * f_u * d * t}{\gamma_{M2}}$ $= 396{,}9\ kN$

The force ranges of both plates for fatigue results:

- Outer plates: $\Delta F = 65kN$
- Central plate: $\Delta F = 130kN$

Outer plate proposed and control

The reference value of this connection is $\Delta\sigma_C = 112\ N/mm^2$ (EN 1993-1-9 table 8.1 detail 8) resulting in:

- Reference value: $\Delta\sigma_C = 112\ N/mm^2$
- Constant amplitude fatigue limit: $\Delta\sigma_D = 0{,}737 * 112 = 82{,}5\ N/mm^2$
- Cut off limit: $\Delta\sigma_L = 0{,}549 * 82{,}5 = 45{,}3\ N/mm^2$

The stress range in the gross cross-section of this plate is:

- Gross cross-section: $A_{gross} = 20 * 140 = 2800\ mm^2$
- Stress range: $\Delta\sigma = \frac{65000N}{2800mm^2} = 23{,}2\ N/mm^2$

Central plate

The reference value of this connection is $\Delta\sigma_C = 112\ N/mm^2$ (EN 1993-1-9 table 8.1 detail 8) resulting in:

- Reference value: $\Delta\sigma_C = 112\ N/mm^2$
- Constant amplitude fatigue limit: $\Delta\sigma_D = 0{,}737 * 112 = 82{,}5\ N/mm^2$
- Cut off limit: $\Delta\sigma_L = 0{,}549 * 82{,}5 = 45{,}3\ N/mm^2$

The stress range in the gross cross-section of this plate is:

- Gross cross-section: $A_{gross} = 25 * 100 = 2500\ mm^2$
- Stress range: $\Delta\sigma = \frac{130000N}{2500mm^2} = 52\ N/mm^2$

Bolt rod

The reference value of this connection is $\Delta\sigma_C = 100\ N/mm^2$ (EN 1993-1-9 table 8.1 detail 15) resulting in:

- Reference value: $\Delta\sigma_C = 100\ N/mm^2$
- Constant amplitude fatigue limit: $\Delta\sigma_D = 0{,}737 * 100 = 73{,}7\ N/mm^2$
- Cut off limit: $\Delta\sigma_L = 0{,}549 * 73{,}7 = 40{,}5\ N/mm^2$

The stress range in the gross cross-section of this plate is:

- Cross-section: $A_s = 459\ mm^2$
- Stress range: $\Delta\tau = \frac{130000N}{459mm^2} = 283{,}2\ N/mm^2$

Design calculations using a preload of $200\ kN$

Design slip resistance outer plates:

- Bolt in oversized hole: k_s $= 0{,}85$
- Friction coefficient: μ $= 0{,}40$
- Number of surfaces: n $= 4$
- Safety factor: γ_{M3} $= 1{,}35$
- Slip resistance: $F_{s;Rd} = \frac{k_s * n * \mu}{\gamma_{M3}} * F_{p;C}$ $= 200{,}5\ kN$
- Slip resistance per connection: $F_{s;Rd} = \frac{200{,}5}{2}$ $= 100{,}25\ kN$

Design slip resistance central plate best case:

- Bolt in regular hole: k_s $= 1{,}00$
- Friction coefficient: μ $= 0{,}40$
- Number of surfaces: n $= 2$
- Safety factor: γ_{M3} $= 1{,}35$
- Slip resistance: $F_{s;Rd} = \frac{k_s * n * \mu}{\gamma_{M3}} * F_{p;C}$ $= 118{,}5\ kN$

Design slip resistance central plate worst case:

- Bolt in regular hole: k_s $= 1{,}00$
- Friction coefficient: μ $= 0{,}30$
- Number of surfaces: n $= 2$
- Safety factor: γ_{M3} $= 1{,}35$
- Slip resistance: $F_{s;Rd} = \frac{k_s * n * \mu}{\gamma_{M3}} * F_{p;C}$ $= 89\ kN$

Bolt shear resistance:

- Completely threaded rod: α_v $= 0{,}5$
- Safety factor: γ_{M2} $= 1{,}25$
- Shear resistance: $F_{v;Rd} = \frac{\alpha_v * f_{ub} * A_S}{\gamma_{M2}}$ $= 183{,}6\ kN$

Coated area of specimens

- Cover plate surface area: $A_{cover} = 100 * 100 = 10000\ mm^2$
- Washer surface area: $A_{washer} = \pi * 25^2 = 2000\ mm^2$
- Surface area normal hole: $A_{normal\ hole} = \pi * 15^2 = 700\ mm^2$
- Surface area large hole: $A_{large\ hole} = \pi * 30^2 = 2800\ mm^2$

Total coated interface area:

- $A_{total} = 8 * A_{cover} + 6 * A_{washer} - 14 * A_{normal\ hole} = 82.200\ mm^2$

Partially compress coated interface area:

- $A_{compressed} = 4 * A_{cover} + 6 * A_{washer} - 10 * A_{normal\ hole} = 45.000\ mm^2$

Total coated interface area with large holes:

- $A_{less} = A_{total} - 8 * (A_{large\ hole} - A_{normal\ hole}) = 65.400\ mm^2$

Reduction in contact area with large holes:

- $100\% - \left(\frac{A_{less}}{A_{total}}\right) * 100 \cong 20\%$

Area of total coated area that is compressed:

- $\frac{A_{compressed}}{A_{total}} * 100 \cong 55\%$

APPENDIX B. ADDITIONAL GRAPHS

FEA Stiffness graphs:

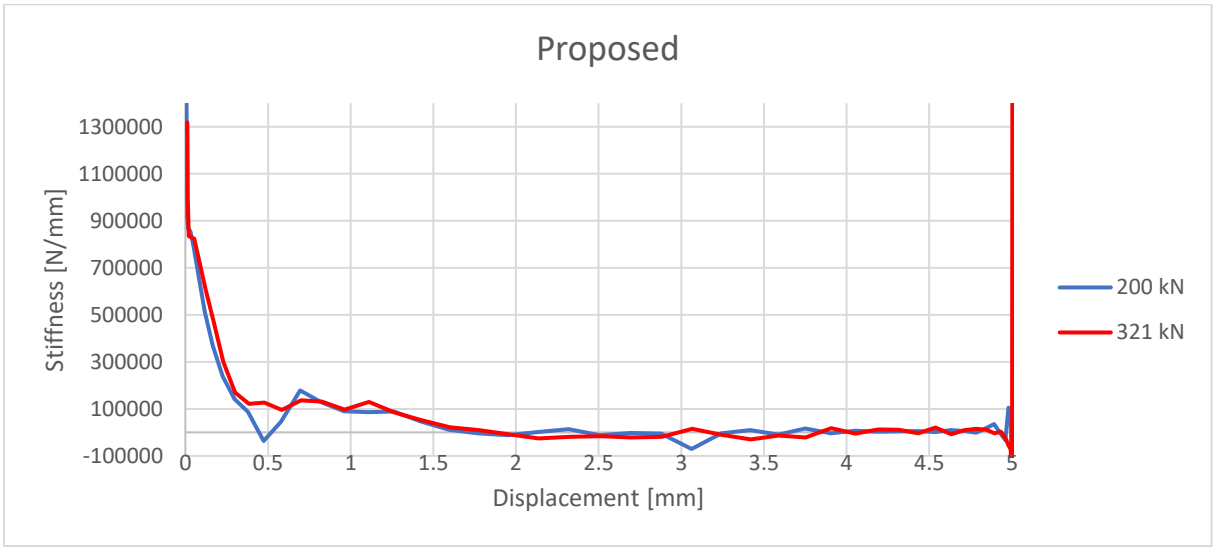

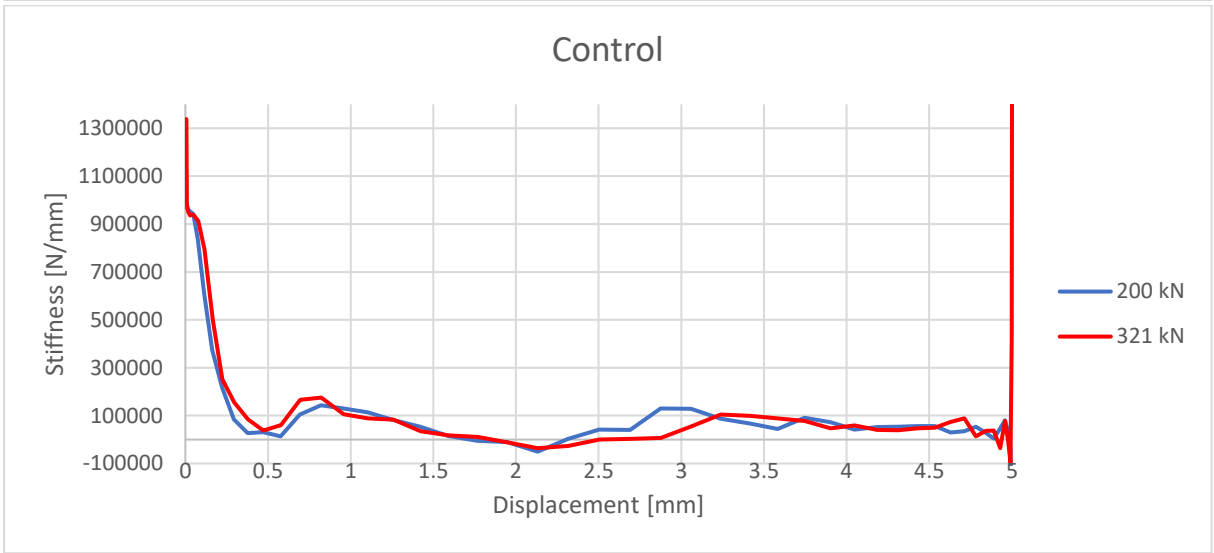

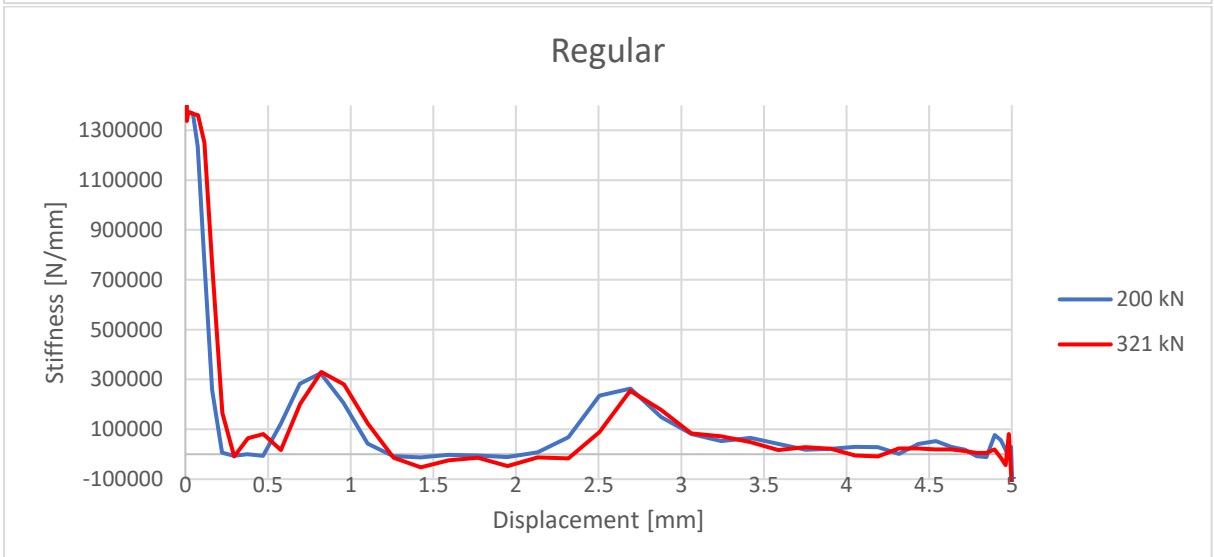

FEA Stiffness comparison graphs:

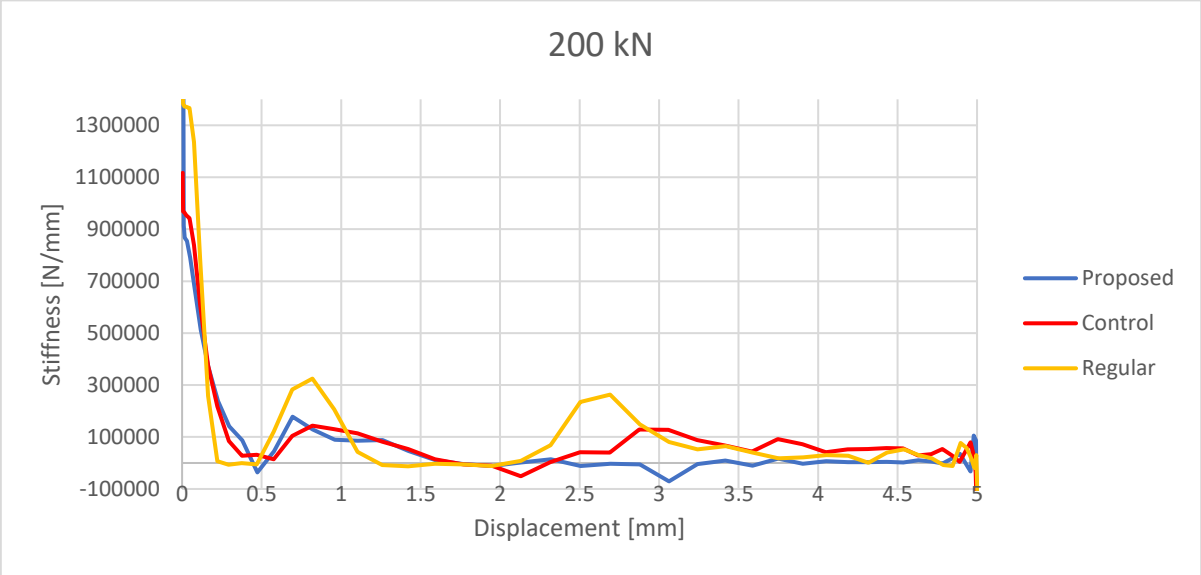

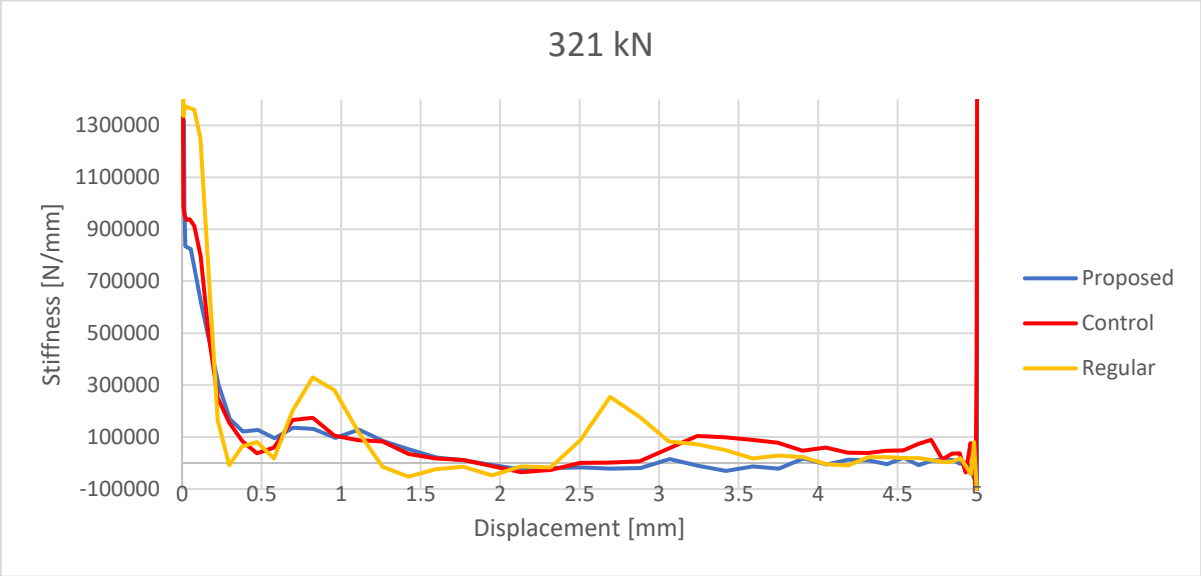

Relative preload short term relaxation:

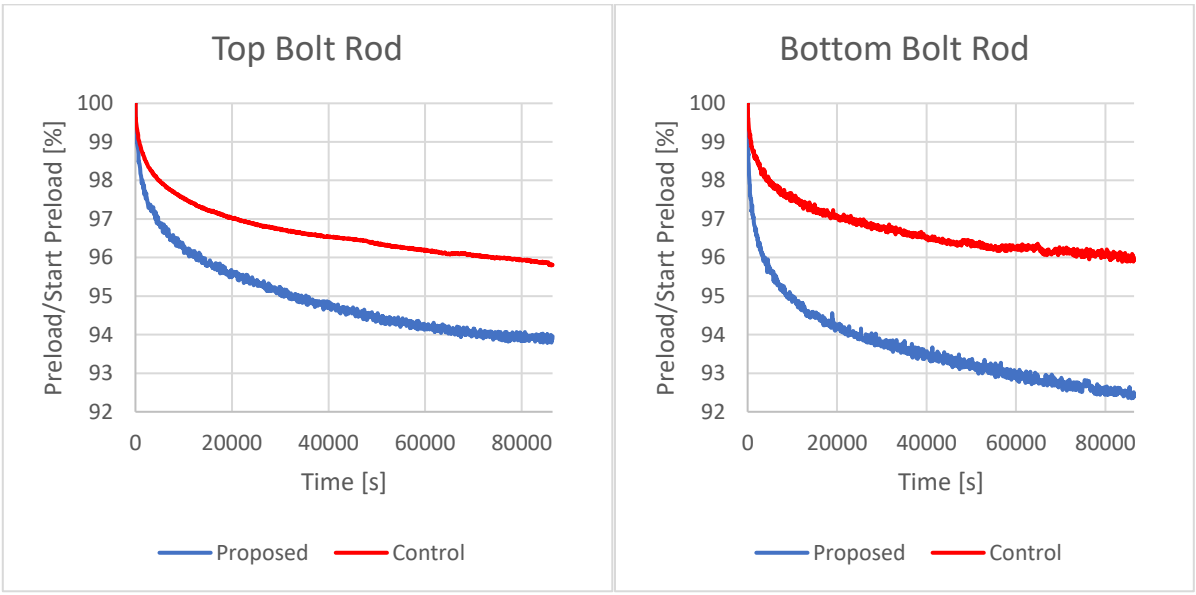

Length gain short term relaxation:

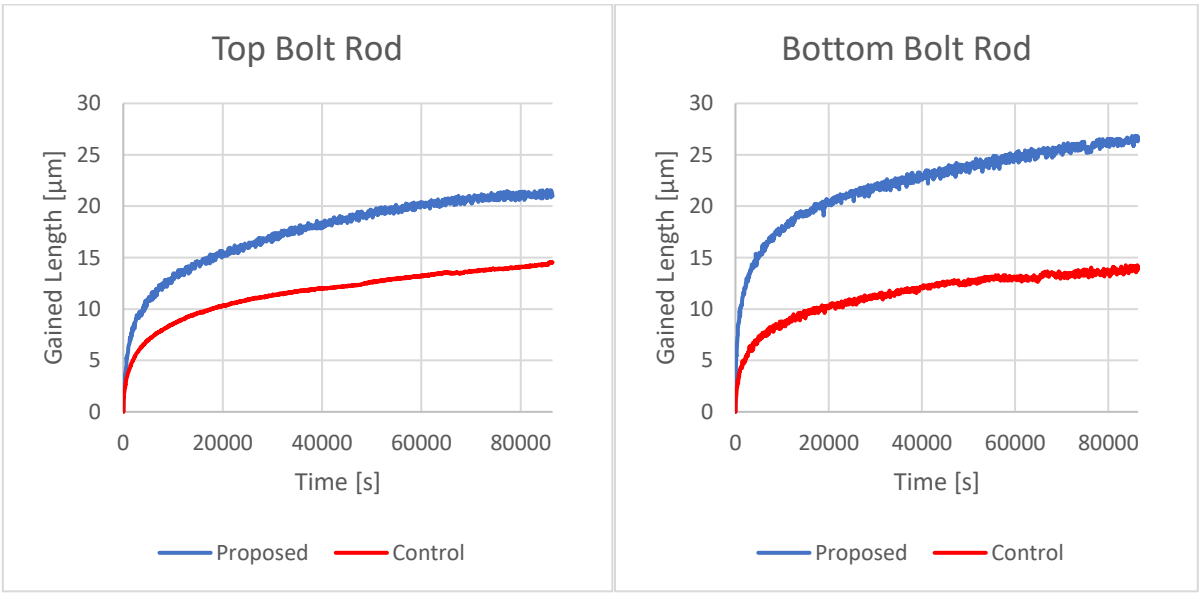

APPENDIX C. ABAQUS MODEL IMAGES

Proposed deformed (Top: $200\ kN$; Bottom: $321\ kN$):

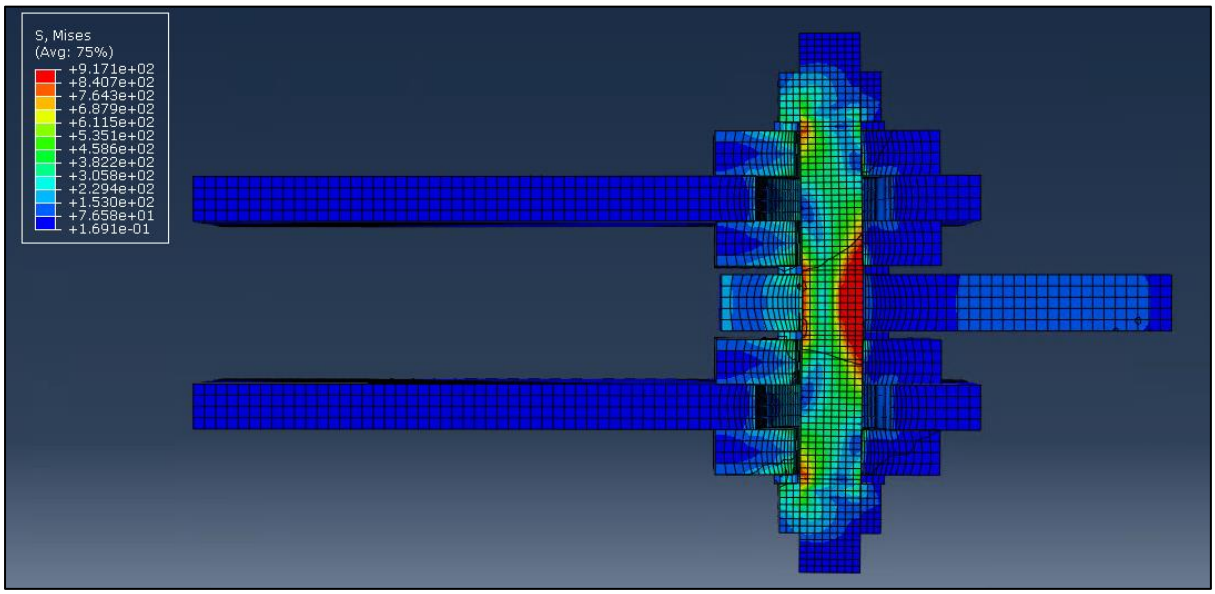

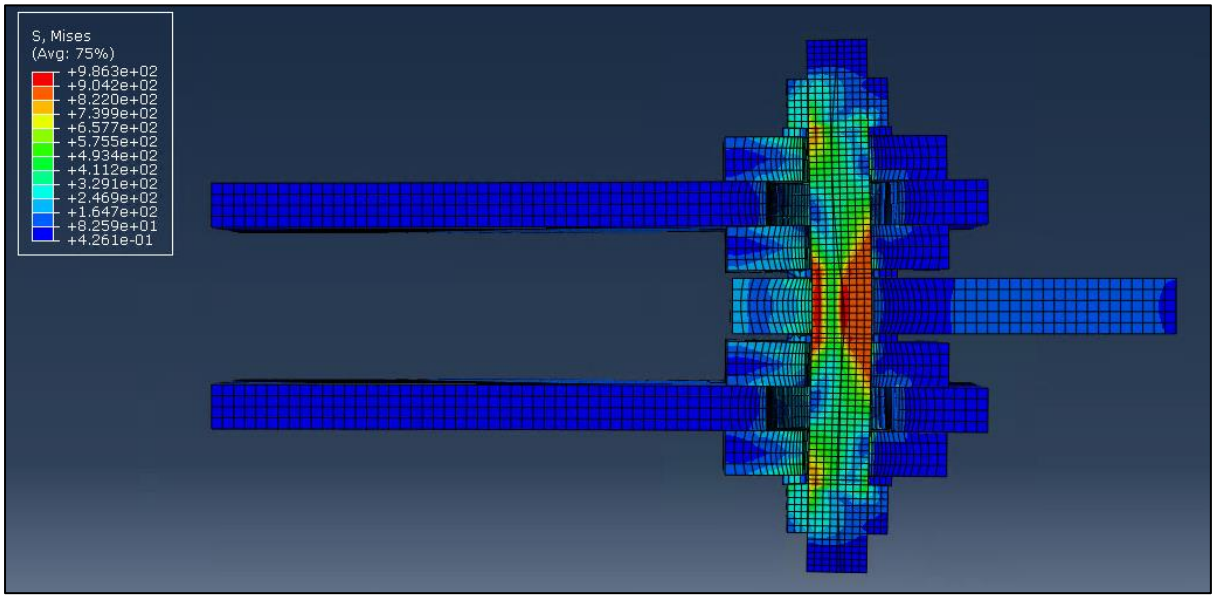

Control deformed (Top: $200\ kN$; Bottom: $321\ kN$):

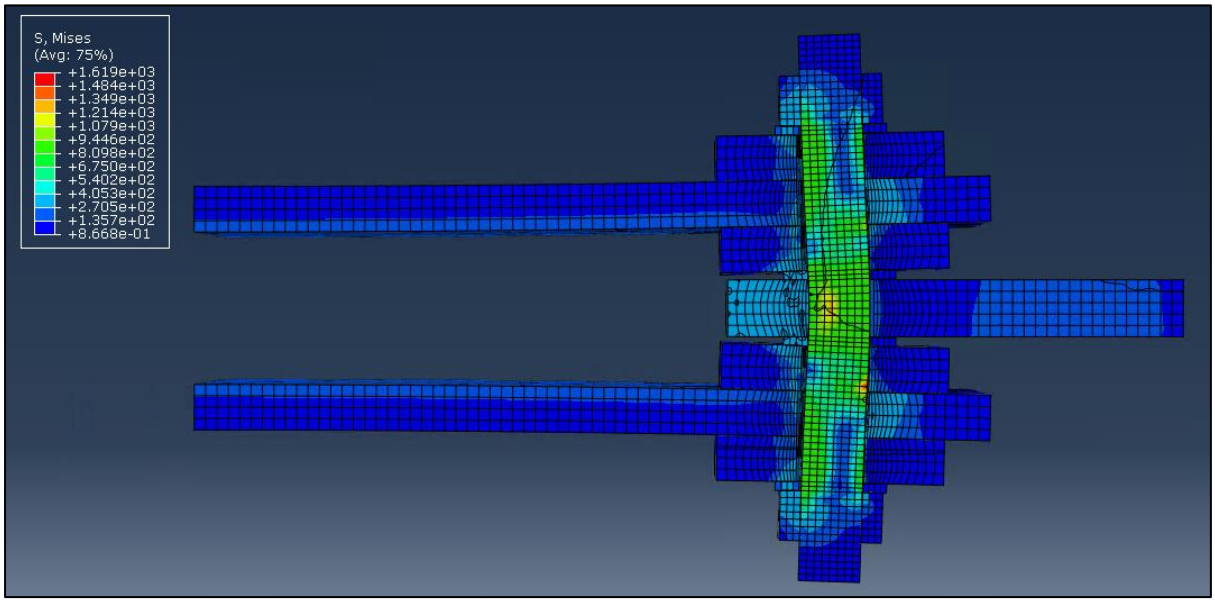

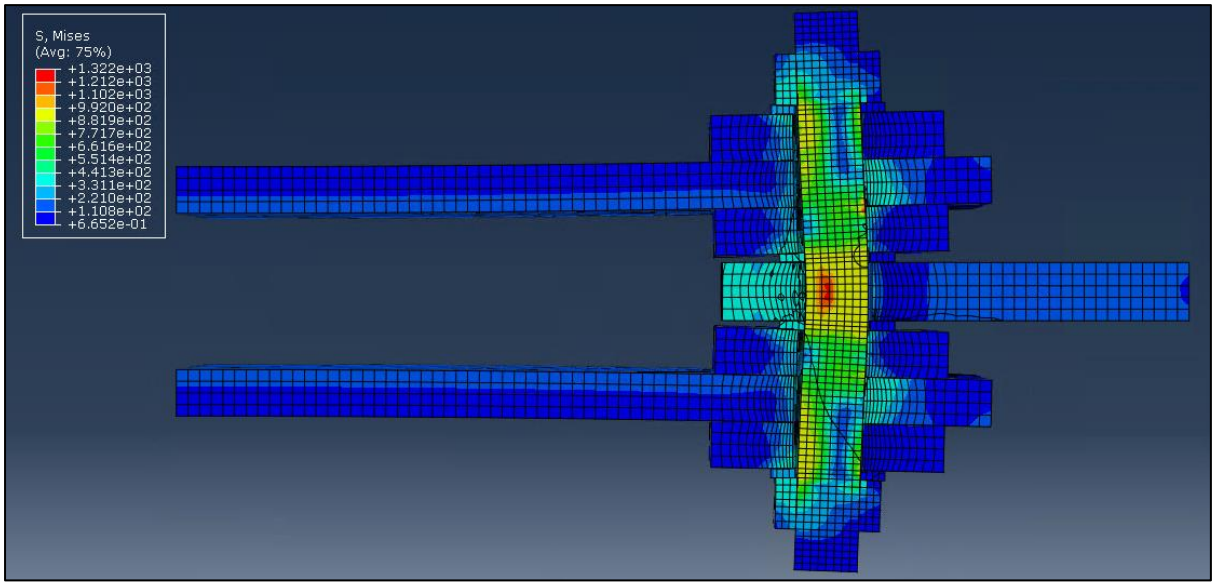

Regular deformed (Top: $200\ kN$; Bottom: $321\ kN$):

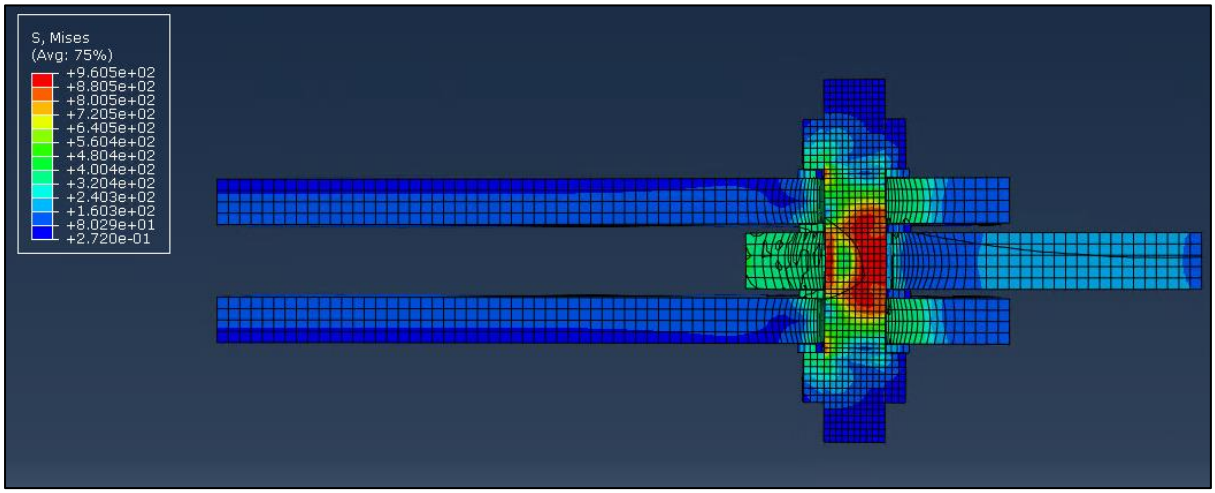

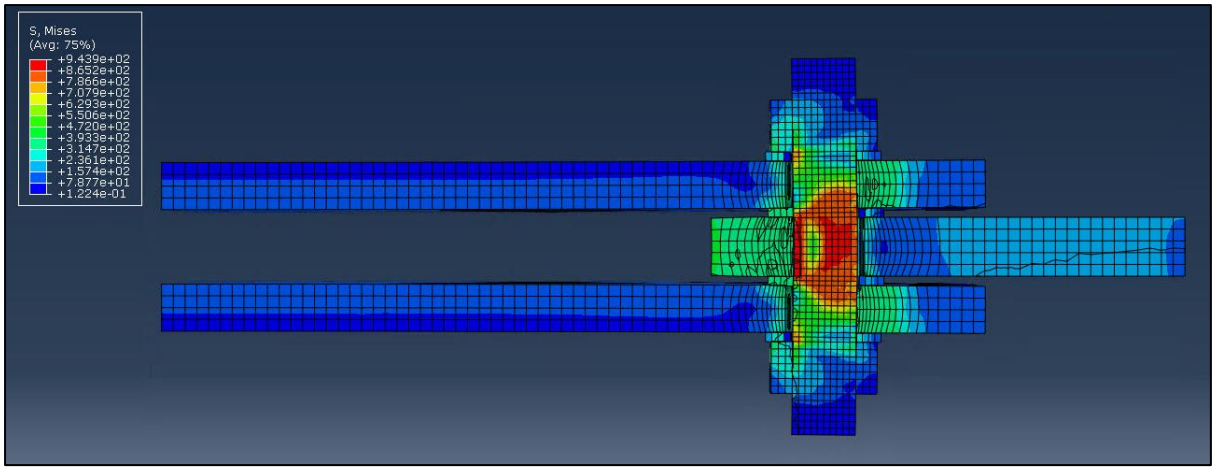

APPENDIX D. TIPS FOR FUTURE EXPERIMENTS

This appendix notes a number of small tips for future experiments using the same specimens.

If unused parts for each test are not available, it can help to flip over the cover plates between the proposed and control tests. This will reduce the number of pre-compressed coating layers at the start of the control test. It is also preferred to use new washers for each test.

For specimens using cover plates and disc springs it is recommended to place an additional washer, that has a larger diameter than the disc spring, between the cover plates and disc springs. This will prevent the significant damage they inflict on the coating of the cover plates.

Use 20 mm high supports for the central plates and cover plates to prevent sagging during assembly and preloading.

The bolt rod must be centred during preloading of the bolts to prevent interaction between the bolt rod and hole edge during fatigue loading.

During and after preloading, retighten both bolts the same number of time to prevent differences from occurring.

Let the test specimen rest after preloading:

- If testing short term relaxation: let rest for 24 hours.
- If not testing short term relaxation: let rest for 1 hour.
- Retighten the bolts to the required preload prior to fatigue loading.